CHANGED

NACA

RESEARCH MEMORANDUM

for the

U. S. Atomic Energy Commission

AERODYNAMIC CHARACTERISTICS OF A 1/4-SCALE MODEL OF

THE DUCT SYSTEM FOR THE GENERAL ELECTRIC P-1

NUCLEAR POWERPLANT FOR AIRCRAFT

By Charles C. Wood and John R. Henry

Langley Aeronautical Laboratory
Langley Field, Va.

AUG 1 5 1955

THIS DOCUMENT CONTAINS RESTRICTED DATA AS
DEFINED IN THE ATOMIC ENERGY ACT OF 1954. ITS
TRANSMITTAL OR DISCLOSURE OF ITS CONTENTS IN
ANY MANNER TO AN UNAUTHORIZED PERSON IS
PROHIBITED.

NATIONAL ADVISORY COMMITTEE
FOR AERONAUTICS
WASHINGTON
AUG 1 5 1955

TABLE OF CONTENTS

NATIONAL ADVISORY COMMITTEE FOR AERONAUTICS

RESEARCH MEMORANDUM

for the

U. S. Atomic Energy Commission

AERODYNAMIC CHARACTERISTICS OF A 1/4-SCALE MODEL OF

THE DUCT SYSTEM FOR THE GENERAL ELECTRIC P-1

NUCLEAR POWERPLANT FOR AIRCRAFT

By Charles C. Wood and John R. Henry

SUMMARY

A 1/4-scale model of the General Electric P-1 nuclear powerplant was investigated to determine the internal aerodynamic characteristics. More specifically, the primary purposes of the investigation were to measure the mass-flow distribution of air in the simulated reactor, to measure the total-pressure losses for the duct components and for the complete model, and to determine model modifications necessary to produce the desired performance characteristics. Secondary objectives were to determine the effects of flow asymmetry (simulation of less than four engines in operation) on the aerodynamic performance, to determine the total-pressure profiles at the entrance to the simulated reactor, and to determine whether the path of a specific segment of air flow could be traced from the simulated reactor to a specific turbine inlet pipe.

The original mass-flow distribution in the simulated reactor was not acceptable; minor alterations to the guide vanes produced an acceptable distribution. The original performance of the inlet diffuser was not acceptable and was corrected by modifying the inlet header plate. The inlet and exit collector rings both affected the aerodynamics of the flow through adjacent duct components to a high degree. The overall loss of total pressure for the final model configuration was equivalent to 6.66 times the dynamic pressure in the compressor discharge pipes, which corresponded to the inlet of the 1/4-scale model.

INTRODUCTION

At the request of the Atomic Energy Commission, an investigation was conducted in the Langley Internal Flow Section to determine the

aerodynamics of the internal flow for a 1/4-scale model of the duct system for the General Electric P-1 nuclear powerplant for aircraft. A general description of the powerplant and specifications are given in reference 1. The configuration consisted of four turbojet engines in parallel with provisions for heating in the conventional manner by chemical combustion or for heating by bypassing the four compressed airstreams through a single atomic reactor to the four turbine inlets. A preliminary analysis is presented in reference 2 which determines the proper model scale and flow simulation for the investigation reported herein. An estimate of the pressure losses of an early version of the duct system is presented in reference 3. The NACA investigation was based on the performance requirements for the FTB (Flying Test Bed) version of the powerplant. Reference 4 presents a summary of part of the NACA investigation and is based on material transmitted by the NACA to the General Electric Company by means of informal progress reports.

The primary objectives of the investigation were to determine the effects of various duct components on the mass-flow distribution in the simulated reactor, to modify the model components to obtain acceptable reactor mass-flow distributions, to measure the total-pressure loss characteristics for the component parts of the model as well as for the complete model, and to determine means of reducing the total-pressure losses of components which produced losses too high to be acceptable. Secondary objectives were to determine the effects of asymmetry (simulation of less than four engines in operation) on the loss of total pressure for the complete model and on the distribution of air flow in the simulated reactor, to determine the total-pressure profiles just downstream from the entrance to the simulated reactor, and to determine if the paths of specific segments of air flow could be traced from the simulated reactor to a specific turbine inlet pipe.

The objective of obtaining uniform mass-flow distribution in the reactor was considered to be most important since nonuniform distributions would cause local regions of excessive temperature and possible destruction of the reactor. The total-pressure losses of the model had to be kept within reasonable limits to avoid excessive losses in thrust. The total-pressure or velocity distributions at the entrance of the simulated reactor were required to estimate the reactor heat transfer and performance. The air-flow traces were required to determine whether samples of concentration of fissionable products in the turbine inlet pipes could be used to detect and locate a structural failure in the reactor.

Near the completion of the experimental phase of the investigation reported herein, a decision was made which affected the remainder of the 1/4-scale model tests. The decision is described in the following quotation from reference 5:

"During the quarter ended June 30, 1953, the General
Electric ANP Project experienced a change in immediate objec-
tive as a consequence of governmental consideration of pro-
grams and budgets. The government has now asked that the
general direction of the program be aimed at development of
components for a power plant of direct military utility rather
than at the early acquisition of experience with reactors and
systems of aircraft type but built primarily for flight
demonstration."

The immediate effect of the change in general direction on the subject
program was to curtail the air-flow tracer tests, which were the last
item on the test program and incompleted at that time. It was also
decided that no effort would be made to analyze the data in more detail
than the analyses contained in the periodic informal progress reports
transmitted to the General Electric Company. Consequently, the material
contained herein represents a rearrangement and summary of the informal
progress reports and was prepared to establish a permanent record of the
data for use where applicable to future powerplant or duct designs.

Design Mach number at the entrance to the simulated reactor was
0.135; however, tests were conducted for the Mach number range from
approximately 0.085 to 0.16. The test Reynolds number based on the
hydraulic diameter at the inlet station of the inlet annulus was 240,000
at design Mach number; this value was 15.8 percent of the full-scale
Reynolds number.

SYMBOLS

H total pressure

p static pressure

ρ density

q compressible dynamic pressure in individual reactor passages
        upstream of orifice plate

μ coefficient of viscosity

M Mach number

V velocity

A duct area

L   length along the center line of air passage

r   radius of duct elements, inches

$\overline{H}$ mass-weighted total pressure, $\dfrac{\displaystyle\int_{r_x}^{r_y} \rho V H\, d(r^2)}{\displaystyle\int_{r_x}^{r_y} \rho V\, d(r^2)}$

$$\overline{V} = \dfrac{\displaystyle\int_{r_x}^{r_y} V\, d(r^2)}{\displaystyle\int_{r_x}^{r_y} d(r^2)}$$

D   hydraulic diameter, $\dfrac{4 \times \text{Cross-sectional area of duct}}{\text{Perimeter of duct}}$

R   Reynolds number, $\rho \overline{V} D / \mu$

Subscripts:

x   reference to inner wall

y   reference to outer wall

v   indication that a specific term is based on venturi measurements
           (see discussion in "Basis of Comparison")

i   inlet of a particular duct element

e   exit of a particular duct element

B,1,2,3,4⎫
6,7,8,9 ⎭   stations for instrumentation (see fig. 1)

APPARATUS AND METHODS

TEST SETUPS

A drawing of the complete 1/4-scale model, which simulated the section of the powerplant located between the compressor discharge and the turbine inlet, is shown in figure 1. The various components comprising this duct system are the compressor discharge pipes, inlet collector ring, inlet annulus, inlet header, simulated reactor, guide vanes, simulated control rods, exit header, exit annulus, exit collector ring, and the turbine inlet piping. Other components shown in this drawing which were necessary for test purposes but which were not a part of the actual model are the large cylindrical plenum chamber which supplied air to the compressor discharge pipes, and the control valves and venturi meters used for regulating and measuring the flow, respectively, in both the compressor discharge and turbine inlet pipes. Air from a laboratory blower discharged into the plenum, entered the compressor discharge pipes through bellmouth-shaped venturi meters, flowed through the duct system, and was discharged to atmosphere downstream of the valves in the turbine inlet pipes. This model configuration will be referred to as test configuration 4 since tests of other configurations were necessary prior to the testing of this complete configuration.

Drawings of other test configurations are shown in figures 2, 3, and 4. Configuration 1 (fig. 2) was tested for purposes of calibrating the simulated-reactor assembly and consisted of cylindrical and conical ducting which connected the model to the blower, the simulated reactor including the orifice plate, conical and cylindrical ducting connected to the exit of the simulated reactor, and a venturi meter. Each annulus of the simulated reactor was calibrated separately by sealing the inlets of all other annuli with tape supported by wooden backing rings. Several sizes of venturi meters were necessary to cover the required air-flow ranges.

Test configuration 2 (fig. 3) included the simulated reactor and downstream ducting of configuration 1 in addition to the inlet annulus fitted with an adapter cone and collar and upstream cylindrical ducting. The purpose of the tests of configuration 2 was to determine the performance of the inlet annulus and header and the effect of the inlet annulus and header on the simulated-reactor performance under conditions of ideal flow at the inlet to the annulus.

Test configuration 3 (fig. 4) consisted of test configuration 2 with the ideal inlet replaced by the inlet collector ring and the same upstream ducting as configuration 4 (fig. 1). Configuration 3 represents, therefore, complete model simulation up to and including the reactor, and

permitted the evaluation of the effect of the inlet collector ring on
the performance of the duct assembly consisting of the simulated reactor,
inlet header, and inlet annulus.

MAJOR MODEL COMPONENTS

Simulated Reactor

The simulated reactor (shown in fig. 5) consisted of 10 aluminum
concentric cylinders which formed nine annular passages, a circular
plate which contained many bellmouth circular orifices and which will
be referred to hereafter as the multiorifice plate, a rear strut intended
for support purposes in the actual powerplant, and 16 short concentric
cylinders fastened to the longer cylinders in the manner shown in fig-
ure 5. The solid central cylinder, which formed the inner wall of pas-
sage 1, was longer than the other nine cylinders for purposes of struc-
tural support. Each of the nine large cylinders was made in two parts
to permit the orifice plate to be installed as shown; consequently, air
entering the nine passages from an upstream duct flowed through the pas-
sages, through the orifice holes located in the orifice plate, through
the nine passages downstream of the orifice plate, and into some down-
stream duct. The total area of the nine annular passages was 101.56 square
inches. The areas of passages 1 and 2 were 3.25 and 9.14 percent, respec-
tively, of the total area; the areas of the remaining passages varied from
11 to 14.19 percent of the total area. The design mean inlet Mach number
to the reactor was 0.135. Since the air was to be heated in the actual
reactor, the design exit Mach number was 0.22. The total area of the
orifice holes in the orifice plate in each annulus was fixed, according
to an approximate design procedure, to produce at the design inlet Mach
number of 0.135 a total-pressure loss of 9.3q, where q is the inlet
dynamic pressure in the simulated reactor passages. During the calibra-
tion tests, it was found necessary to add in series with the circular
orifices the annular orifices formed by the 16 short concentric cylinders
in order to obtain approximately equal total-pressure losses across all
annuli. Detailed drawings of the rear strut, the support member of the
reactor, are shown in figure 6(a). Drawings of the rear-strut modifica-
tion, which was intended to simulate insulation and was not derived from
aerodynamic considerations, are shown in figure 6(b). Data showing the
percent blockage (reduction in area) of each annular passage of the reac-
tor produced by both the original and modified rear struts are included.

Inlet Annulus and Header

A drawing of the inlet annulus together with a table of dimensions
is shown in figure 7. The annular passage had practically a constant

area from the entrance or upstream end of the annulus through the 90° turn, which is located near the annulus exit and which directs the air flow radially towards the model center line. Downstream of the 90° bend in the region adjacent to the header plate, the area increased rapidly at a rate equivalent to that of a conical diffuser with a 28° cone angle. The downstream end of the inlet annulus, referred to herein as the header plate, was redesigned so that the rate of area increase was reduced to that of an equivalent 12° conical diffuser; a table of dimensions for the redesigned header plate is also shown in figure 7.

Exit Annulus and Header

A drawing of the exit annulus and a table of dimensions is shown in figure 8. This duct element was similar to the inlet annulus in that it consisted of a section of constant area followed by one with rapidly increasing area. The constant area section began in the region of the header plate (station 6) at the entrance to the exit annulus, continued through the large angle turn which directed the air flow towards but at an angle to the center line, and continued downstream through the other minor turns to the section approximately parallel to the center line which begins 5.9 inches from the downstream end. The rate of area expansion of this 5.9-inch section was equivalent to that of a 28° conical diffuser. No alterations to this duct element were made.

Inlet Collector Ring

Drawings of the inlet collector ring together with all important dimensions are shown in figure 9. This duct collected the flows discharged from the four $4\frac{1}{2}$-inch-diameter compressor discharge pipes and varied in diameter as shown in figure 9. The compressor pipes, which were in the same vertical plane, all connected to the same side of the collector, two above and two below a horizontal plane through the center of the collector ring. Flow from the two center pipes was directed almost radially towards the collector-ring center, whereas flow from the two outer pipes was directed almost tangential to the collector ring. Short diffusers connected the compressor pipes to the collector-ring passage. The diffusers were approximately 6 inches long and increased in diameter from $4\frac{1}{2}$ to approximately $5\frac{1}{4}$ inches. The downstream end of the collector ring had an annular opening which matched the upstream end of the inlet annulus to which the collector discharged. No modifications to the inlet collector ring were made.

Exit Collector Ring

Drawings of the exit collector ring and important dimensions are shown in figure 10. The exit and inlet collector rings were somewhat similar in that one end was an annulus and the other was four circular pipes; however, the orientation of the annulus and pipes of the exit collector ring was opposite to that of the inlet collector. The entrances to the turbine inlet pipes, which were built into the exit collector ring in a manner similar to the exits of the compressor discharge pipes, were of a diameter equal to that of the turbine pipes and were not enlarged as were the pipe connections in the inlet collector ring.

Guide Vanes

Detail drawings of the guide vanes and tables of dimensions for the two vane configurations tested are shown in figure 11. The guide vanes were attached to the downstream end of the simulated reactor with the exception of annulus 1, where the vane was fastened to the header plate. The vanes were intended to turn the flow 90° to a direction parallel to the header plate with a minimum of total-pressure loss and without disturbing the balance of flow in the reactor. Vane configuration 1 differed from vane configuration 2 in that configuration 2 included the vane for annulus 1 and a completely redesigned vane for annulus 2. The vane heights of vanes 3 to 7 were reduced by cutting off short sections of the base whereas that for vane 9 was increased by inserting shims at the base. This configuration increased the minimum spacing between adjacent vanes in the annuli near the center of the reactor and in annulus 9, while decreasing the minimum spacing in the annuli in the outer part of the reactor.

Control Rods

Detailed drawings of the simulated control rods, together with tables of dimensions, are shown in figure 12. Control rod configuration 1 was used in conjunction with guide vanes whereas configuration 2 was used without guide vanes. The control rods for both configurations were airfoil-shaped and of the same profile; the arrangement for use without guide vanes had a slightly higher aspect ratio and a flat tip for attachment to the reactor. Configuration 1 fastened directly to the curved guide vanes. An end view of the reactor, figure 13, shows the circumferential and radial positions of the control rods. Figure 14, a photograph of the exit end of the reactor, with guide vanes and rods in quadrant D (see fig. 1) removed, is included for illustrative purposes.

AUXILIARY EQUIPMENT

The several venturi meters required for this investigation were all designed to produce a sinusoidal acceleration distribution in which the acceleration at the inlet and exit was zero. The ratio of the upstream area to the venturi throat area was 10 for all venturi meters except the ones located in the compressor discharge and turbine inlet pipes, the area ratios of which were dictated by the pipe sizes and quantities of air to be passed and which equaled 1.65 and 1.45, respectively. A drawing of a typical venturi meter is shown in figure 15; a table listing the various venturi throat diameters required is also included.

Special equipment required for the air-flow tracing investigation consisted of a supply of dichlorodifluoromethane (Freon 12), a water-heated Freon vaporizer, a tube for injecting the Freon vapor into the model, and equipment for measuring the specific gravity of the mixture of air and Freon 12, which will be discussed in the following section. The design condition for the vaporizer was the vaporization of 1/2 pound of Freon per second at pressures up to 300 pounds per square inch. The injection tube was a 5/16-inch outside-diameter cylindrical tube with three short 3/16-inch outside-diameter tubes attached perpendicular thereto. The center lines of these short tubes, which were parallel to the model center line, were located the same radial distance from the model center as were the midpoints of annular passage numbers 4, 5, and 6. (See fig. 16.) The exit ends of the short tubes were located about 1/32 inch upstream of the simulated reactor entrance; consequently, Freon entered the model in annuli 4, 5, and 6 in a direction parallel with the airstream. Injection tubes were located simultaneously at the 45° position in all four quadrants.

INSTRUMENTATION

For test configuration 1 (fig. 2), flow measurements were made in the venturi meter, at the orifice plate in the simulated reactor (station 3), and in the cylindrical duct upstream of the reactor. The instrumentation in the orifice plate consisted of a pressure orifice on both the upstream and downstream face in each of the four quadrants of the nine annuli. Instrumentation upstream of the reactor was limited to a single total-pressure tube (designated as H_{1a}), which determined the mean total pressure since the velocity was extremely small in this region.

For test configuration 2, instrumentation, in addition to that for test configuration 1, consisted of wall static-pressure orifices in the

inlet annulus and traversing total-pressure instruments in the inlet annulus at stations 2i and 2e. Both the total-pressure survey instruments and wall static-pressure orifices were located at four circumferential positions, on a 45° location in each quadrant; unless noted otherwise, all instrumentation discussed hereafter may be assumed to be located similarly. Surveys at stations 2i and 2e were not made simultaneously. The total-pressure tube of station 1a was moved to a position upstream from the inlet annulus.

The instrumentation for test configuration 3 included that for test configuration 2 in addition to instrumentation located in the compressor discharge pipes. The total-pressure tube H_{1a} was omitted. A special tube was used for determining the whirl angle of the flow at stations 2i and 2e. Four wall static-pressure orifices and a single total-pressure tube were located in each of the compressor discharge pipes at station 1 and in each throat of the venturi meters located at station B. For this and later test configurations, station 1 was the reference station, replacing the station for other test configurations which was designated 1a.

Instrumentation for test configuration 4 consisted of that for test configuration 3 in addition to longitudinal wall static-pressure orifices on both walls of the exit annulus, traversing total-pressure rakes in the exit annulus at station 6, traversing total-pressure and whirl-angle rakes in the exit annulus at stations 7 and 8, and four wall static-pressure orifices and a total-pressure tube in the throat of each venturi meter at station 9. Station 6 was located in the upstream part of the exit annulus and immediately downstream of the header section at the discharge of the simulated reactor, station 7 was in the exit annulus at the entrance to the section in which the large area increase occurred, and station 8 was upstream of the exit collector ring. Surveys in this annulus, as noted previously for the inlet annulus, were made at one station at a time.

A traversing rake consisting of two 0.040-inch-diameter, total-pressure tubes spaced 0.08 inch between centers was located at the 45° position in quadrant A, $2\frac{1}{2}$ inches downstream from the upstream end of the simulated reactor passages. This rake permitted total-pressure measurements from the outer to inner wall of each annulus.

The two primary parts of the instrumentation necessary for determining the specific gravity of the Freon and air mixture were sampling tubes and an instrument for measuring the specific gravity. One sampling tube was located in each turbine inlet pipe, approximately midway between the exit collector ring and station 9. The cylindrical sampling tube was placed transverse to the flow with three holes at the leading edge which were located to sample segments of equal area. Each tube was

located at 45° relative to either the horizontal or vertical planes. The instrument for determining the specific gravity was a commercial instrument which operated on a mechanical principle and determined the specific gravity of the Freon and air mixture relative to that of some reference gas. The accuracy of this instrument was about ±10 percent for Freon-to-air concentrations of 1 percent by volume.

TEST PROCEDURE

Tests were conducted with test configurations 1, 2, 3, and 4 in that order. The primary purpose of testing configuration 1 was to develop an orifice configuration which at a passage inlet Mach number of 0.135 would produce in each passage a total-pressure loss between stations 1a and 4 equal to approximately 9.3 times the dynamic pressure in the passage at the inlet. Such an aerodynamic configuration was required to simulate the flow resistance of the reactor. The secondary purpose was to determine the flow coefficient of the final orifice arrangement in each annulus in order that the orifices could be used as flow measuring devices. As noted previously, each annulus was tested with all other annuli sealed at their inlets. In addition, configuration 1 was tested with all annuli open, with and without the rear strut in place. The purposes of the tests were to determine the uniformity of the flow distribution in the simulated reactor without the rear strut, and to determine the nonuniformity of the flow due to strut blockage.

Configurations 2, 3, and 4 were tested for the purpose of determining the effect of a single duct element or a group of duct elements on the distribution of mass flow per unit area in the simulated reactor, for the purpose of determining whether the total-pressure loss of a particular duct element was excessive, and for the purpose of determining the general flow characteristics of each duct element. The aforementioned objectives dictated a test procedure whereby the complete model assembly had to be broken up into sections for individual testing. Configurations 2, 3, and 4 represent the breakdown adopted.

Configuration 2 permitted the evaluation of the inlet annulus and header section design relative to the reactor mass-flow distribution and total-pressure loss characteristics. Similarly, configuration 3 permitted evaluation of the inlet-collector design. With respect to the ducting downstream from the simulated reactor, the design in the immediate region of the exit header section was considered to be the only unit which could affect the reactor mass-flow distribution appreciably; therefore, the downstream ducting was evaluated with the complete model assembled, configuration 4. During the investigation, changes to certain duct elements appeared desirable; some of these desirable changes were made and tested with the complete model configuration, test configuration 4.

Table I lists the various test configurations and the particular original or redesigned duct elements tested with each configuration. In general, all configurations were tested over the largest flow range permitted by the equipment in order to obtain an indication of Reynolds number effects.

A limited number of tests were conducted with test configuration 4c with various compressor discharge and turbine inlet pipes closed. Since these investigations were intended to represent conditions prevailing when certain of the four engines were not in use, it was always necessary to have corresponding turbine and compressor pipes shut simultaneously. For these asymmetrical test conditions, as for the symmetrical test conditions, the mass flow per unit area in the compressor discharge and turbine inlet pipes was adjusted to within ±1 percent of the mean mass flow per unit area in the pipes through which air was flowing. The corresponding total-pressure deviation in any pipe at design Mach number never exceeded $0.15(H - p)_{v1}$.

BASIS OF COMPARISON

The performance indices of most importance in the subject investigation were the distribution of mass flow and the total-pressure loss coefficient. The distribution of flow in a particular duct element is generally presented as the percent deviation from the mean mass flow per unit area in that particular duct element. The total-pressure loss is generally presented as the difference from the mass-weighted total pressure in the four compressor discharge pipes, $\overline{H}_1$, and the station of

interest. The loss, in most cases, is presented in terms of a calculated

compressible dynamic pressure at station 1, $\left[(H - p)_{v1}\right]$. This is the

pressure corresponding to an assumed rectangular velocity profile, an air-flow quantity corresponding to that measured by the venturi meters at station B, a flow area corresponding to the sum of the area of the pipes at station 1 through which air was flowing, and a total pres-

sure $\overline{H}_1$. The parameter $\left[(H - p)_{v1}\right]$ is convenient for use in making

engine performance estimates since it is a one-dimensional quantity which satisfies continuity. Conversion factors which permit evaluating similar one-dimensional values of compressible dynamic pressure at other duct stations in addition to mass-weighted mean values are also presented in order to facilitate further aerodynamic analysis of the performance of individual duct elements. Similarly, one-dimensional values of Reynolds and Mach numbers, R_v and M_v, were evaluated and are presented. In the case of station 3, $\overline{M}_3$ is defined as a one-dimensional value of Mach number corresponding to the mass-weighted total pressure and the total mass flow of the nine reactor passages as measured by the orifices in the multiorifice plate.

Results of the gas sampling tests are presented as the percentage concentration of Freon to that of air noted in a particular turbine inlet pipe to the mean concentration of Freon to air in the turbine inlet pipes through which the mixture was flowing.

RESULTS AND DISCUSSION

STATION CONVERSION DATA

Pertinent information necessary to facilitate comparison of data for the various test configurations and to permit further analysis of these data is presented in figure 17. The relations of test Reynolds number R_{v2i} and Mach numbers M_{v1}, M_{v2i}, M_{v2e}, M_{v7}, M_{v8}, and M_{v4} are presented as a function of mean simulated-reactor passage Mach number $\bar{M}_3$ in figure 17(a). The relations of the ratio of calculated dynamic pressure at station 1 and the calculated dynamic pressures at stations 2i, 2e, 3, 4, 7, and 8 are shown as a function of mean passage Mach number in figure 17(b). The relation of the ratio of the calculated dynamic pressure and the measured dynamic pressure at stations 1, 2i, 2e, 7, and 8 is shown as a function of mean passage Mach number in figure 17(c). Figure 17 permits converting the data into terms of conditions at any reference station desired. The Reynolds number obtained at design Mach number is 240,000, which is 15.8 percent of the full-scale Reynolds number. A range of Reynolds number between 162,500 and 288,000 was covered in the test. Design Mach number at the inlet and exit of the simulated reactor, stations 3 and 4, was 0.135 and 0.22, respectively.

PERFORMANCE OF THE SIMULATED REACTOR UNDER

IDEAL INLET CONDITIONS

Before the investigation of the duct system could proceed, it was necessary to develop a satisfactory orifice configuration and to calibrate the simulated reactor under ideal conditions similar to those imposed by test configuration 1. The simulated reactor which met the prescribed performance is that shown in figure 5; data from tests of this reactor under ideal inlet conditions (configuration 1) are presented in figures 18, 19, and 20. The loss coefficients of each passage of the reactor are presented as a function of reactor passage Mach number in figure 18. The loss coefficients at design Mach number 0.135 vary from 10.17 for annulus 1 to 9.38 for annulus 9. This represents a

variation of $\dfrac{H_3 - H_4}{q}$ of about 8 percent. The fact that the mean loss
coefficient of all annuli was approximately 9.8 instead of 9.3, the
design loss coefficient, was not considered significant because the coef-
ficient was so large in order of magnitude. Figure 19 presents the vari-
ation of the mean mass flow per unit area for each annulus in terms of
percentage of the mean mass flow per unit area for the entire model for
the condition where all annuli were operating in parallel. Data are pre-
sented over a passage Mach number range of 0.095 to 0.152. The maximum
variation of mass flow per unit area for the Mach number nearest to
design (0.138), with the exception of annulus 1, was from 0.55 (annulus 7)
to -0.62 percent (annulus 2). Annulus 1 was deficient by 6.48 percent;
this deficiency was attributed to the rear strut located near the exit of
the simulated reactor, which effectively reduced the annulus exit area
39 percent. (See fig. 6(b).) Data taken during another set of runs
indicated that the maximum variation of mass flow per unit area at a Mach
number of 0.140 was ±0.4 percent with the rear strut removed. In addi-
tion to the variations between annuli, there were also some variations
between quadrants in any one annulus. These data are presented in fig-
ure 20 at a Mach number nearest the design. The variations were small,
most data falling within ±0.4 percent. The results of the orifice cali-
bration tests are presented in figure 21 as a function of Mach number.
The data indicate the effect of Mach (or Reynolds) number to be small and
the magnitude of the orifice coefficients to conform to standard values
for bellmouthed orifices.

PERFORMANCE OF THE DUCT SYSTEM UPSTREAM OF THE ORIFICE

PLATE IN THE SIMULATED REACTOR

Pressure and Velocity Distributions

Inlet annulus and header, ideal inlet.- The radial variation of the
ratio of the local to the mean velocity at the inlet station of the inlet
annulus, station 2i, for test configuration 2 is shown in figure 22.
Variations in distribution with changes in Mach number were negligible,
as were variations between the four quadrants at which surveys were made.
The outer-wall portion of the bellmouthed inlet located immediately
upstream of station 2i produced somewhat thicker boundary layers than
did the center portion; however, the flow was representative of an ideal
inlet.

The wall static-pressure measurements along the length of the inlet
annulus for test configuration 2 are represented nondimensionally in fig-
ure 23 as the ratio of the difference between the static pressure at the
fictitious station v2i and the local static pressure to the dynamic

pressure at the fictitious station v2i. This static-pressure drop coef-
ficient is plotted against the nondimensional flow length along the pas-
sage center line. The static-pressure deviations between quadrants in
any one transverse plane were not large; therefore, the points plotted
are presented as an average of the four quadrants. The curve fairings
are somewhat arbitrary because several times the available number of
longitudinal stations would be required to obtain an accurate trace of
the static-pressure changes. The curves indicate that, at corresponding
locations on the inner and outer walls, differences in the coefficient
of as much as 0.08 existed. These differences were presumably set up by
a combination of centrifugal forces and changes in local wall shape and
were not considered serious. No evidence of appreciable change in the
coefficient with speed is apparent up to the entrance of the diffuser
preceding the header plate. Downstream from this point, there are indi-
cations of depreciating performance with increasing speed or Reynolds
number and this is a typical diffuser effect. Its seriousness cannot be
evaluated without consideration of the total-pressure-loss data to be
discussed in a following section. The overall static-pressure drop coef-
ficient for the approximately constant area portion of the inlet annulus
was about 0.44, which is larger than the total-pressure loss coefficient
by the amount of increase in mean dynamic pressure due to changes in
velocity distribution and density.

The radial variation of total pressure at the exit station of the
inlet annulus, station 2e, for test configuration 2 is shown in figure 24.
Variations in distribution between the four survey quadrants were negli-
gible, except in a small region near the inner wall; however, extremely
large radial variations were present. The highest loss, $1.19(H - p)_{v2i}$,
occurred at the inner wall adjacent to the header plate, while the mini-
mum loss, $0.14(H - p)_{v2i}$, occurred at the 75-percent-area point, refer-
enced to the inner wall. The same data are plotted as a velocity distri-
bution in figure 25. The distorted condition of the boundary layer on
the inner wall is apparent, with magnitudes of the velocity in this
region ranging from 8 to 35 percent of the mean velocity according to
what quadrant is considered. The peak velocity obtained was 140 percent
of the mean. The velocity distribution is what might be expected down-
stream from the large and rapid increase in area (equivalent to a $28°$
conical diffuser) adjacent to the header plate. The boundary layer at
the entrance to this increasing area section was probably thick, which
penalized the performance further. The boundary-layer profiles for sta-
tion 2e were such that flow separation and instabilities are likely to
occur at full-scale Reynolds number.

Inlet-collector-ring exit.- Radial variations of the angle at which
the flow is whirling (whirl angle), the total pressure, and the ratio of
the local to the mean velocity at station 2i for test configuration 3
are shown in figures 26, 27, and 28, respectively. Variations in the

distributions with Mach number were again negligible; however, variations between the four survey quadrants were large. The whirl angles of the flow increased gradually from approximately 0° near the outer wall to approximately 15° about midway between the outer and inner walls, and were essentially constant thereafter. (See fig. 26.) The flow in quadrants A and D whirled counterclockwise whereas the flow in quadrants B and C whirled clockwise as viewed from downstream; this variation appears logical when one considers the details of the inlet collector ring and the circumferential locations of the four survey quadrants.

The loss of total pressure in the four quadrants, figure 27, was approximately equal at the outer wall and was large in magnitude. The loss in quadrants A and B decreased progressively over the larger portion of the duct width from the high value near the outer wall to a low value near the inner wall. The loss in quadrants C and D was practically constant and was large over the major portion of the duct width.

Velocity distributions developed from these data and presented in figure 28 indicate maximum velocities for quadrants A and B to be approximately equal and to be 125 percent of the mean velocity. The maximum velocities for quadrants C and D were approximately equal, but only 90 percent of the mean. The boundary layer occupied a relatively small percentage of the inlet area and presumably represented only minor losses of energy. The velocity profiles realized with an ideal inlet flow, test configuration 2, are presented in this figure for comparison purposes. The unsymmetrical flow and, consequently, the gross deviation from that obtained with an ideal inlet flow is attributed directly to the inlet collector ring. This unsymmetrical flow would be expected to produce greater losses between station 2i and the simulated reactor than were realized with the ideal inlet flow. Improvement in the total-pressure distribution at the inlet-collector-ring exit (station 2i) is desirable and could possibly be accomplished by relieving the sharp radius of turn on the outer wall of all quadrants of the collector-ring exit (see fig. 9) in order to reduce the losses shown in figure 27 in this region.

Inlet header, collector ring in place.- Results of surveys at station 2e obtained with the inlet collector ring in place, test configuration 3, are shown in figures 29, 30, and 31. Variations in the distributions with Mach number were small; however, variations between the four quadrants at which surveys were made, although being considerably less than at station 2i for the same test configuration, were significant. The whirl angle of the flow was small, never increasing beyond 8°. (See fig. 29.) The radial variations of total pressure (fig. 30) were large; the total-pressure loss for quadrants A and B varied from a value of $2.25(H - p)_{vl}$ at the inner wall to a low of $0.74(H - p)_{vl}$ near the outer wall. Total-pressure losses in quadrants C and D were less in the inner half, but larger in the outer half.

The same data are plotted in figure 31 as velocity distributions in terms of the mean velocity. The variations between velocities in the four quadrants were small near the inner wall, but quite large in a section near the outer wall that represented about 60 percent of the annulus area. The maximum velocities for quadrants A and B were approximately equal and 135 percent of the mean. The maximum velocities for quadrants C and D were approximately equal but only 112 percent of the mean. The decrease in the circumferential variations obtained between stations 2i and 2e resulted from natural mixing which was probably accelerated by the whirling motion of the flow known to be present in the inlet annulus. Figure 31 also indicates practically no boundary layer on the outer wall, and boundary layers at the inner wall which extended over 90 percent of the duct area. Comparison of these profiles with those obtained with an ideal inlet flow, test configuration 2, indicates the effects of the inlet collector ring to be favorable with respect to radial distributions but unfavorable with respect to the circumferential variations. The improvement in radial distribution was realized by a radial shifting of the flow toward the inner wall, which originated at the collector-ring exit, resulting in significantly greater velocities in a region near the inner wall that represented approximately 30 percent of the annulus area and slightly lower velocities in the remaining portions.

Redesigned inlet header.- With the inlet collector ring in place, the velocity distributions at station 2e were substantially better than obtained without the collector ring but were not considered satisfactory; consequently, efforts were directed towards improving the velocity distributions. A reduction in the rate of area change in the diffuser section adjacent to the header plate was the most obvious solution; therefore, a header plate designed to provide an increasing area section which expanded at a rate equivalent to that of a 12° conical diffuser was constructed. In designing the header plate, an effort was also made to maintain constant velocity as the flow progressed from the exit of the diffuser section towards the center line of the model; this was not feasible near the model center as the distance between the header and the upstream end of the simulated reactor was prescribed. Drawings and dimensions of this header plate, number 2, are shown in figure 7. The redesigned header plate was tested with the complete model, configuration 4b. Radial variations of performance indices obtained from measurements at station 2e for test configuration 4b are shown in figure 32. Also presented are data from figures 30 and 31 which were obtained with test configuration 3 and header plate 1. The differences between data for these two configurations were due only to changes in the header plate since tests with configuration 4 with the original header plate showed the model components downstream of the reactor to have no influence on the total-pressure characteristics of the upstream components. Significant circumferential variations were again observed because no action was undertaken to reduce them. The radial variations

of total-pressure loss coefficient were large, varying from approximately $1.8(H - p)_{v1}$ near the outer wall to approximately $0.7(H - p)_{v1}$ at the 90-percent-area point (referenced from the inner wall). However, header plate 2 was responsible for significant decreases in the total-pressure losses between the inner wall and the 90-percent-area point, which produced significant improvements in the velocity profiles. Increased velocities were obtained near the inner wall and decreased velocities near the outer wall. To be more specific, the minimum mean velocity for the four quadrants (observed near the inner wall) and the maximum mean velocity (observed at the 90-percent-area location) were 50 and 107 percent of the calculated velocity; whereas, with header plate 1, the mean velocities were 30 and 127 percent, respectively. The velocity profiles obtained with header plate 2 were not ideal, but were considered satisfactory since the profiles indicated little likelihood of flow separation and instabilities at full-scale Reynolds number.

Simulated-reactor inlet profiles.- Results from total-pressure surveys in each of the nine annuli of the simulated reactor $2\frac{1}{2}$ inches downstream from the leading edge are presented in figure 33. These data were obtained with test configuration 4c. Results for a particular annulus are presented in terms of H_{local}/H_{max}, and are plotted against percent of the distance across the annulus. At the wall positions, the curves have been faired to values corresponding to static pressures computed from the reactor mass-flow data and the total pressure H_3 in that particular annulus (where H_3 is the stagnation pressure on the upstream face of the orifice plate in the reactor). Surveys were made at a mean reactor passage Mach number $\bar{M}_3$ of approximately 0.135. Results from the two survey tubes have been superimposed in figure 33 and, in most circumstances, form a single well-defined curve. Readings from the two total-pressure tubes in annulus 1 were not in perfect agreement. The air flowing into this annulus was complicated somewhat by the main stem of the survey rake which was located immediately upstream of the leading edge of the annulus. Interference effects, which changed with radial position of the survey tubes, could not be eliminated and were considered possible causes of these minor differences. These effects were not noted in the other eight annuli. For annuli 2 to 8, the maximum total-pressure location occurred at approximately the 90-percent-gap location. Between the location of maximum total pressure and the outer wall, the total pressures decreased gradually at a rate which depended on the annulus location. Annulus 3 had a total-pressure ratio near the outer wall of 0.9877, which is equivalent to a V/V_{max} of 0.49; this value was lower than noted for any other annuli. For annulus 1, the location of maximum velocity was at the 10-percent location. For annulus 9, the total-pressure distribution was practically constant across the entire annulus or gap. Flow into the nine passages was steady; no evidence of actual or incipient flow separation was noted.

Simulated-reactor total pressures.- The total-pressure loss between the reference station la for test configuration 2 (inlet annulus with ideal inlet) and the face of the orifice plate, station 3, as measured by the upstream pressure orifices on the orifice plate, is presented as a function of Mach number in figure 34. The vertical displacement of the curves indicates the variation of total pressure with position of the passage in the reactor. The loss coefficient tended to increase with Mach number since it was partially determined by the diffuser performance, which was shown in figure 23 to deteriorate with increasing Mach number. This tendency was less in passages 6 to 9, probably because of the larger friction losses in these passages. The losses in the various passages tended to decrease progressively with increasing passage number with the exception of passage 9, which had large losses. The boundary layer which developed in the diffuser along the header plate obviously affected the loss coefficient of the inner passages. The high loss in passage 9 was probably due to the fact that the air entering this passage consisted of the outer-wall boundary layer.

Similar data for tests with the collector ring in place (configuration 3) are presented in figures 35 and 36. Data in these two figures were obtained with the same model configuration. Data in figure 35 were obtained simultaneously with surveys at station 2i and data in figure 36 were obtained simultaneously with surveys at station 2e. The trends of these curves with Mach number are the same as observed with test configuration 2, as is the orientation of the curves for the various passages. The only effect of the inlet collector ring on the loss coefficients to station 3 was a change in the magnitude. Loss coefficients in each annulus in figure 36 are larger (by 6 percent or less) than the loss coefficients for the corresponding annuli presented in figure 35. Data for figure 36 were obtained at a later date than were data for figure 35; minor uncontrollable changes in contour of the wooden collector ring were probably responsible for these changes. Almost identical loss coefficients with those in figure 36 were observed with test configuration 4a; however, data for test configuration 4b (header plate 2) presented in figure 37 indicate somewhat lower loss coefficients in all annuli. The loss coefficients decreased with increases in Mach number below the design value and remained practically constant for increases in Mach number above the design value. The orientation of the loss coefficients for the various annuli remained unchanged. The changes in loss coefficient to station 3 were small but favorable. Results from test configuration 4c (header plate 2, guide vane configuration 2, and rear strut 2) shown in figure 38 were similar to those in figure 37. A cross plot of the data from figure 38 is shown in figure 39 to illustrate the variation in loss coefficient between passages. Only data at design Mach number are presented. The effect of the thick boundary layer adjacent to the header plate on the total-pressure distribution within the reactor is evident.

The circumferential variations in flow pattern which originated in the inlet collector ring and were observed, for test configurations 3,

4a, 4b, and 4c, at the inlet-collector-ring exit and throughout the inlet annulus were still present to some extent in the simulated reactor at station 3 and are presented in figure 40. The percentage deviation of the total pressure in a particular quadrant at station 3 from the mean total pressure at station 3 is presented for test configuration 4c as a function of annulus number for a Mach number $\bar{M}_3$ of 0.135. At design speed, the deviations increased gradually from a value of ±2 percent for annulus 1 to a maximum of ±10 percent for annuli 6, 7, and 8, then decreased to approximately ±3 percent for annulus 9. These variations, although substantially larger than noted for ideal inlet conditions, were not considered serious.

Mean Loss Coefficients

Referenced to $\bar{H}_1$ or H_{1a}.- The mass-weighted mean loss coefficients up to the two inlet annulus stations and the orifice plate observed with test configuration 2 (inlet annulus with ideal inlet) are presented as functions of Mach number in figure 41. The loss coefficient to station 2i was practically constant with Mach number; however, the loss coefficients to stations 2e and 3, which were both located downstream of the diffusing section, increased gradually with increasing Mach number. The variations between quadrants were small. Similar mass-weighted loss-coefficient data obtained with test configuration 3 (inlet annulus with collector ring) are presented in figure 42. As previously noted, variations in contour of the inlet collector ring occurred in the time interval between total-pressure surveys at stations 2i and 2e. Therefore, the loss coefficients to station 3, both before and after the changes, are presented in order to determine the losses of the individual duct elements. Mass-weighted loss-coefficient data to stations 2e and 3 for test configuration 4b (redesigned header plate) are shown in figure 43. Differences between the loss coefficients on figures 42 and 43 for either station 2e or 3 are due to changes in the header plate, since data for test configuration 4a (not included) showed the model components downstream of the reactor to have no effect on the loss of total pressure upstream of the simulated reactor. Variations in loss coefficient with Mach number in both figures 42 and 43 are small; however, the variations between quadrants are large. The redesigned header plate was responsible for decreases in the loss coefficient to stations 2e and 3. A more detailed study of this will be made in the following paragraph.

Individual duct elements.- The loss coefficients of each duct element upstream from station 3 for test configurations 2, 3, and 4b were determined from figures 41, 42, and 43 and are presented as a function of Mach number in figure 44. The mean loss coefficient of the inlet collector ring decreased with increasing Mach number. At design Mach number, the collector ring loss coefficient was 0.64, which is equivalent to a total-pressure ratio $\overline{H_{2i}}/\overline{H_1}$ of 0.98 and was not considered

to be excessive. A characteristic with increasing Mach number of an increasing loss coefficient for the inlet annulus and a decreasing loss coefficient for the duct element between stations 2e and 3 was observed with test configuration 2. This is opposite from trends noted for test configuration 3. The values of losses obtained at the design Mach number are summarized in the following table:

	Loss of total pressure in terms of $(H - p)_{v1}$; $\overline{M}_3 = 0.135$ for -		
	Test configuration 2	Test configuration 3 (header plate 1)	Test configuration 4b (header plate 2)
(1) Inlet collector ring (from station 1 to 2i)	-----------	0.640	0.640
(2) Inlet annulus including the diffuser (from station 2i to 2e) (a) Calculated friction . . . . . . (b) Turning and diffusion . . . . . Totals of (a) and (b)	0.297 0.206 0.503	0.297 0.173 0.470	0.297 0.031 0.328
(3) Header and upstream reactor passages (from station 2e to 3) . . . . Total	0.230 0.733	0.325 1.435	0.392 1.360

With the collector ring in place, the presence at station 2i of large circumferential and radial variations in the flow and the existence of large whirl angles unquestionably resulted in total-pressure losses in the inlet annulus (between stations 2i and 2e) from turbulent mixing. Such losses would be significantly greater than would have occurred had this unusual inlet flow not existed. Therefore, the lower loss coefficient of the inlet annulus with configuration 3 relative to the loss coefficient observed with configuration 2 can be accounted for only by an improvement in the diffuser performance. The unfavorable effect of the inlet collector ring on the loss of total pressure between stations 2e and 3 can probably be associated with the significant changes in mass-flow distribution which must have occurred between station 2e and the entrance to the simulated reactor with the collector in place since circumferential variations in mass-flow rate between the four quadrants of the simulated reactor were ±3/4 percent of the mean mass-flow rate; whereas, variations in mass-flow rate between the four quadrants at the exit station of the inlet annulus, station 2e, were about 7 percent of the mean. Header plate 2 effectively reduced the loss of total pressure in the inlet annulus and increased the loss between stations 2e and 3. Reasons for the decrease in loss in the inlet annulus are obvious; however, data were not sufficient to determine the reasons for the increased loss between stations 2e and 3.

MASS-FLOW DISTRIBUTION IN THE SIMULATED REACTOR

Symmetrical Conditions

From the operational standpoint of the reactor, the magnitudes of the deviations in mass flow per unit area in each of the nine annuli relative to the mean mass flow per unit area were of great importance. Limits on the deviations were, therefore, specified to be ± 5 percent; these limits have been used throughout this investigation as a gage for determining whether results obtained with a particular configuration were acceptable. The ± 5-percent limit was not considered applicable to annulus 1 in view of the large blockage due to the rear strut in this annulus and in view of the low air-flow capacity of this annulus.

The variations in mass flow per unit area in the various passages of the simulated reactor for test configuration 2 are presented as a function of the Mach number at the inlet-annulus inlet station in figure 45. The curves group between 3.1 and -2.3 percent of the mean for annuli 2 to 9; annulus 1, however, was deficient by a maximum of 10.3 percent. The trends with increasing Mach number or Reynolds number are favorable at speeds above the design value, $M_{v21} = 0.259$. Reactor mass-flow deviations for test configuration 1 (ideal inlet to reactor, fig. 19) were significantly less than for test configuration 2; maximum deviations, with the exception of annulus 1, of 0.9 and -0.85 percent occurred in passages 3 and 9, respectively. The increase in mass-flow deviations caused by the addition of the inlet annulus is attributed to the nonuniform radial total-pressure distribution in the header section (figs. 24 and 34).

Similar data obtained for test configurations 3, 4a, 4b, and 4c are presented in figures 46, 47, 48, and 49, respectively. The orientations of the curves for the various passages were, except for passages 6, 7, and 8 in figure 49, essentially the same for each configuration. The addition of both the inlet collector ring and the duct elements located downstream from the simulated reactor increased the magnitudes of the deviations. Data for the complete model shown in figure 47 were obtained before any alterations to the individual duct elements were made; the curves group between -8.2 percent, for annulus 2, and 7.6 percent, for annulus 8. Annulus 1 was deficient by a maximum of 16.4 percent. Header plate 2 had little effect on the deviation; however, guide vane configuration 2 reduced the deviations substantially in spite of the fact that the tests included rear strut 2, which had poorer characteristics in this respect than rear strut 1.

Figure 50, a cross plot of mass-flow deviations at design Mach number, $\overline{M}_3 = 0.135$, for the model configurations in the last five figures,

permits a better comparison of the data. This figure shows that at design speed with the complete model assembly, guide vane configuration 2 was the only configuration which produced mass-flow deviations in annuli 2 to 9 which fell within the allowable limits. In fact, with this arrangement, only the deviation in annulus 2 was greater than $3\frac{1}{2}$ percent with the exception of annulus 1, which was deficient by 12.1 percent. The distribution of flow obtained with this configuration (4c) was considered satisfactory; consequently, no further changes were made.

Asymmetrical Conditions

The percentage deviations in mass flow per unit area in the simulated reactor passages from the mean mass flow per unit area for the six asymmetrical conditions for which tests were conducted are presented as a function of mean passage Mach number M_3 in figures 51 to 56. Data on these figures were obtained with test configuration 4c. The trends with increasing Mach number as well as the orientation of the curves for the various annuli are similar to results obtained with symmetrical flow. The deviations for several of the asymmetrical conditions increased grossly relative to those observed for symmetrical conditions as is indicated clearly by figure 57, which consists of cross plots of figures 51 to 56. Results for a symmetrical condition at design Mach number are included for comparison purposes. Results for the asymmetrical conditions are presented at some percentage of design Mach number, dependent upon the number of pipes open (75 percent for three pipes, 50 percent for two pipes, etc.). With the compressor and turbine operating at design rating, that is, the same operating positions on the performance curves as for the complete model at design speed, the Mach number in the simulated reactor for the various asymmetrical conditions would correspond to those for which data in figure 57 are presented. With pipe 3 closed, the deviations change little relative to those for the symmetrical condition; with pipe 4 closed, the only significant change was in annulus 1 where the deviation increased to 25 percent. With pipes 1 and 4 and pipes 2 and 3 closed, the deviations in annuli 1 and 2 were large; however, deviations in the remaining annuli were less than 7 percent. For the two conditions having three pipes closed, no annulus had deviations within the 5-percent limit. In annulus 1, there was little, if any, flow (deviation of -100 percent), while in annulus 9 the deviation was 62 percent. The other condition having three pipes (1, 2, and 4) closed had deviations of somewhat less magnitude, -100 percent in annulus 1 and a maximum surplus in any annulus of 18 percent. According to the mass-flow deviation limits adopted, none of the cases where more than one pipe was closed (less than three-engine operation) would be satisfactory.

Circumferential Variations for Both Symmetrical

and Asymmetrical Conditions

The circumferential variations in mass flow per unit area are pre-
sented in figure 58. Results expressed in terms of the percentage devia-
tions of mass flow per unit area from the annulus mean mass flow per unit
area are presented for each quadrant as a function of annulus number.
The deviations in a particular quadrant were quite erratic from annulus
to annulus. The deviations noted for the symmetrical flow case varied
between approximately ±1 percent. The variations increased as the num-
ber of closed compressor discharge and turbine inlet pipes increased;
maximum variations occurred in quadrants A and C when pipes 2, 3, and 4
were closed. These variations are -56 and 53 percent, respectively.

PERFORMANCE OF THE OVERALL DUCT SYSTEM

Symmetrical Conditions

The loss of total pressure between stations 1 and 9, essentially
the loss for the entire duct system, is shown as a function of mean
reactor passage Mach number in figure 59. Results for two configura-
tions are presented, 4a and 4d. Configuration 4d, not previously dis-
cussed, used control rod configuration 2 and no guide vanes. Configura-
tion 4a, which has been discussed previously, used both guide vanes and
rods. The trend of both curves with Mach number is the same. In the
limited Mach number range below 0.105 for which tests were conducted,
the loss coefficient was nearly constant with increasing Mach number.
For Mach numbers greater than approximately 0.105, the loss coefficient
increased rapidly with increasing Mach number. The loss with guide
vanes was $6.82(H - p)_{v1}$ at design Mach number; the corresponding loss
without vanes was $7.27(H - p)_{v1}$. Figure 60, which presents the loss
coefficient between stations 1 and 9 for configurations 4a and 4b as a
function of passage Mach number, shows that changes to the header plate
reduced the loss coefficient over the entire speed range of the test.
At design Mach number, the loss coefficient was 6.7 with header plate 2,
representing a reduction in overall loss of 1.8 percent. Loss coeffi-
cients obtained with configuration 4c, the final configuration, and pre-
sented in figure 61 were approximately the same as for test configura-
tion 4b. Since the loss coefficient through the simulated reactor varied
substantially with Mach number (see fig. 18), it was desirable to remove
this effect from the measured overall losses of the duct system in order
to determine the Mach or Reynolds number characteristics of the ducting
exclusive of the orifice plate. For determining this effect, the orifice-
plate calibration curve (fig. 18) was used to adjust the overall-duct-
system data to a constant orifice-plate loss coefficient of 9.3. The

results are presented in figure 61(b) as a function of Mach number. At design Mach number, the adjusted loss coefficient $\dfrac{\overline{H}_1 - \overline{H}_9}{(H - p)_{v1}}$ was 6.53, while the measured loss coefficient was 6.66. At Mach numbers of 0.09 and 0.145, the adjusted loss coefficients were 6.65 and 6.56, respectively, while the measured coefficients were 6.26 and 6.96. Thus, practically all the measured variation of the overall loss coefficient with Mach number was due to the orifice-plate characteristics.

Asymmetrical Conditions

The overall measured loss coefficients of the model determined with asymmetrical conditions are presented as a function of mean passage Mach number in figure 62. Also included for comparison purposes are results for a symmetrical condition. This figure shows that for the asymmetrical conditions an increasing number of closed pipes decreased the loss coefficient significantly, that the variation in loss coefficient with Mach number was small, and that with the outer pipes (number 4 or both 1 and 4) closed, the loss coefficient was somewhat greater than with the inner pipes closed. The reason for the large reduction in loss coefficient was because the mass flow per unit area throughout the model was reduced in proportion to the number of pipes closed; whereas, the dynamic pressure on which the coefficient is based was not reduced. A true comparison of the aerodynamic performance may be obtained by multiplying the coefficients for the 1-, 2-, and 3-pipe-closed conditions by 1.78, 4, and 16, respectively.

PERFORMANCE OF THE DUCT SYSTEM DOWNSTREAM FROM THE

ORIFICE PLATE IN THE SIMULATED REACTOR

Pressure and Velocity Distributions

Simulated-reactor exit.- Total pressures in the individual annuli at station 4, expressed in terms of loss coefficients, are presented in figure 63 as a function of annulus number. Data in this figure, obtained with test configuration 4c, are for one Mach number only, $\overline{M}_3 = 0.141$. The data were not measured directly, but were computed using data at stations 3 and 1 and the orifice-plate calibration curve of figure 18. The loss coefficient $\dfrac{\overline{H}_1 - \overline{H}_4}{(H - p)_{v1}}$ increased from a value of 4.95 for annulus 1 to 5.84 at annulus 5, decreased to a value of 5.34 for annuli 7 and 8, then increased to a value of 5.6 for annulus 9. Similar trends

were noted for other header plate, guide vane, and rear strut configura-
tions. The loss distribution was just opposite from what might normally
have been expected. The characteristics of the orifice plate, when the
flow rates were approximately equal, were such that losses through the
individual annuli at design Mach number were less in the outer annuli
than in the annuli comprising the center portions. The loss distribution
to station 3, figure 39, was similar to the loss distribution through the
simulated reactor. The deficiencies in flow rate through annuli 1, 2, 3,
and 4 (test configuration 4c) produced lower orifice-plate losses by not
only reducing the dynamic pressure in the passages but also by reducing
M_3 and thus the orifice loss coefficient, as shown in figure 18. These
factors were thus responsible for the change in distribution at station 4
from that normally expected. As the mass-flow deviations were, to some
extent, a function of the total pressure at station 4, it must be con-
cluded that the orifice-plate characteristics determined to some extent
the mass-flow deviations. Unless the actual reactor has the same Mach
number characteristics as the orifice plate (simulated reactor for these
tests), flow-rate deviations with the actual reactor may differ somewhat
from those for the model, especially in annulus number 1. For instance,
if the loss coefficient of the actual reactor does not vary with changes
in passage Mach number, mass-flow deviations in the actual reactor will
be larger than reported herein.

Exit-header exit.- The results of total-pressure surveys at the
exit of the exit header (station 6) for test configuration 4c are pre-
sented in figure 64 for quadrant A. Total-pressure measurements at
positions in quadrant A other than the 45° position indicated total
pressures at station 6 to be asymmetrical due to wakes from model com-
ponents located upstream (rear strut and control rods); consequently,
the attainment of reliable data at this station was impractical. The
curve presented is merely for the purpose of illustrating the general
type of total-pressure profile obtained at this station.

Exit annulus.- The wall static-pressure measurements along the
length of the exit annulus for test configuration 4a are represented
nondimensionally in figure 65 as the ratio of the difference between
the static pressure at station 1 and the local static pressure to the
calculated dynamic pressure at station 1. The static pressures in quad-
rants A and B were approximately equal and have been averaged and plotted
in figure 65(a). Similarly, static pressures in quadrants C and D have
been plotted in figure 65(b). The curve fairings are somewhat arbitrary
because several times the present number of longitudinal stations would
have been required to obtain an accurate trace of the static-pressure
changes. The static pressures on the outer and inner walls of the duct
system were essentially equal at station 6 $\left(\dfrac{L}{D_6} = 0\right)$, in the diffuser

between stations 7 and 8 $\left(\dfrac{L}{D_6} = 6.3\right)$, and at station 8 $\left(\dfrac{L}{D_6} = 7.3\right)$. The

static-pressure readings cannot be accurately interpreted due to the fact that static-pressure changes in the annulus were due to a number of inseparable effects, such as changes in local and general directions of flow, in velocity distributions, in flow area, and in angle of whirl.

Exit diffuser.- The results of total-pressure and whirl-angle surveys in the exit diffuser at stations 7 and 8 are presented in the form of radial distributions in figure 66. The total-pressure data at station 7 were obtained with test configuration 4c; the remaining data in this figure were obtained with test configuration 4a. At station 7, total-pressure data in quadrants A and C are available; whirl-angle measurements at station 7 and both total-pressure and whirl-angle measurements at station 8 are available in all four quadrants. At stations 7 and 8, significant circumferential, as well as radial, variations of total pressure were observed. Whirl-angle distributions at both stations 7 and 8 were practically independent of airspeed; thus, the results presented represent an average for all speeds tested. At station 7, the whirl-angles were practically zero in a region near the outer wall which represented approximately 25 percent of the duct area, but increased gradually to a maximum angle of approximately 20° near the inner wall. The whirl was induced by the exit collector and flows in quadrants A and D whirled in a direction opposite from flows in quadrants B and C. The whirl angle of the flow increased in the diffuser (between stations 7 and 8) reaching, at station 8, a maximum angle of approximately 50°. The increase in whirl angle was due to the reduction in the axial velocity component due to diffusion. Larger circumferential variations were observed at station 8 than at station 7; however, the radial variations noted were somewhat less than at station 7.

The total-pressure data from stations 7 and 8 (fig. 66) are plotted as velocity distributions in terms of the calculated axial velocities in figure 67. The velocities presented are the total velocities; thus, the velocity ratios for the quadrants at stations 7 and 8 will not average 1.0 since the flow was whirling. The velocity distributions were practically constant with speed. The variation of velocity between quadrants increased in the direction of flow; at station 8, maximum velocities varied from 157 percent of the calculated axial velocity (noted for quadrant B) to 86 percent (noted for quadrant D). The boundary layer along both walls thickened as the flow progressed through the diffuser. At the diffuser exit, station 8, the boundary layers near the inner wall in quadrants C and D extended over approximately 40 percent of the duct or annulus area. The boundary-layer profiles indicated no actual or incipient flow separation.

Mean Loss Coefficients

Referenced to $\overline{H}_1$.- The measured mean loss coefficients at stations 4, 7, and 8 are presented as a function of mean passage Mach

number in figure 68. Data at stations 4 and 7 (as noted for figs. 63 and 66) were obtained with test configuration 4c; whereas, data at station 8 were obtained with test configuration 4a. For Mach numbers greater than approximately 0.105, the loss coefficient at each station increased rapidly with increasing Mach number. The major portion of the variation in loss coefficient with Mach number is attributed to the orifice-plate characteristics, as previously discussed. At design Mach number, the loss coefficients at stations 4, 7, and 8 were 5.4, 5.74, and 6.14, respectively.

Individual duct elements.- Loss-coefficient data for the various duct elements downstream from the simulated reactor were necessary for estimating the performance of the actual powerplant which, due to the heat addition, has different values of design Mach number upstream and downstream of the reactor. Loss coefficients for the individual duct elements are presented in figure 69 as a function of mean passage Mach number. Total-pressure surveys at station 8 were not made for the final model configuration (test configuration 4c); thus, it was necessary to assume a loss coefficient $\dfrac{\overline{H}_8 - \overline{H}_9}{(H - p)_{v1}}$ for this model configuration equal to that measured for the same duct element when tested with test configuration 4a. In interpreting these data, the Mach number trends should be disregarded because the magnitudes of the changes in loss coefficient are of the same order as the accuracy of the data. The loss coefficients from stations 4 to 7, stations 7 to 8, and stations 8 to 9 were 0.33, 0.27, and 0.68, respectively, at $\overline{M}_3 = 0.135$.

It was impractical to calculate the loss of total pressure due to wall friction between stations 4 and 6; however, the duct length between the two stations was short and the loss from friction small. The loss from friction between stations 6 and 7, however, was calculated to be 16.5 percent of the measured loss between stations 4 and 7. The total-pressure loss associated with flow over the rear strut and control rods probably constituted a high percentage of the remaining loss and was not considered excessive.

The measured loss between stations 7 and 8 was equivalent to $0.39(H - p)_{v7}$. The loss from wall friction in this duct element was approximately 5 percent of the measured loss; consequently, the loss from other sources was approximately $0.371(H - p)_{v7}$. The total loss in a conical diffuser having the same area ratio (1.57:1) and equivalent conical expansion angle (28°) is 7.5 percent of the inlet dynamic pressure. Thus, the loss between stations 7 and 8 (diffusing section) from sources other than friction was several times larger than the loss in an equivalent conical diffuser including loss from friction. The velocity distribution at station 7 was not particularly undesirable,

and no evidence of boundary layer separation was obtained at station 8. The high loss apparently cannot be attributed to flow separation; consequently, it must be associated with the whirling motion and resulting flow asymmetry induced by the exit collector ring.

The loss coefficient of the exit collector ring and turbine inlet piping $\dfrac{\overline{H}_8 - \overline{H}_9}{(H - p)_{v1}}$ was 0.68. It was estimated that 30 percent of this loss resulted from friction in the turbine inlet pipes, thus giving a net loss through the collector ring of $0.48(H - p)_{v1}$ or $1.73(H - p)_{v8}$. This loss of $1.73(H - p)_{v8}$ was substantially greater than the $0.65(H - p)_{v1}$ loss which was measured between station 1 and station 2i (through the inlet collector ring and an 18-inch length of compressor discharge piping). However, in terms of the dynamic pressure at the point of entry of air into the inlet-collector-ring passage, the loss coefficient of the inlet collector ring was approximately 1.2, which is about 69.5 percent of the exit-collector-ring loss coefficient. The remaining 30.5-percent difference cannot be broken down because of insufficient data; however, it could be due to a number of reasons, that is, differences in inlet conditions, whirl effects, dump and turn losses, and exit losses.

AIR-FLOW TRACING INVESTIGATION

The scope of the air-flow tracing tests consisted of determining whether the flow in the simulated reactor followed a specific path throughout the downstream duct elements and whether the techniques used were satisfactory. The investigations were conducted with test configuration 4c. Results are presented in figures 70 and 71. The overall quantity of Freon injected into the model was controlled but the manner in which the flow divided among the three annuli into which it was injected simultaneously (annuli 4, 5, and 6) was uncontrolled. Six test conditions were investigated - four symmetrical and two asymmetrical. For five of these test conditions, Freon was injected individually in quadrants A, B, C, and D; for the sixth condition, Freon was injected in quadrant B only.

Results are presented in figure 70 in terms of percent of mean concentration for the symmetrical condition with approximately constant injection in quadrants A, B, C, and D for three airspeeds corresponding to values of $\overline{M}_3$ of approximately 0.112, 0.129, and 0.145. Also included are results for a higher percentage injection in quadrant B. When the volume of Freon injected in quadrant A was equivalent to 0.8 percent of the total air-flow volume, the results indicate percentages of mean concentration in the turbine inlet pipes 1, 2, 3, and 4

to have been 40, 300, 40, and 20 percent, respectively. With injection in quadrant B, inlet pipes 1, 2, 3, and 4 had percentages of mean concentration of 10, 30, 265, and 95 percent, respectively. Thus, with injection in quadrant A, the major part of Freon flowed into pipe 2, and with injection in quadrant B, the Freon flowed into pipe 3. With injection in quadrants C or D, similar trends were observed. The flow paths indicated by the data agreed with what would be expected from the model geometry. Neither increasing nor decreasing the Mach number with approximately constant injection had any noticeable effect, nor did increasing the percentage injection for a particular Mach number.

The results for the two asymmetrical conditions, pipe 1 and pipe 2 closed, obtained at a Mach number $\bar{M}_3$ of 0.108 with approximately 1 percent injection are presented in figure 71. Results for the symmetrical test condition for a Mach number $\bar{M}_3$ of 0.129 are also included. The percentage concentrations are presented as the ordinates and pipe number as the abscissa. Lines of constant quadrant of injection are drawn. The dashed lines are used to connect the reading for pipes having air flow with the readings obtained in closed pipes. For the asymmetrical conditions, as noted for the symmetrical conditions, there appeared to be a definite concentration pattern in the turbine inlet pipes for each quadrant in which Freon was injected. The changes in the distribution of air flow between the various annuli of the reactor or even between quadrants of a particular annulus resulting from the injection of Freon in various quadrants of annuli 4, 5, and 6 were negligible. It is of interest to note that closing a particular turbine pipe did not prevent a high concentration of Freon from appearing in the pipe if the Freon injection pattern was the same as the one which produced this result in the symmetrical case (see pipe-2-closed case, quadrant A).

SUMMARY OF RESULTS

The following conclusions are drawn as to the air-flow characteristics of the 1/4-scale model of the duct system for the General Electric P-1 nuclear powerplant for aircraft:

1. The inlet annulus, the inlet collector ring, the rear strut and the original design of the exit header section, all increased the mass-flow deviations from uniformity in the simulated reactor.

2. The guide vanes at the exit of the reactor were the most convenient means of reducing mass-flow deviations in the simulated reactor; by this means, the deviations in all except annulus 1 were reduced to within ±5 percent of the mean, an improvement of 38 percent relative to the complete model deviations before vane alterations.

3. Changes to the contour of the inlet header plate had little effect on the mass-flow deviations in the simulated reactor.

4. The mass-flow deviations in the reactor passages increased for the asymmetrical conditions as the number of closed compressor discharge and turbine inlet pipes increased; with three of the four pipes closed, the velocity of air flow was essentially zero in some annuli near the center of the reactor.

5. Mass-flow deviations in the simulated reactor for all configurations tested became smaller with increasing Mach number and Reynolds number.

6. The total-pressure losses in the inlet collector ring were not considered excessive.

7. Although the inlet collector ring established a whirl motion and considerable circumferential asymmetry in the flow, the velocity profiles in the inlet annulus exit station (station 2e) were improved, the loss of the inlet annulus and diffuser (stations 2i to 2e) was reduced by 6.5 percent, and the loss of the inlet header section (stations 2e to 3) was increased. The net result was an increase in loss between stations 2i and 3 of 8.5 percent relative to the loss with ideal flow at the inlet annulus inlet station.

8. The expansion angle of the diffuser in the inlet-header-plate region was judged to be too high to permit satisfactory performance at full-scale Reynolds numbers. A redesigned header plate provided an expansion angle of 12°, which improved the velocity profile in the inlet annulus exit station (station 2e), reduced the combined loss of the inlet annulus and diffuser (stations 2i to 2e) by 30 percent, and increased the header section loss (stations 2e to 3). The net result was a decrease in loss of 10 percent between stations 2i and 3.

9. Flow in each of the nine annuli of the simulated reactor $2\frac{1}{2}$ inches downstream from their entrance was stable with relatively high velocities near both the inner and outer walls of each passage.

10. Wakes from the rear strut and control rods were present in the exit annulus at station 6 and prevented the attainment of reliable measurements at station 6.

11. The loss of total pressure in the exit header and annulus between stations 4 and 7 was not considered to be excessive.

12. Although boundary-layer profiles at the end of the exit annulus diffuser (station 8) showed no evidence of actual or impending separation, the loss through the diffuser (stations 7 and 8) was excessive,

and was believed to be associated with the whirl motion imparted to the flow by the exit collector ring.

13. The losses in the exit collector ring were appreciably larger than losses in the inlet collector ring. The exit collector ring was responsible for considerable flow asymmetry in the exit annulus, particularly in a circumferential direction, and probably responsible for somewhat higher losses in all duct elements affected.

14. The measured loss coefficient for the entire model for the configuration giving acceptable mass-flow distributions in the reactor (header plate 2, guide vane configuration 2, and rear strut 2) was 6.66, which was 2.4 percent less than observed with the original configuration (header plate 1, guide vane configuration 1, and rear strut 1). The measured variation with increasing Mach and Reynolds number was attributed almost entirely to the orifice-plate characteristics.

15. The sampling technique used in the air-flow tracing investigation proved to be satisfactory for this type of investigation.

16. The data indicated that paths of specific segments of air flow could be traced from the simulated reactor to a specific turbine inlet pipe, and that, within the limits of the tests, the paths were not significantly affected by Mach number or by the concentration of Freon-12 vapor introduced.

Langley Aeronautical Laboratory,
    National Advisory Committee for Aeronautics,
        Langley Field, Va., July 25, 1955.

Charles C. Wood
Aeronautical Research Scientist

John R. Henry
Aeronautical Research Scientist

Approved:

for John V. Becker
Chief of Compressibility Research Division

ecc

REFERENCES

1. Anon.: Aircraft Nuclear Propulsion Project Engineering Progress
   Report No. 4, April 1, 1952 - June 30, 1952. Apex-4, (Contract
   No. AF 33(038)-21102; Contract No. AT (11-1)-171), Aircraft Gas
   Turbine Div., General Electric Co., June 1952.

2. Schmill, W. C., and Heddleson, C. F.: Preparation of Ducting Devel-
   opment Program for the Direct Cycle Power Plant. No. DC-51-11-20,
   General Electric Co., Nov. 28, 1951.

3. Heddleson, C. F.: Analysis of a Direct Cycle Air Pressure Drop.
   No. DC-51-32-19, General Electric Co., Dec. 28, 1951.

4. Heddleson, C. F.: An Investigation of the Flow Characteristics of
   the Reactor and Shield Ducting Using a One-Quarter Scale Airflow
   Model - Task 7117. Milestone III-4 - Tests of the Reactor Shield
   Ducting from Inlet to the Forward Distributor through the Simulated
   Reactor Core. No. DC-53-4-123, General Electric Co., Apr. 15, 1953.

5. Anon.: Aircraft Nuclear Propulsion Project, Engineering Progress
   Report No. 8, April 1, 1953 - June 30, 1953. Apex-8, (Contract
   No. AF 33(038)-21102), Aircraft Gas Turbine Div., General Electric
   Co., June 1953.

TABLE I

TEST CONFIGURATIONS AND PARTICULAR ORIGINAL OR REDESIGNED

DUCT ELEMENT TESTED WITH EACH CONFIGURATION

Test configuration	Header plate		Guide vane configuration		Rear strut		Control rod configuration	
	1 original	2 redesigned	1 original	2 redesigned	1 original	2 redesigned	1	2
1					x			
2	x				x			
3	x				x			
4a	x		x		x		x	
4b		x	x		x		x	
4c		x		x		x	x	
4d	x				x			x
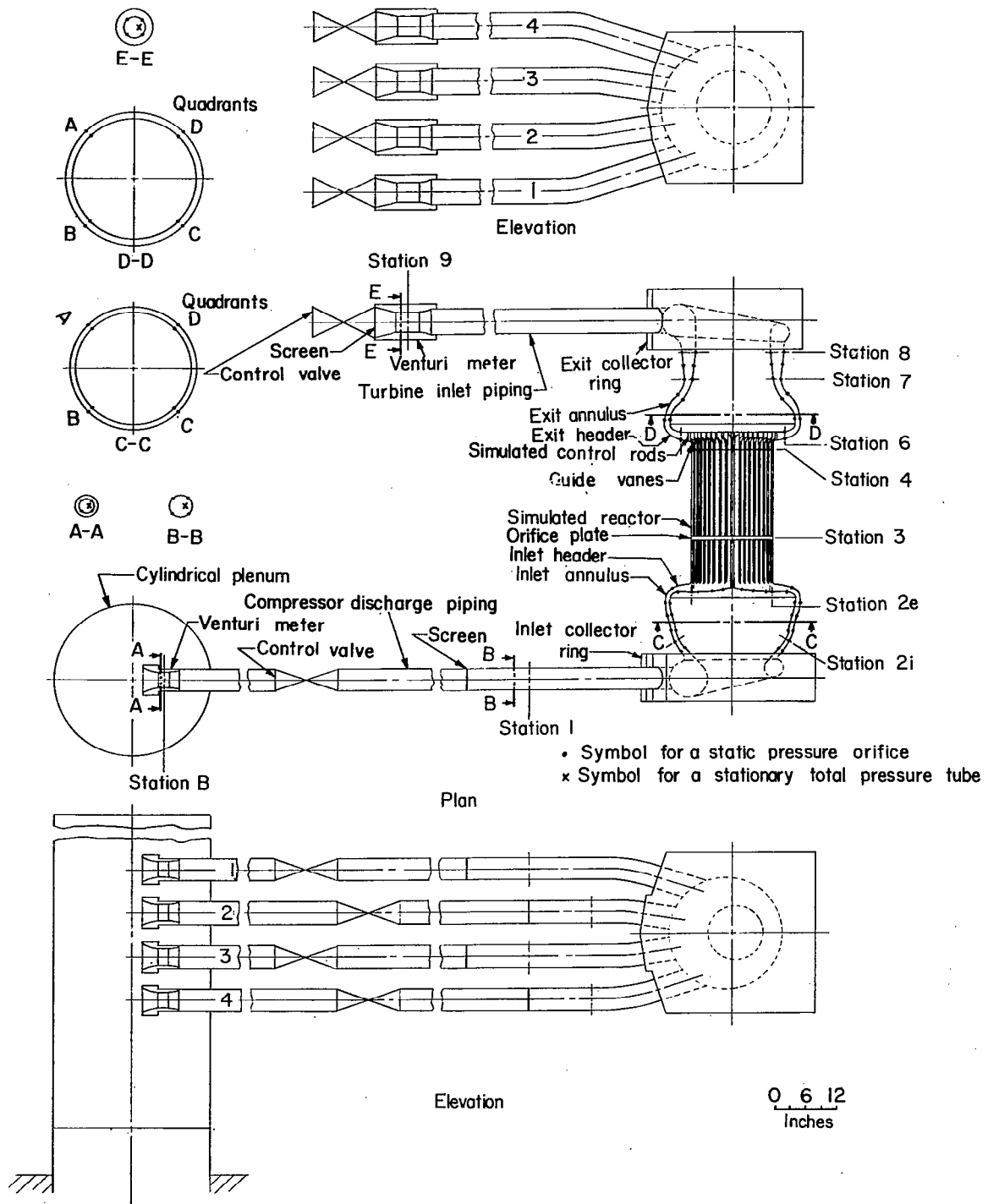
Figure 1.- Diagram of the complete duct system. Test configuration 4.

Static pressure orifices located similarly
on downstream face of orifice plate

• Symbol for a static pressure orifice
× Symbol for a stationary total pressure tube

Quadrant

Quadrant

A   D

B   C

A-A

A   D

B   C

B-B

Cylindrical ducting

Simulated reactor

Orifice plate

B

Venturi meter

A

x

A

B

Station ía.   Station 3   Station 4

0   6   12

Inches

Figure 2.- Diagram of the setup with which the flow characteristics of
the simulated reactor were determined. Test configuration 1.

- Symbol for a static pressure orifice
x Symbol for a stationary total pressure tube

Quadrant
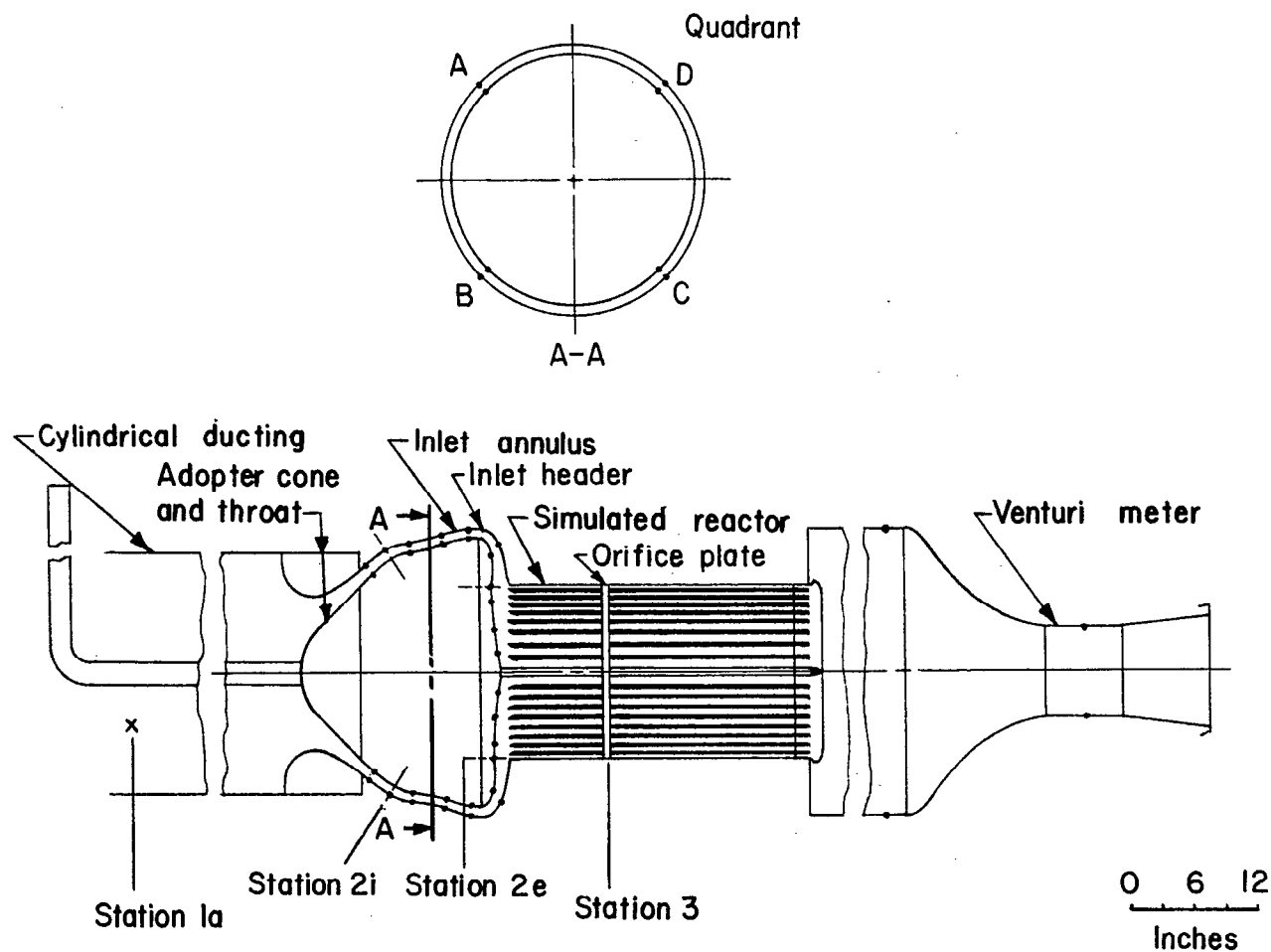
Figure 3.- Diagram of test configuration 2.

A-A   B-B

• Symbol for a static pressure orifice
× Symbol for a stationary total pressure tube

Venturi meter

Simulated reactor
Inlet header
Inlet annulus

Station 3

Station 2e

Station 2i

Cylindrical plenum

Compressor discharge piping

Venturi meter

Control valve

Screen Inlet collector
ring

Station B

Station I

Plan

Elevation

0 6 12
Inches
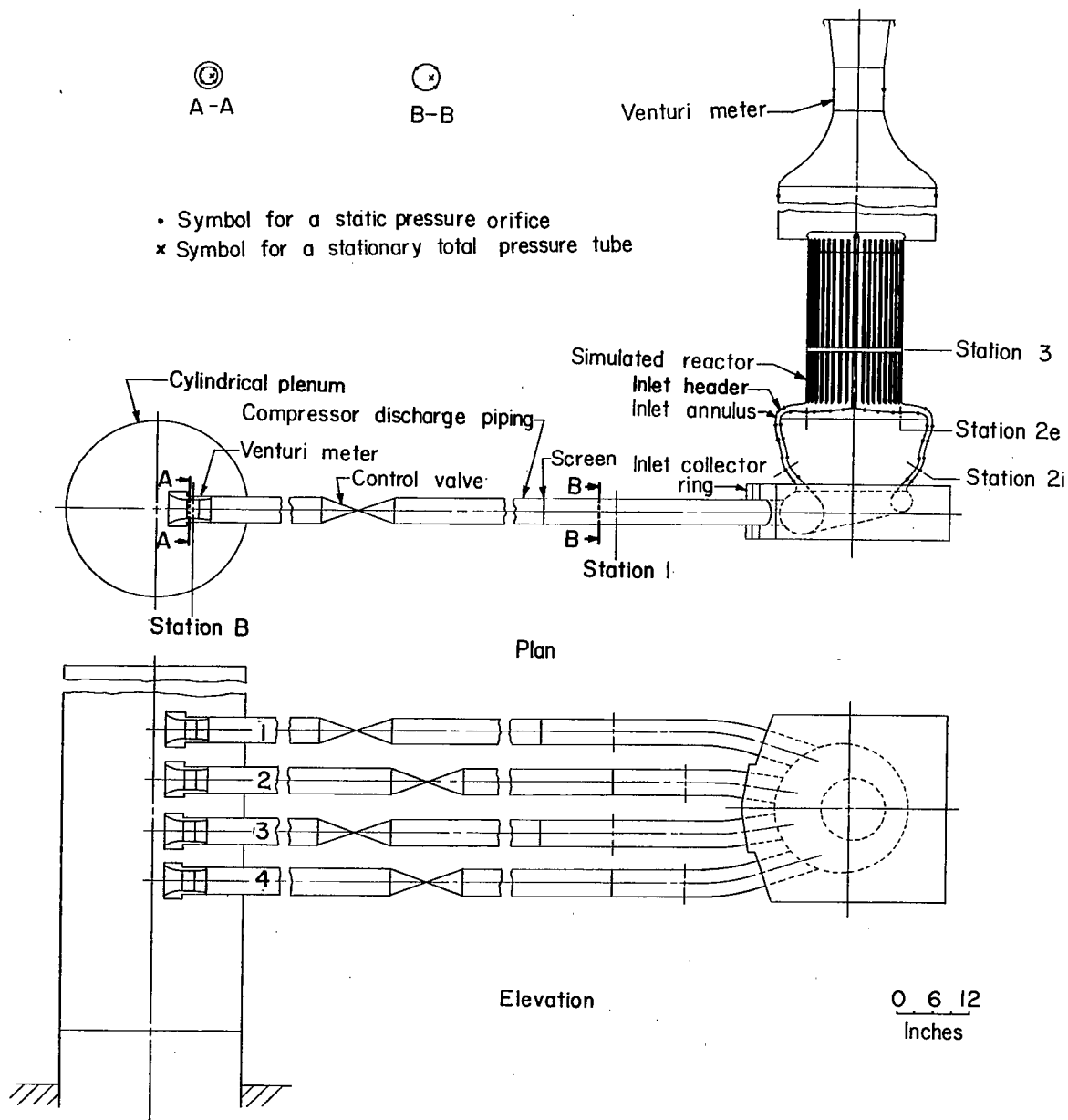
Figure 4.- Diagram of test configuration 3.
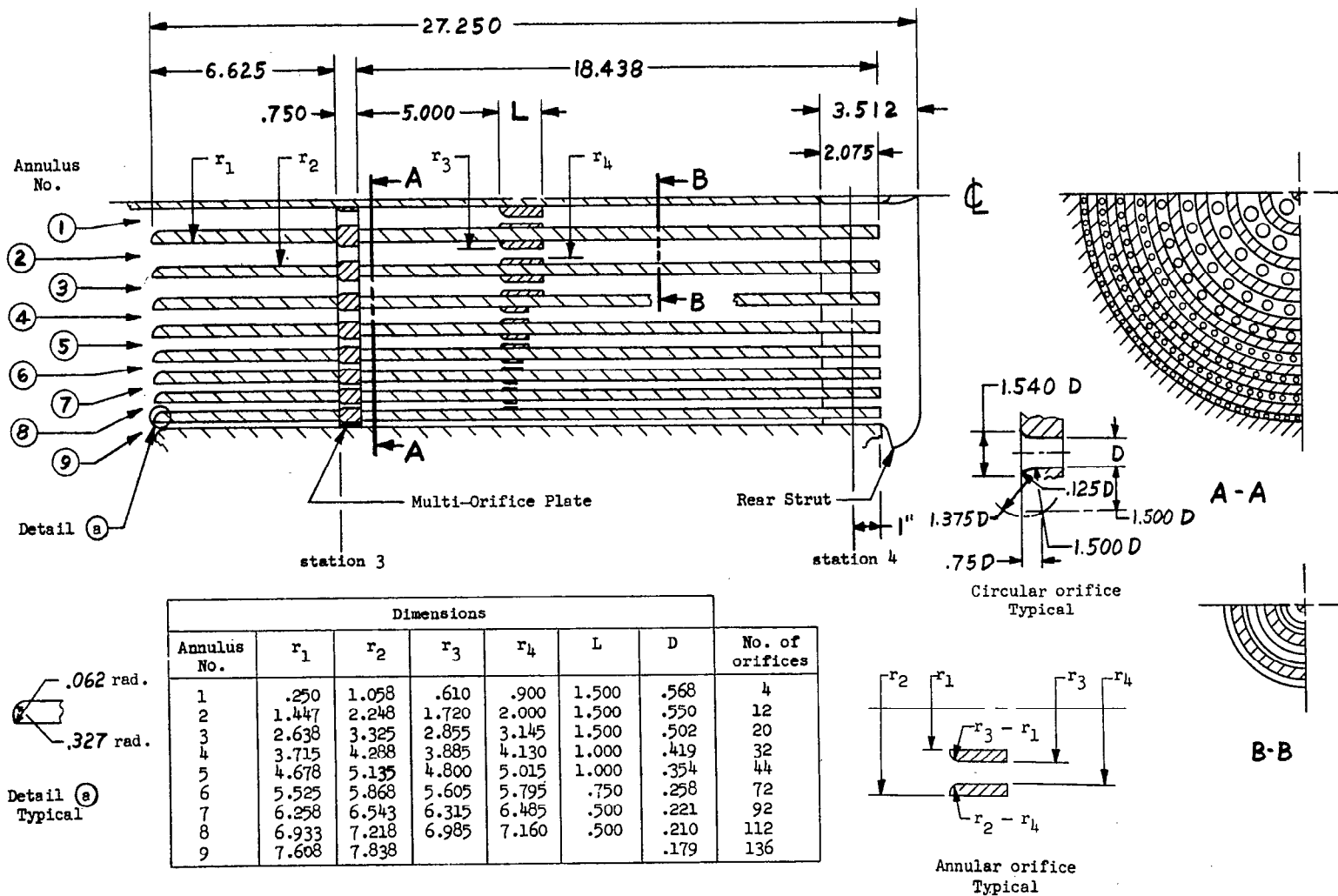
Figure 5.- Detail drawings and dimensions of the simulated reactor.
Dimensions in inches.

Dimensions							
Annulus No.	r_1	r_2	r_3	r_4	L	D	No. of orifices
1	.250	1.058	.610	.900	1.500	.568	4
2	1.447	2.248	1.720	2.000	1.500	.550	12
3	2.638	3.325	2.855	3.145	1.500	.502	20
4	3.715	4.288	3.885	4.130	1.000	.419	32
5	4.678	5.135	4.800	5.015	1.000	.354	44
6	5.525	5.868	5.605	5.795	.750	.258	72
7	6.258	6.543	6.315	6.485	.500	.221	92
8	6.933	7.218	6.985	7.160	.500	.210	112
9	7.608	7.838				.179	136

3.512

15.664

.408

2.075

Coincidental with the downstream ends of the annular passages
which comprise the simulated reactor.

0   2   4
Inches

(a) Strut 1.

Figure 6.- Drawings and dimensions of rear struts.

Rear Strut 2 is identical with Rear Strut 1 except for the
small members attached thereto as shown.
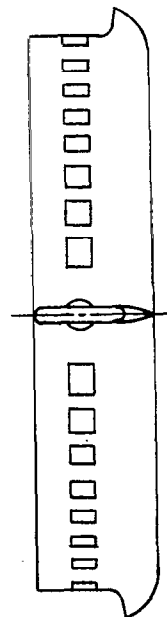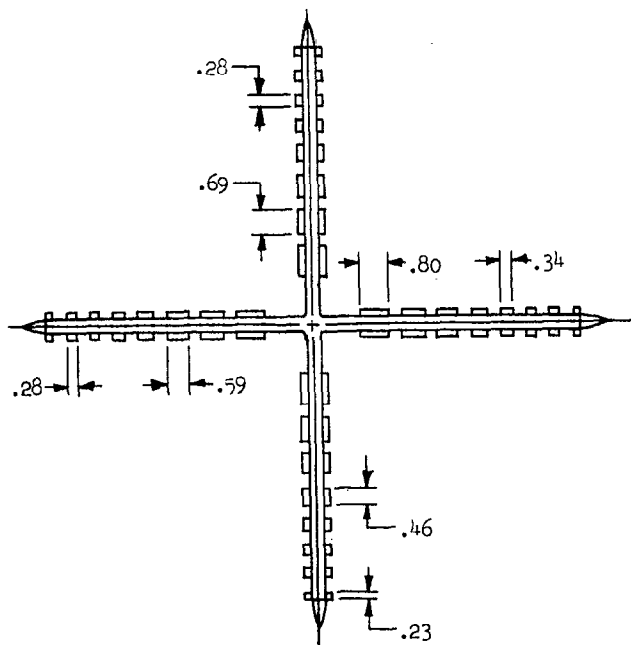
Percentage reduction in passage area attributable to the Rear Strut		
Annulus Number	REAR STRUT	
	1	2
1	39	39
2	14.5	26.5
3	8.2	17.7
4	6.2	12.8
5	5.5	10.3
6	4.8	9.
7	4.4	8.3
8	3.8	7.5
9	3.3	6.8

0 2 4

Inches

.20

2.00 rad.

Section view of
small members
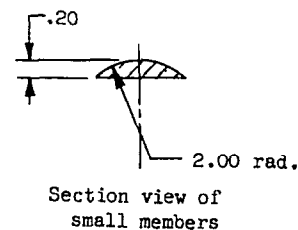
(b) Strut 2.

Figure 6.- Concluded.

section view of
support strut

3.113   .676

support strut
8 equally spaced

Header Plate

2.187

8.337

station 2i

station 2e
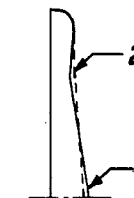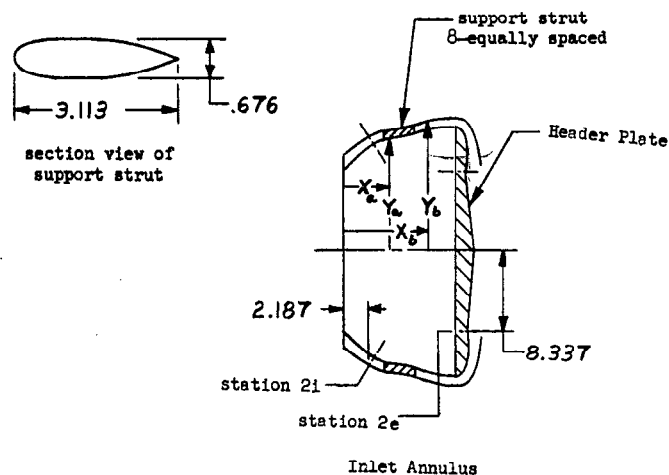
Inlet Annulus

Header Plate

Dimensions for the Inlet Annulus exclusive of the Header Plate			
X_b	Y_b	X_a	Y_a
0	9.281	0	7.922
1.000	10.176	1.000	8.955
1.775	10.799	1.500	9.471
2.876	11.326	2.225	10.131
3.967	11.550	2.673	10.402
4.994	11.568	3.578	10.727
5.932	11.658	4.500	10.813
6.873	11.910	5.006	10.814
7.345	12.103	6.068	10.924
7.833	12.355	7.127	11.226
8.909	12.778	8.168	11.740
9.981	12.951	9.091	12.126
10.500	12.959	9.555	12.231
11.000	12.959	10.019	12.283
11.548	12.938	10.500	12.291
11.846	12.874	11.125	12.291
12.446	12.592		
12.902	12.176		
13.215	11.661		
13.409	10.320		
13.684	8.338		

Dimensions			
Header Plate 1		Header Plate 2	
X_a	Y_a	X_a	Y_a
11.125	12.291	11.125	12.291
11.250	12.291	11.250	12.291
11.452	12.276	11.452	12.276
11.855	12.150	11.855	12.150
12.251	11.856	12.251	11.856
12.535	11.389	12.535	11.389
12.612	10.875	12.612	10.875
12.604	10.424	12.588	10.000
12.250	7.837	12.550	8.500
13.625	0	12.546	7.837
		12.575	7.235
		12.628	6.565
		12.685	5.880
		12.750	5.155
		12.830	4.300
		12.927	3.335
		13.050	2.250
		13.208	1.060
		13.344	0

Figure 7.- Drawings and dimensions of the inlet annulus.

section view of
support strut

.676

2.113

Rear Header Plate

X_b

X_a

Y_a Y_b

17.337

11.827

9.625

Station 6

support strut
8 equally spaced

Station 7

Station 8

Exit Annulus
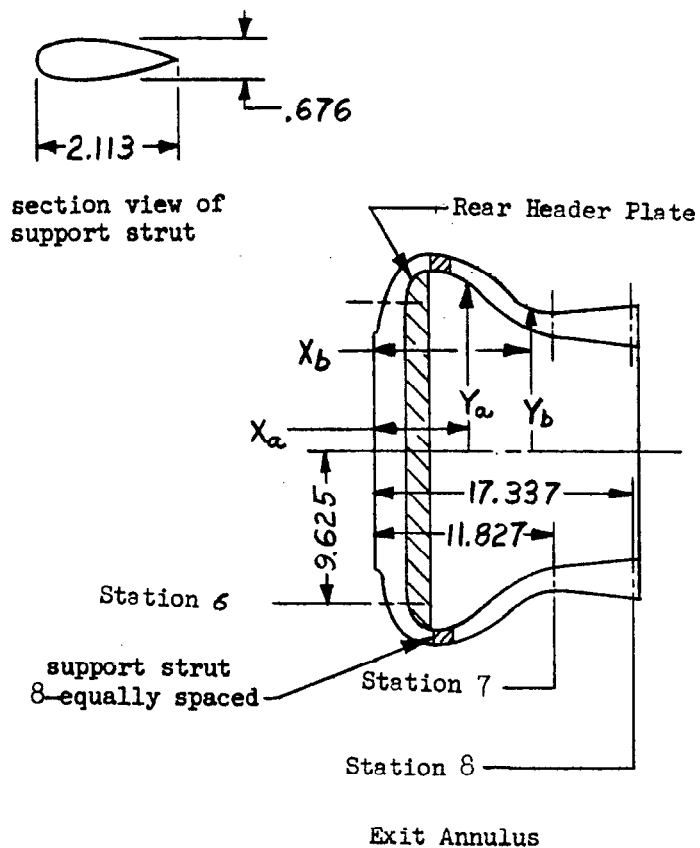
Dimensions			
X_b	Y_b	X_a	Y_a
0	7.837		
.109	7.867	1.816	10.125
.159	8.000	1.864	10.717
.342	9.000	1.944	10.957
.506	10.125	2.029	11.138
.708	11.095	2.302	11.514
1.043	11.746	2.682	11.824
1.521	12.307	3.071	12.006
2.140	12.756	3.465	12.091
2.751	13.013	3.661	12.101
3.357	13.134	5.161	12.101
3.659	13.149	5.359	12.091
5.160	13.149	5.556	12.059
5.462	13.134	5.948	11.929
6.068	13.013	6.334	11.689
6.679	12.756	6.536	11.497
7.321	12.284	7.242	10.742
8.079	11.579	7.962	9.962
8.859	10.860	8.455	9.427
9.366	10.401	9.005	8.938
9.816	10.069	9.563	8.557
10.477	9.716	10.128	8.264
11.124	9.493	10.983	7.964
11.337	9.441	11.559	7.848
11.493	9.370	11.847	7.814
12.186	9.338	12.135	7.796
12.327	9.336	12.328	7.792
18.212	9.851	18.212	7.277

Figure 8.- Drawings and dimensions of the exit annulus.
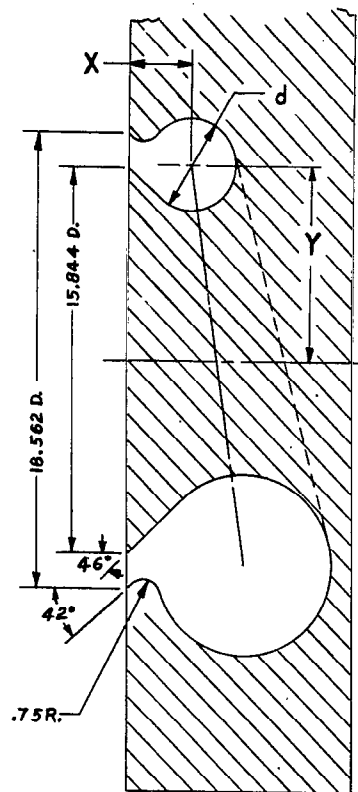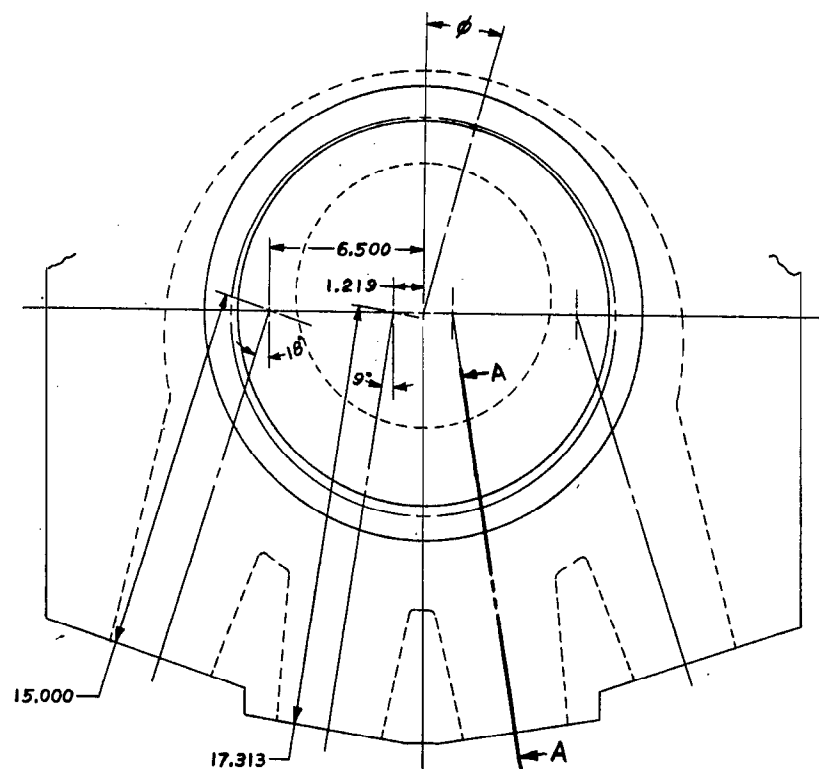
Dimensions			
φ	Y	d	x
0°	7.98	3.81	2.64
10°	7.98	3.84	2.66
20°	7.98	3.91	2.71
30°	7.98	4.03	2.79
40°	7.99	4.20	2.90
50°	8.00	4.40	3.04
60°	8.01	4.65	3.19
70°	8.03	4.92	3.37
80°	8.06	5.22	3.56
90°	8.09	5.54	3.75
100°	8.12	5.86	3.95
110°	8.15	6.18	4.14
120°	8.19	6.49	4.32
130°	8.22	6.77	4.49
140°	8.25	7.02	4.63
150°	8.28	7.22	4.75
160°	8.30	7.37	4.84
170°	8.31	7.47	4.89
180°	8.32	7.50	4.91
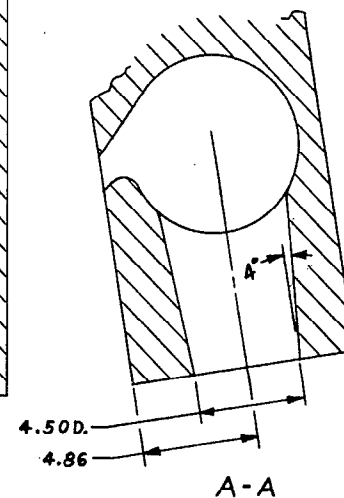
Figure 9.- Drawings and dimensions of the inlet collector ring.

Dimensions			
φ	Y	d	x
0°	9.20	3.84	3.31
10°	9.21	3.86	3.32
20°	9.23	3.90	3.38
30°	9.27	3.99	3.47
40°	9.32	4.08	3.60
50°	9.39	4.22	3.76
60°	9.47	4.38	3.94
70°	9.57	4.58	4.15
80°	9.68	4.82	4.38
90°	9.81	5.06	4.62
100°	9.95	5.38	4.87
110°	10.09	5.62	5.11
120°	10.24	5.92	5.35
130°	10.38	6.20	5.57
140°	10.51	6.46	5.77
150°	10.68	6.68	5.93
160°	10.70	6.86	6.06
170°	10.76	6.96	6.13
180°	10.78	7.00	6.16
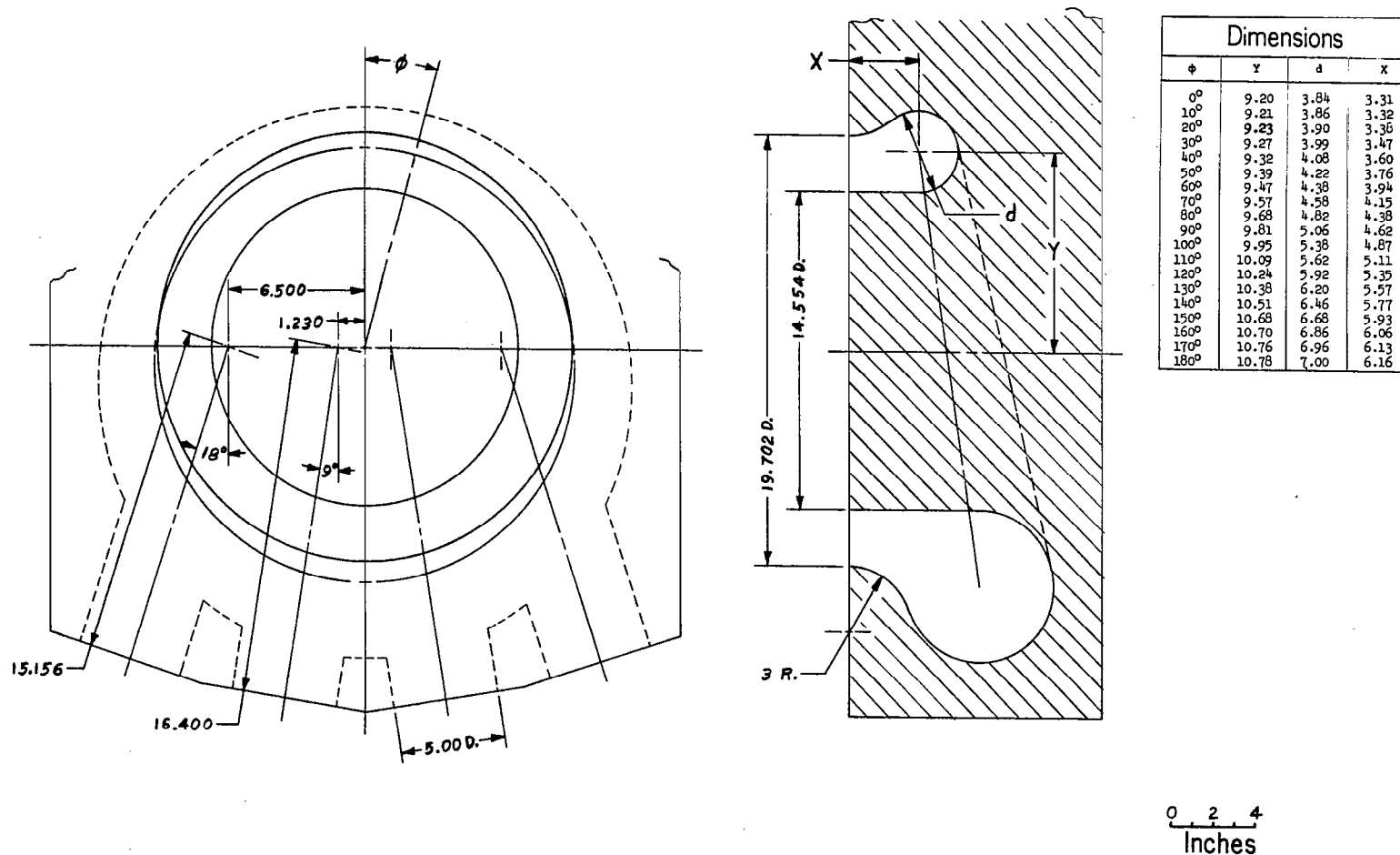
Figure 10.- Drawings and dimensions of the exit collector ring.

cutout for guide vane 2 only

.213

2.437R.

.221R.

22° 30'

.390
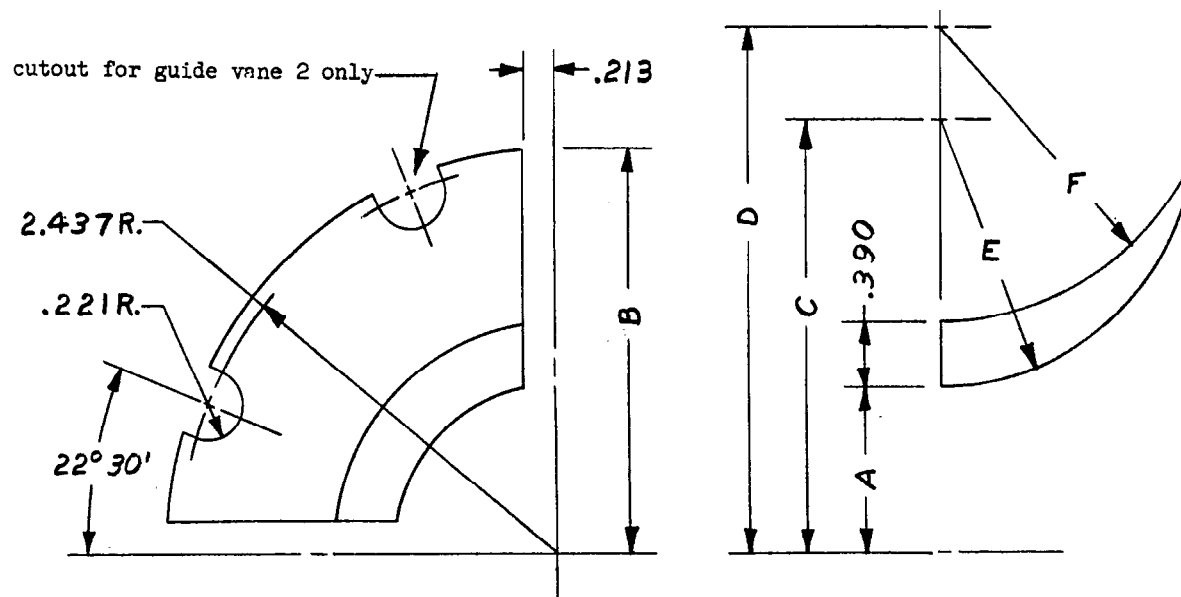
DIMENSIONS								
Vanes	2	3	4	5	6	7	8	9
A	1.058	2.248	3.325	4.288	5.135	5.868	6.543	7.218
B	2.520	3.300	4.225	5.020	5.755	6.520	7.170	7.855
C	2.727	3.447	4.240	5.007	5.635	6.287	6.908	7.467
D	3.252	4.052	4.745	5.557	6.140	6.732	7.312	7.865
E	1.670	1.200	.915	.720	.500	.420	.365	.250
F	1.805	1.415	1.030	.900	.615	.475	.380	.250

(a) Vane configuration 1.

Figure 11.- Drawings and dimensions of the guide vanes comprising guide vane configurations 1 and 2.
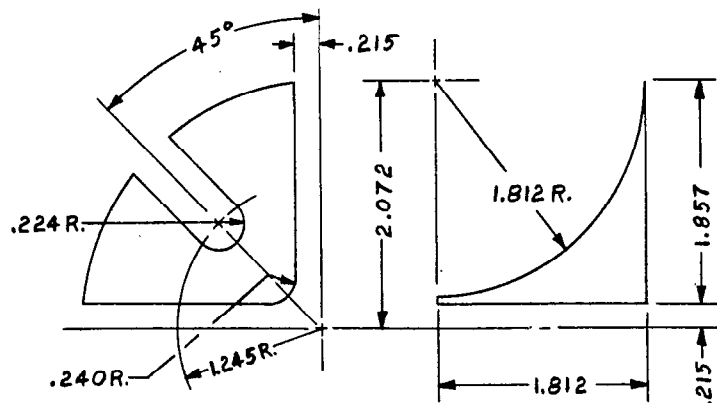
Guide vane 1
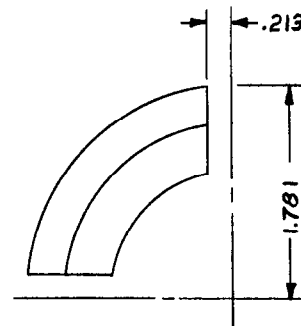
Guide vane 2
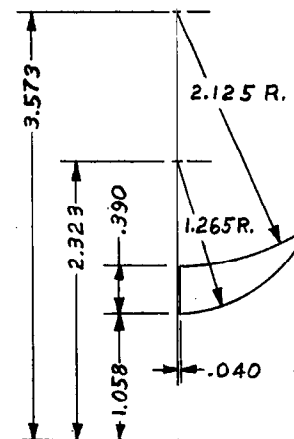
Guide vanes 3 through 9 are, except for changes to the vane heights as shown below, identical with vanes 3 through 9 used for guide vane configuration 1

Vane height, inches		
Vanes	Vane configuration	
	1	2
3	1.192	1.100
4	.908	.808
5	.723	.617
6	.506	.431
7	.444	.384
8	.365	.365
9	—	height for Configuration 1 Plus 1/16"

Spacing
Rear header plate
Vane
3
2
Vane height
Annulus
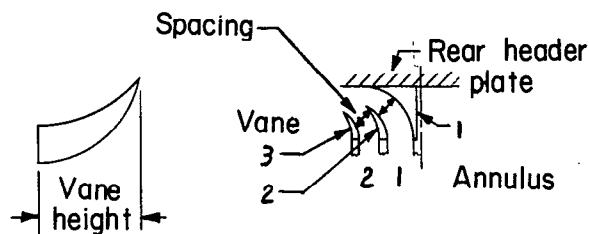
Minimum spacing between adjacent vanes, inches		
Annulus number	Vane configuration	
	1	2
1	.630	.670
2	.820	.849
3	.593	.635
4	.434	.451
5	.436	.416
6	.300	.257
7	.230	.186
8	.230	.174
9	.118	.158

(b) Vane configuration 2.

Figure 11.- Concluded.
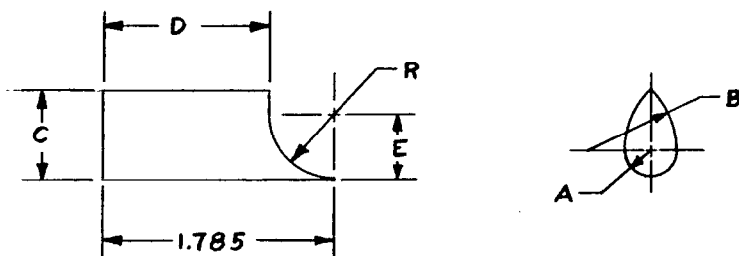
Rod No.	DIMENSIONS					
	A	B	C	D	E	R
1	.205	.750	.721	.300	1.474	1.670
2	.205	.750	.721	.625	1.004	1.200
3	.205	.750	.721	.870	.720	.915
4	.205	.750	.721	1.065	.524	.720
5	.205	.750	.721	1.285	.305	.500
6	.205	.750	.721	1.365	.224	.420
7	.205	.750	.721	1.320	.170	.365
8	.205	.750	.721	1.535	.056	.250

(a) Control rod configuration 1.
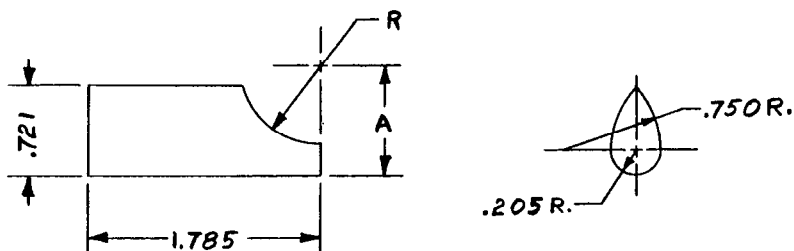
Rod No.	DIMENSIONS	
	A	R
1	2.205	1.805
2	1.815	1.415
3	1.430	1.030
4	1.280	.900
5	1.015	.615
6	.875	.475
7	.780	.380
8	.657	.250

(b) Control rod configuration 2.

Figure 12.- Drawings and dimensions of the control rods comprising control rod configurations 1 and 2.
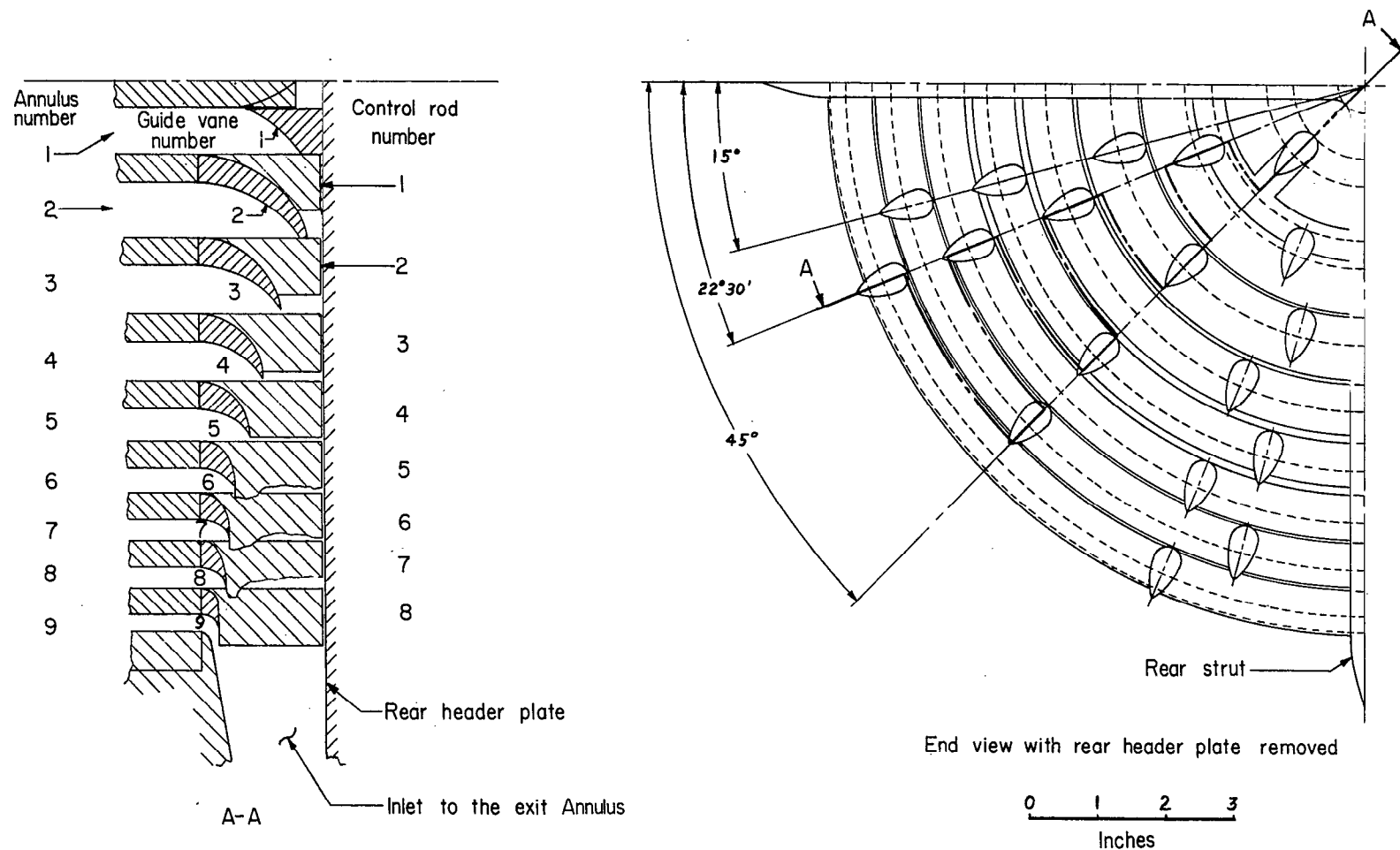
Figure 13.- Drawings of the exit of the simulated reactor showing the relative locations of the annular passages, guide vanes, and control rods. Test configuration 4a.

Part of exit annulus

Annular passages
for quadrant D

Rear strut

Guide vane
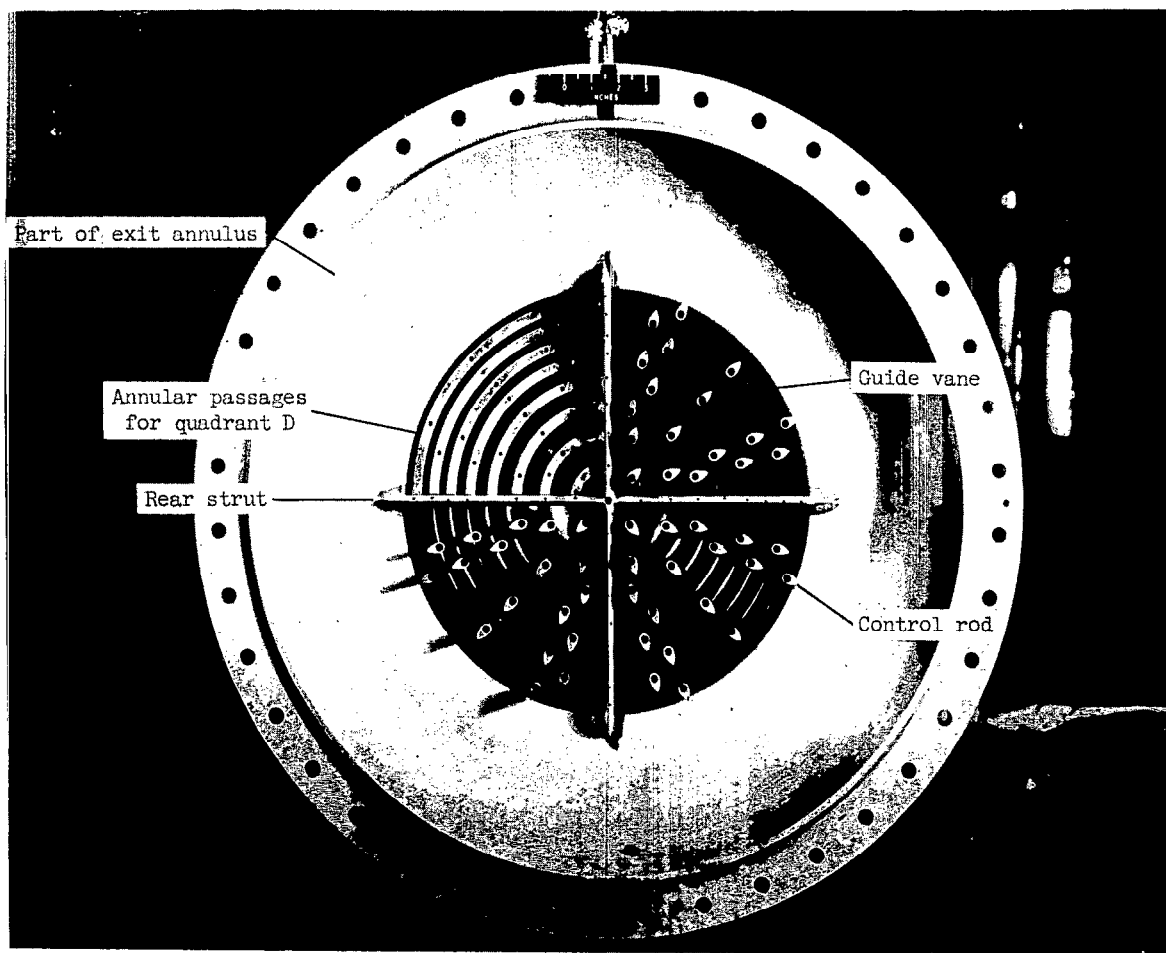
Control rod

RDP No. 248

Figure 14.- Photograph of the downstream end of the simulated reactor
showing the annular passages, rear strut, guide vanes, control rods,
and the upstream outer wall portion of the exit annulus.
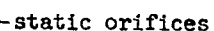
$$\text{Equation} = \left(\frac{A_2}{A_x}\right)^2 = \left[1 - \left(\frac{A_2}{A_1}\right)^2\right]\left[\frac{L_x}{L} - \frac{1}{2\pi}\sin\left(2\pi\frac{L_x}{L}\right) + \frac{1}{\left[\left(\frac{A_1}{A_2}\right)^2 - 1\right]}\right]$$

Venturi meters required
Diameter, d_2, inches
1.250
1.500
2.000
2.500
3.000
4.500
6.750
8.250

Figure 15.- Drawing of a typical venturi meter setup, the equation used to determine the venturi contour, and a table showing the various venturi meters required.
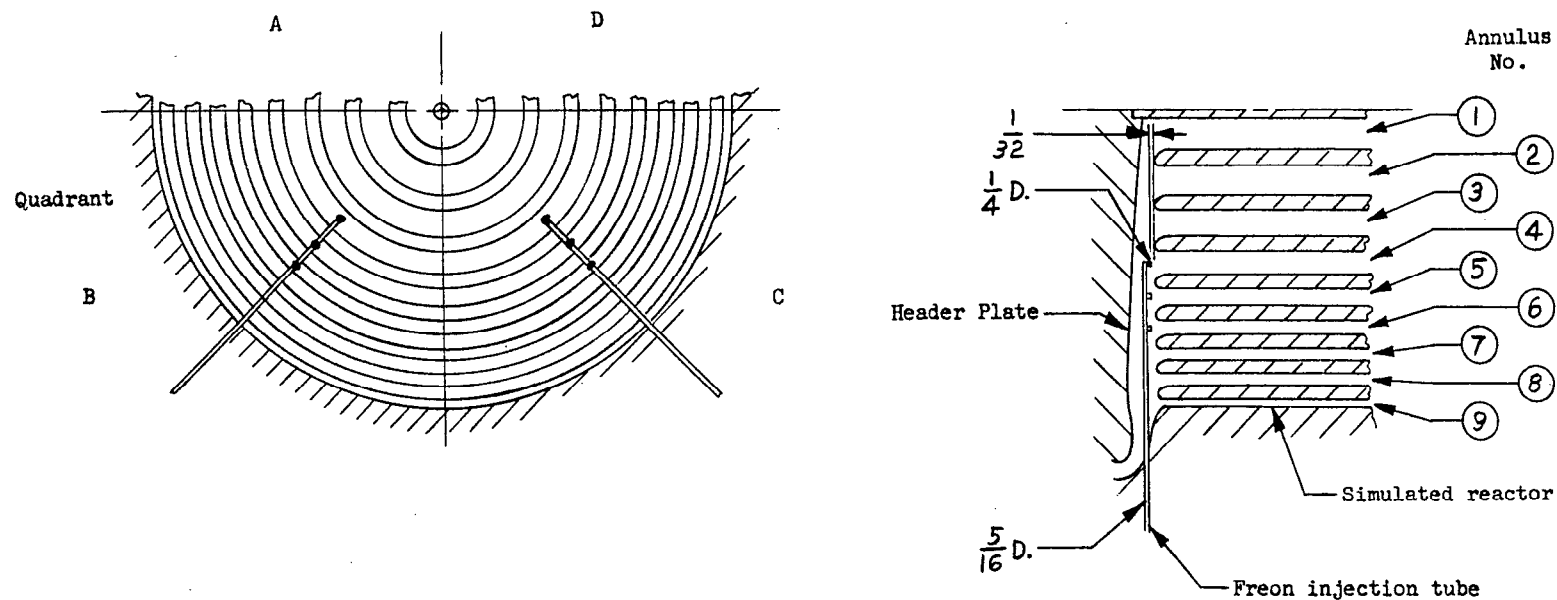
Figure 16.- Diagram showing the Freon injection tube and its location relative to the simulated reactor.
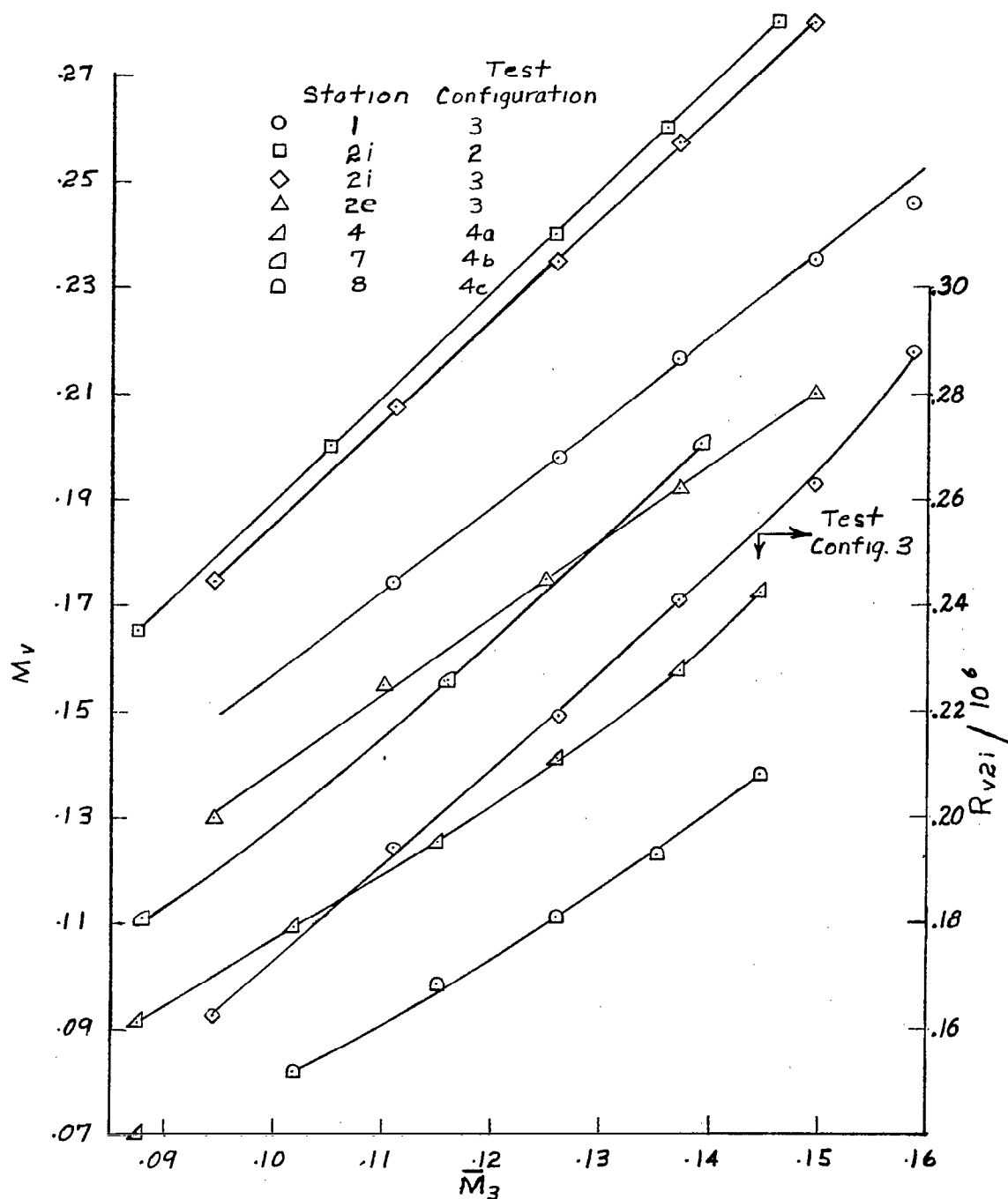
(a) Variation of Reynolds number at station 2i and Mach number.

Figure 17.- Station conversion data at several locations in the duct system as a function of mean reactor passage Mach number.

Test

Station	Configuration
○ 2 i	3
□ 2 e	3
◇ 3	4a
△ 4	4a
◁ 7	4c
◺ 8	4a
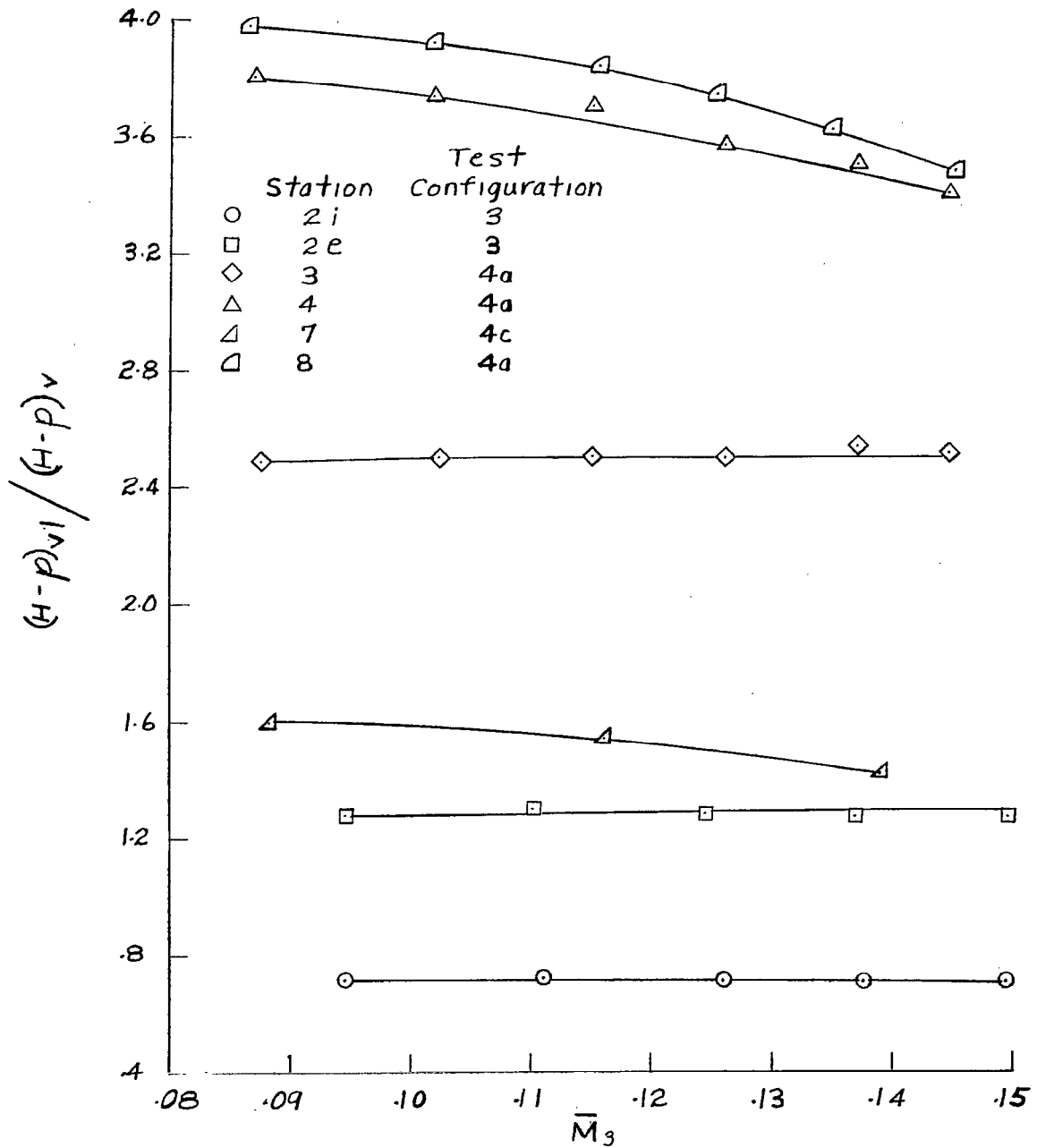
(b) Variation of ratio $(H - p)_{vl}/(H - p)_v$.

Figure 17.- Continued.

	Station	Test Configuration
O	1	3
□	2i	3
◇	2e	3
△	7	4c
◿	8	4a
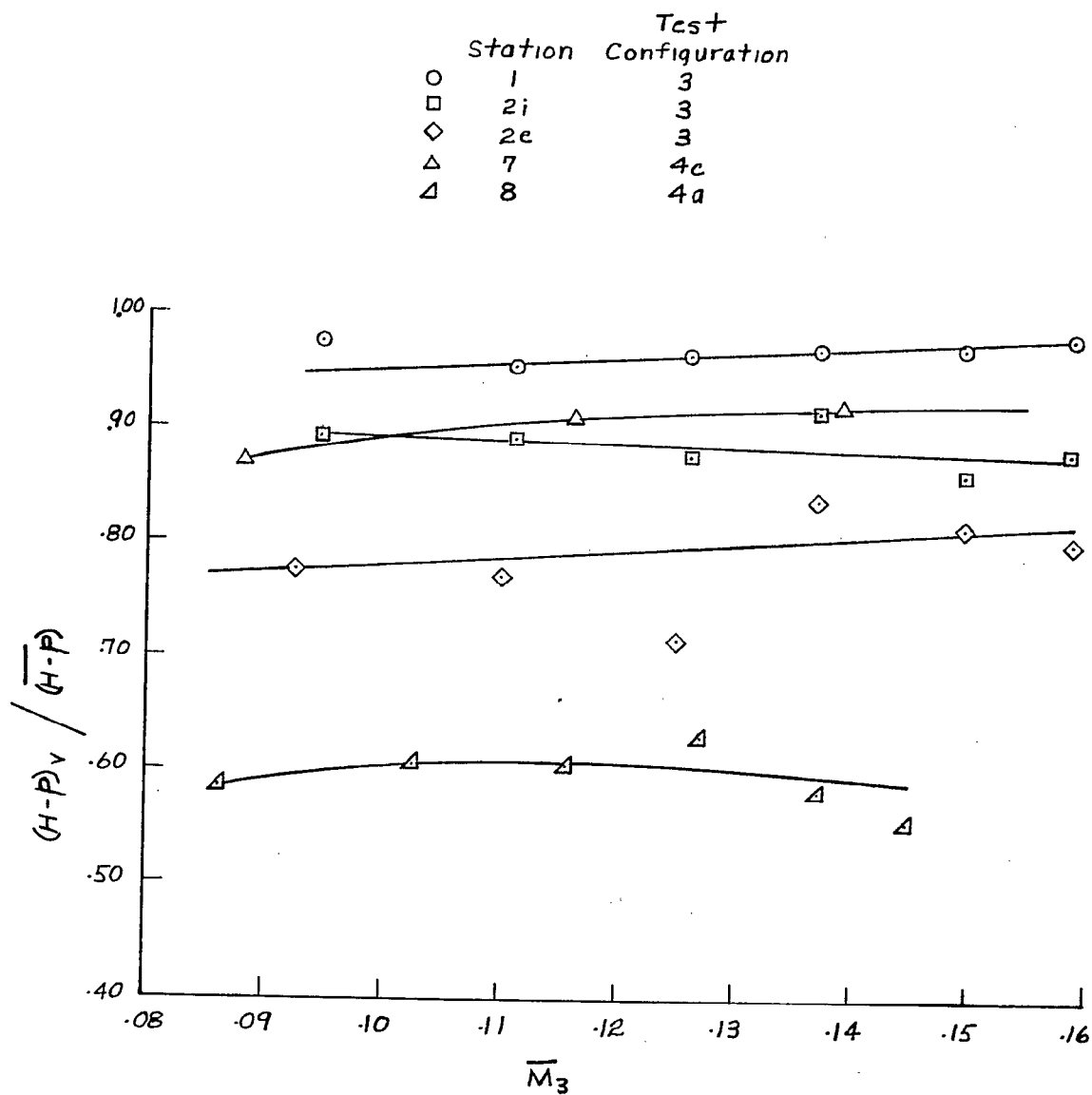
(c) Variation of ratio $(H - p)_V / \overline{(H - p)}$.

Figure 17.- Concluded.
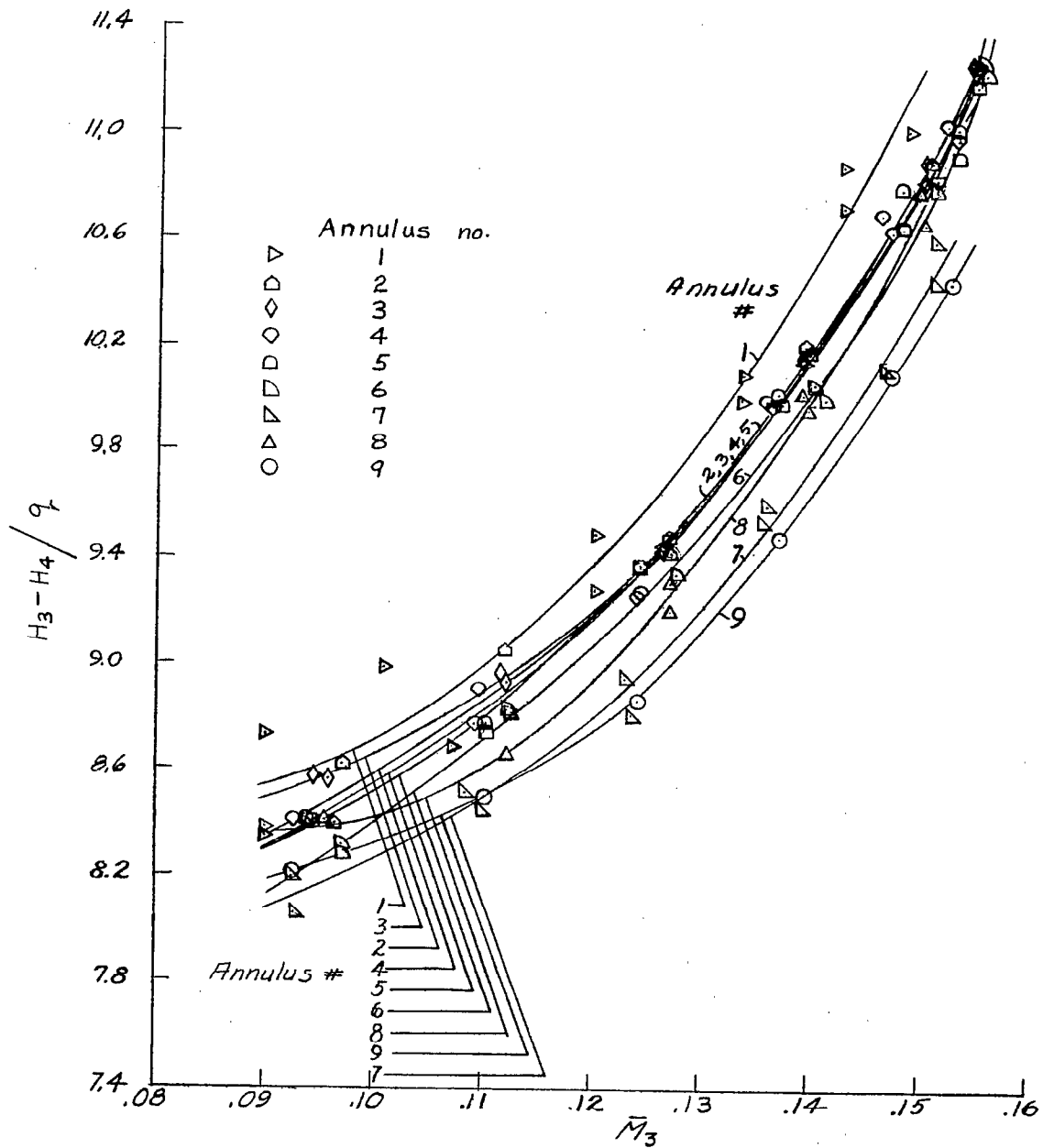
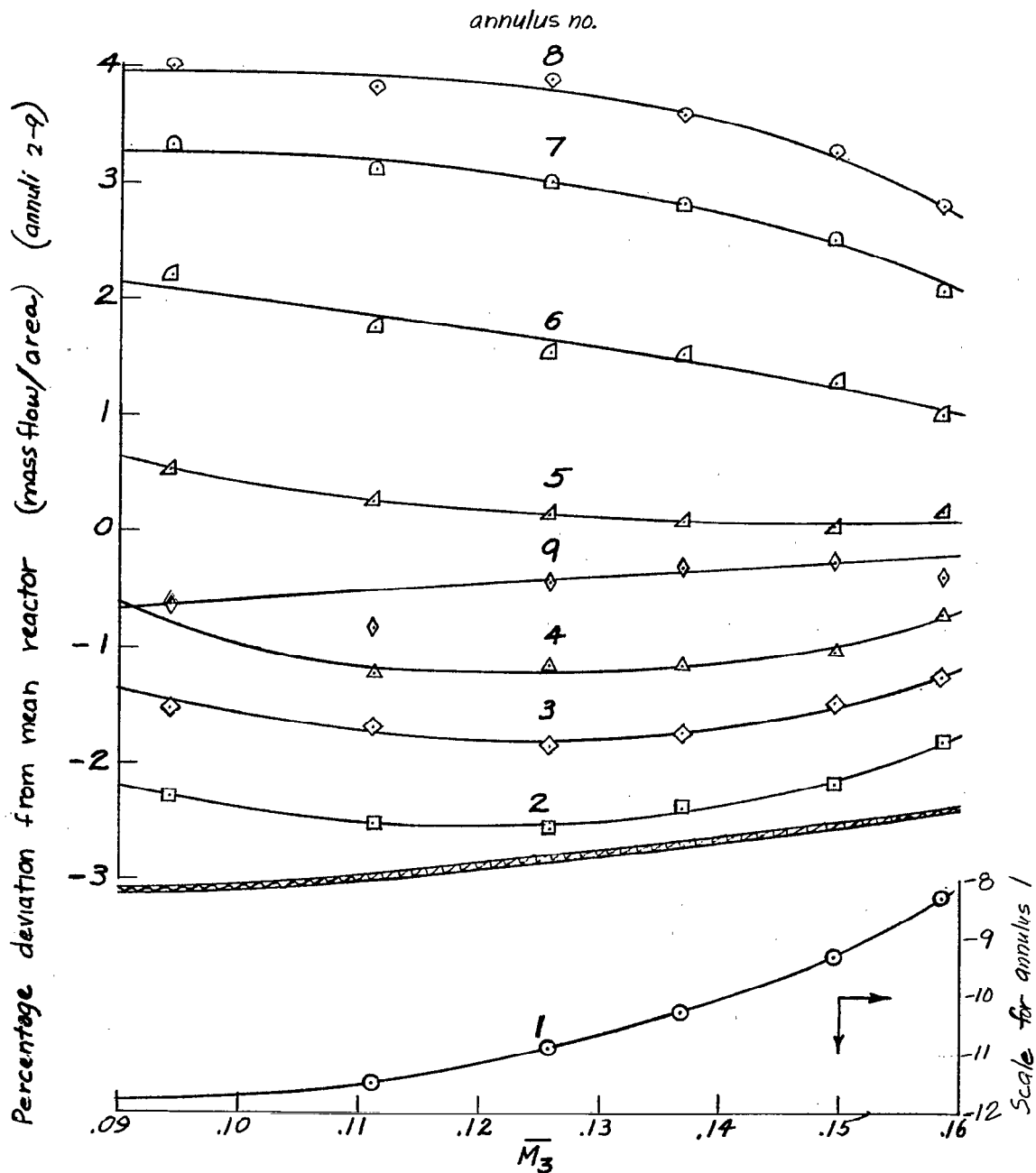Figure 18.- Variations of the loss coefficients for the simulated-reactor assembly with Mach number.
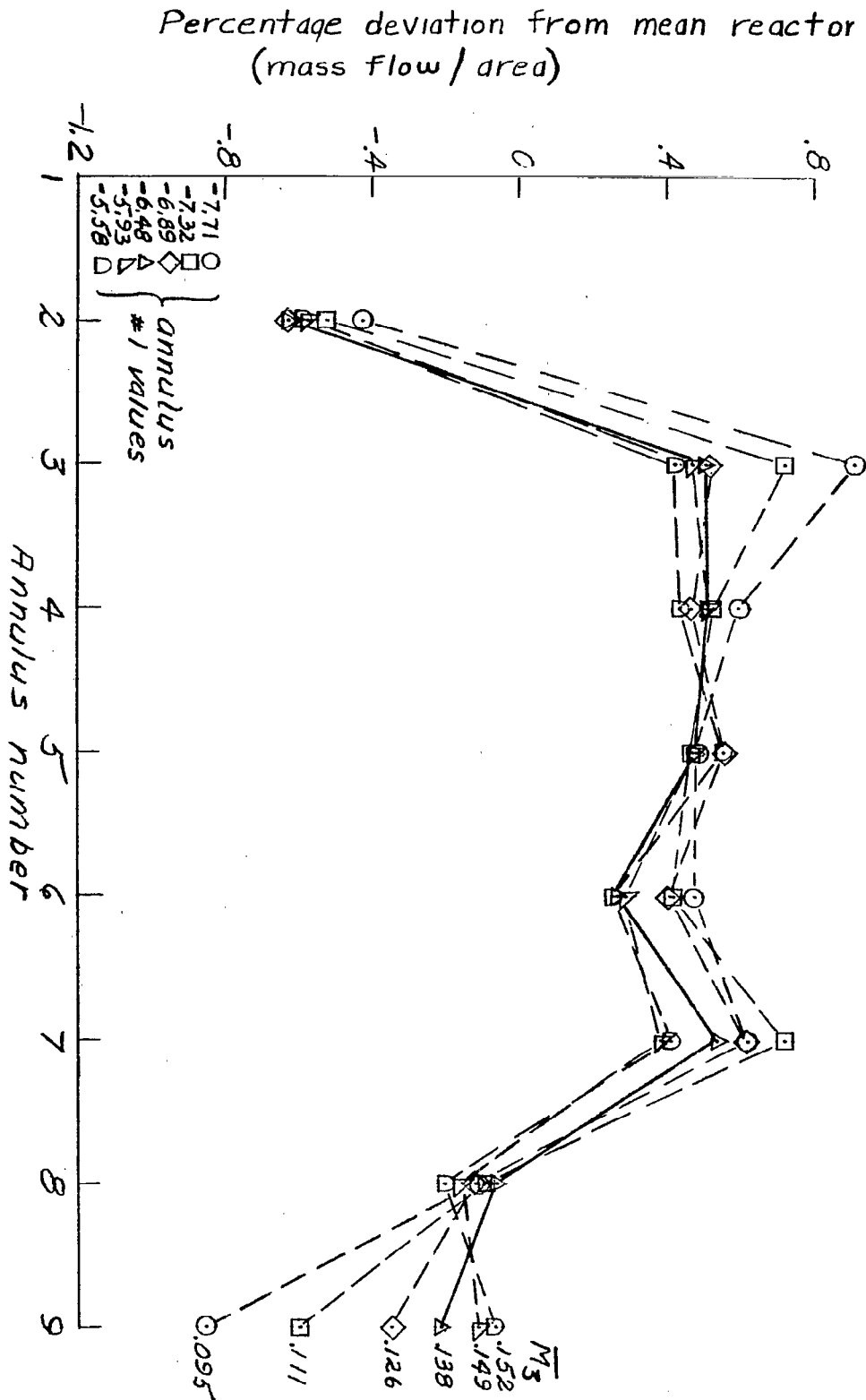
Figure 19.- Variation of the mass-flow deviations in the simulated reactor with Mach number. Test configuration 1.
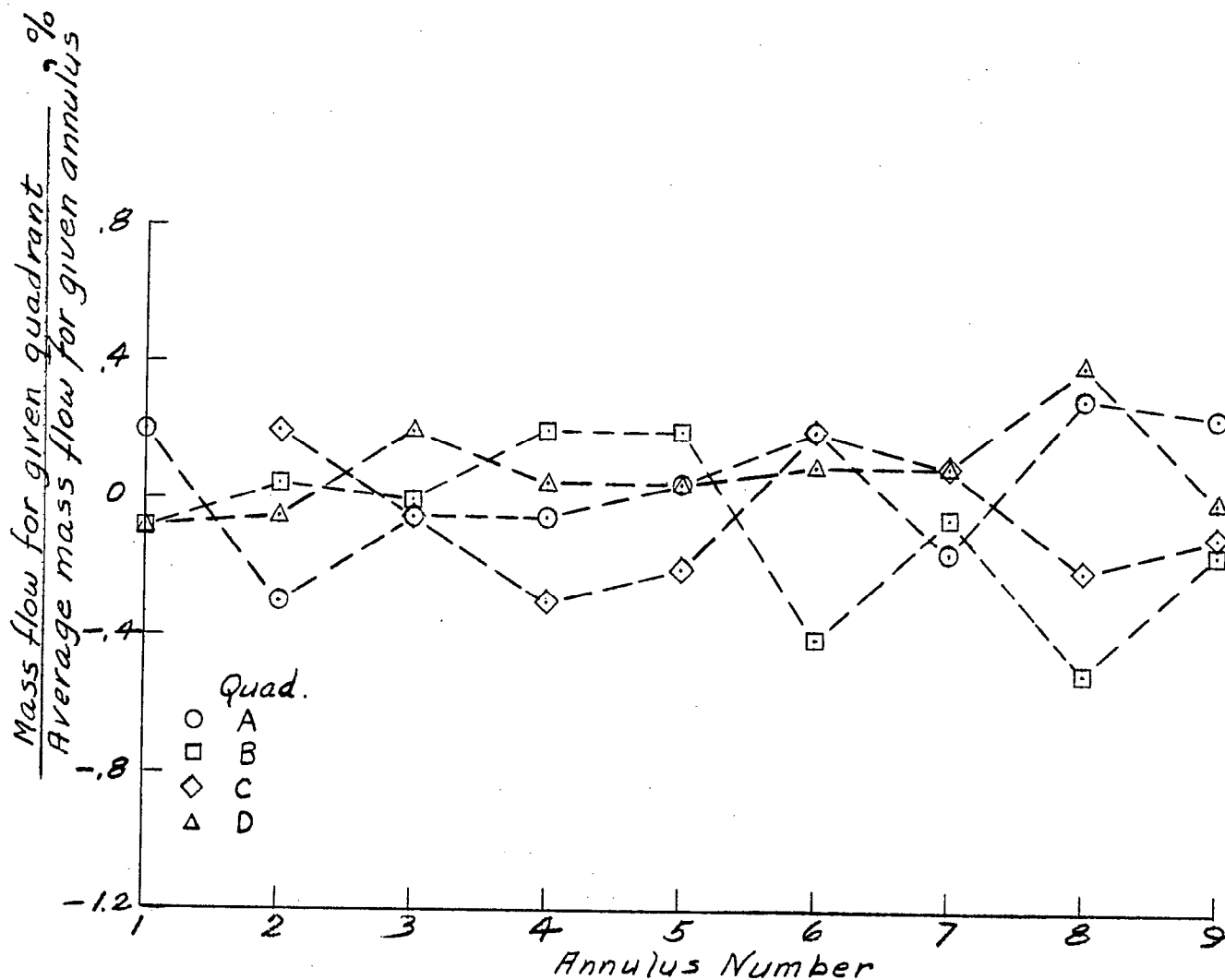
Figure 2Q.- Variation of the mass flow between quadrants in any given
annulus of the simulated reactor. Test configuration 1.
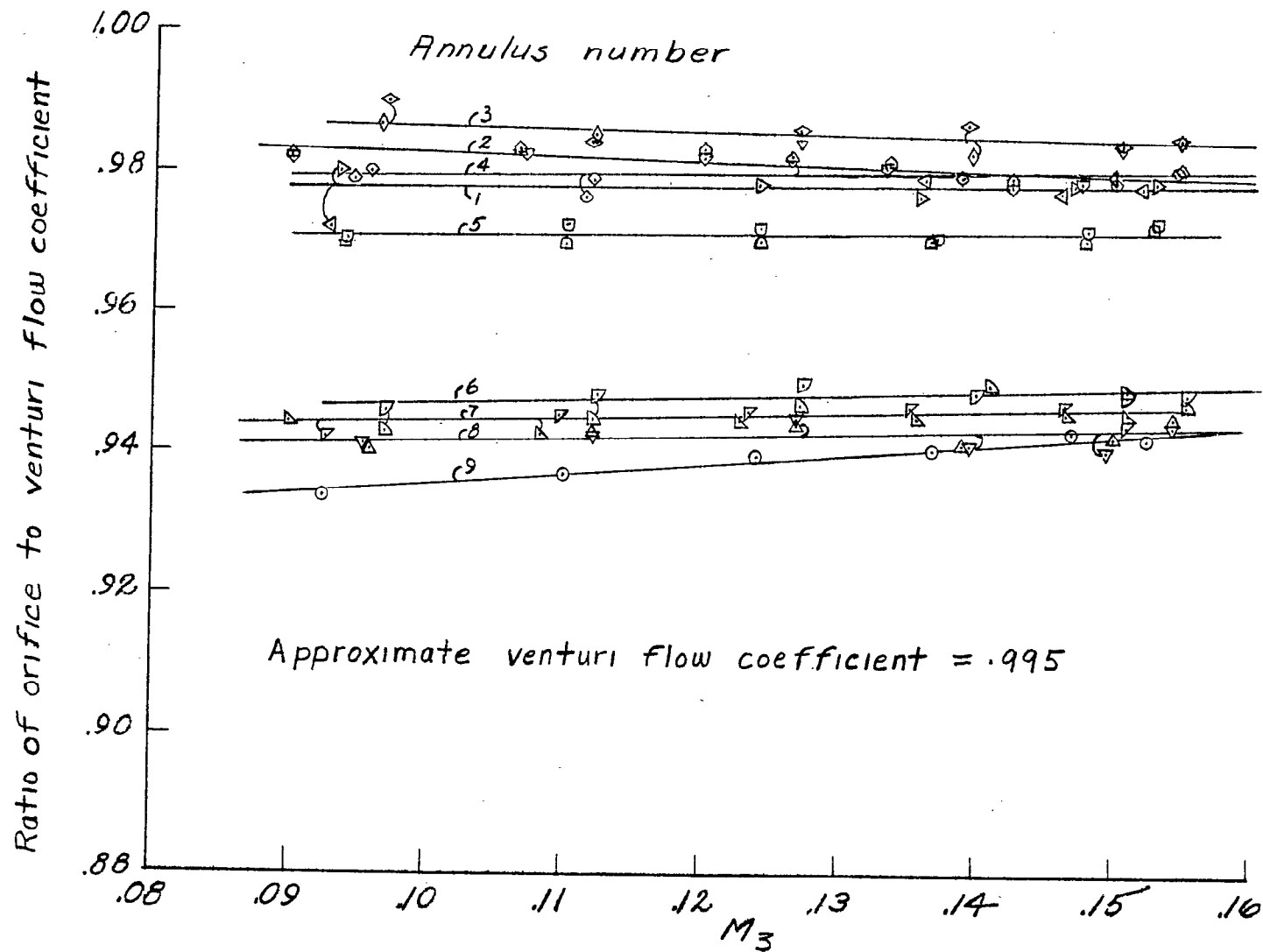
Figure 21.- Calibration curve for multiorifice plate. Test configuration 1.
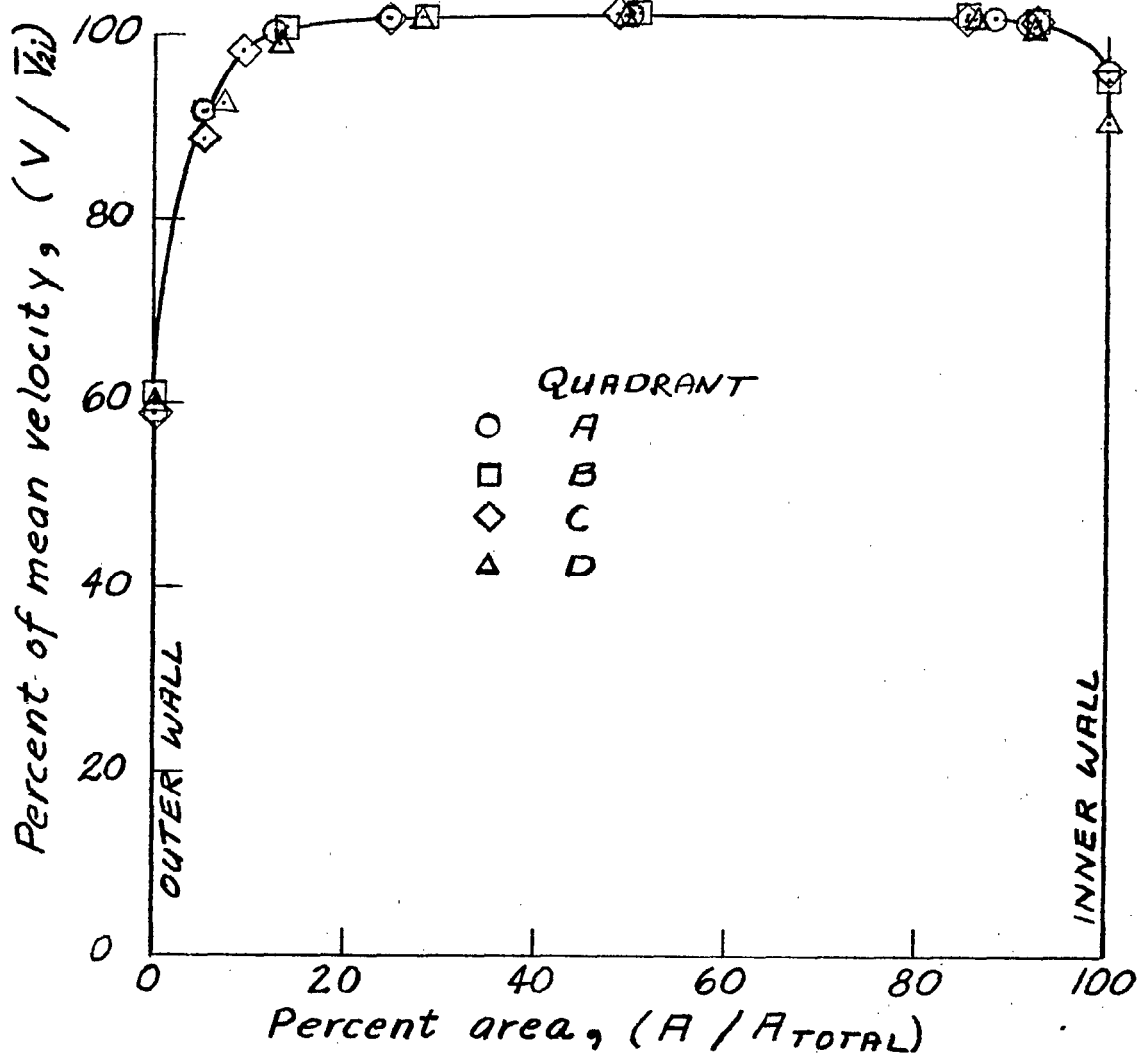
Figure 22.- Radial variation of velocity at station 2i. Test configuration 2.
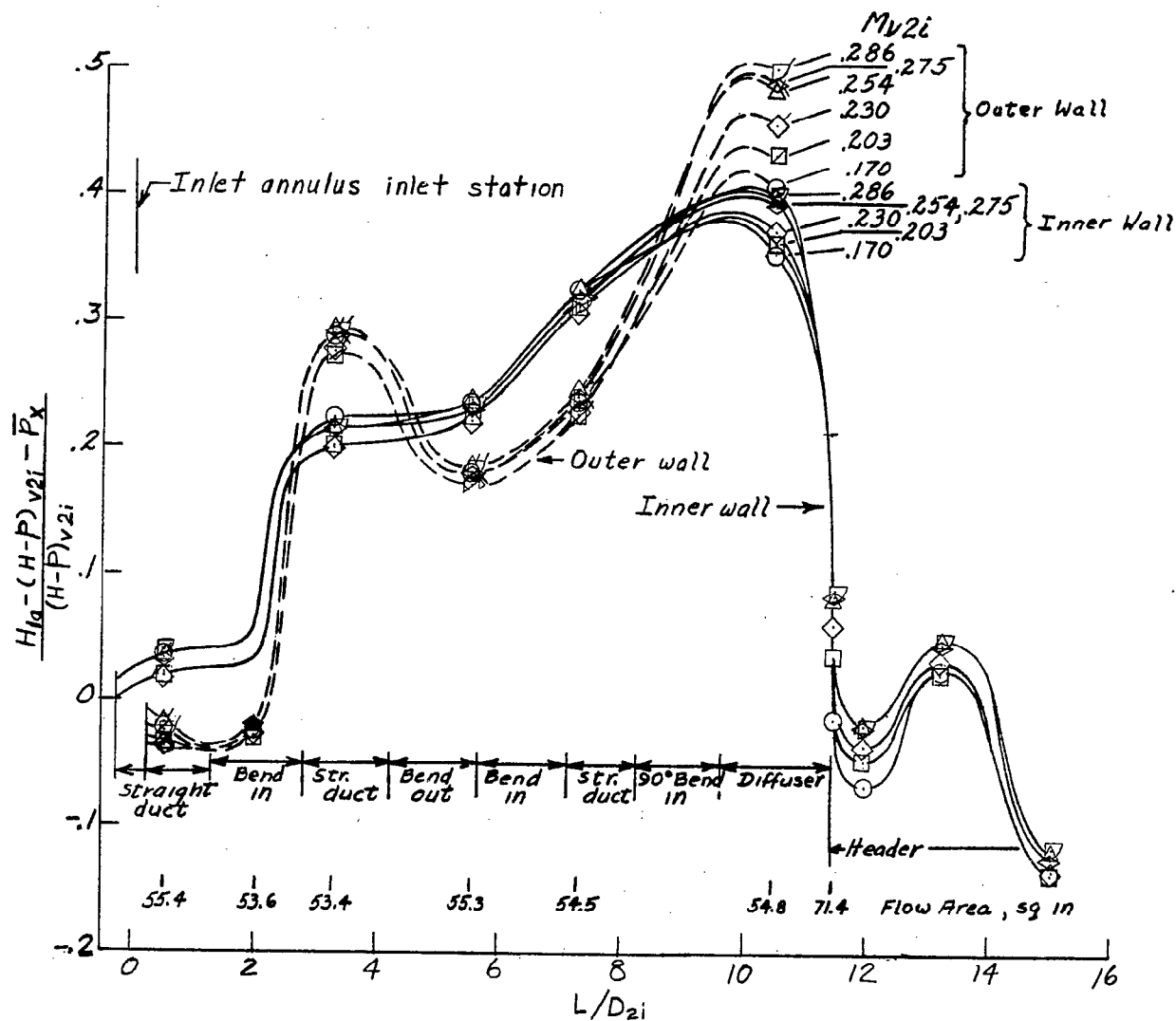
Figure 23.- Longitudinal-static-pressure distribution for inlet annulus. Test configuration 2.
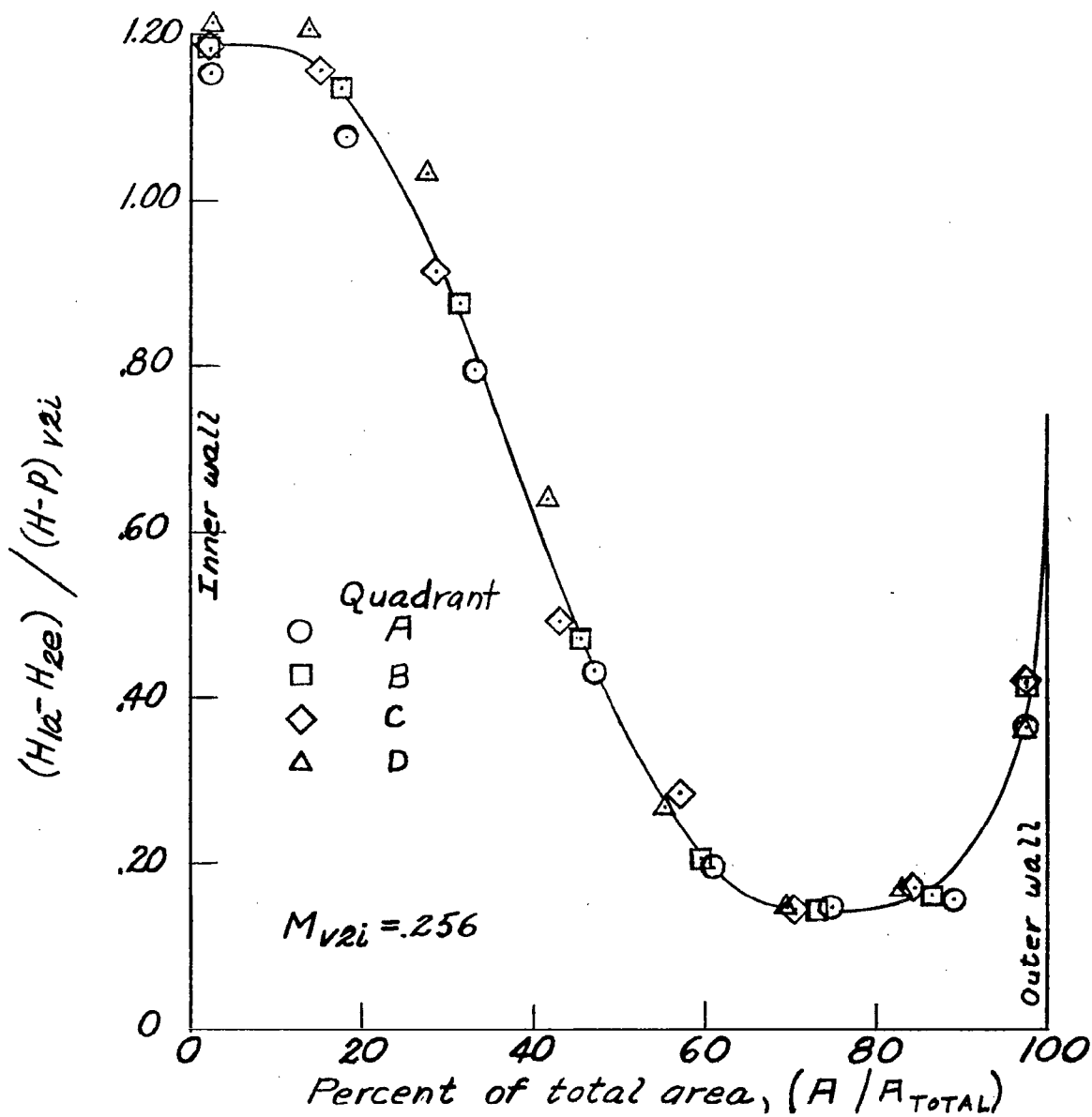
Figure 24.- Radial variation of total pressure at station 2e. Test configuration 2.
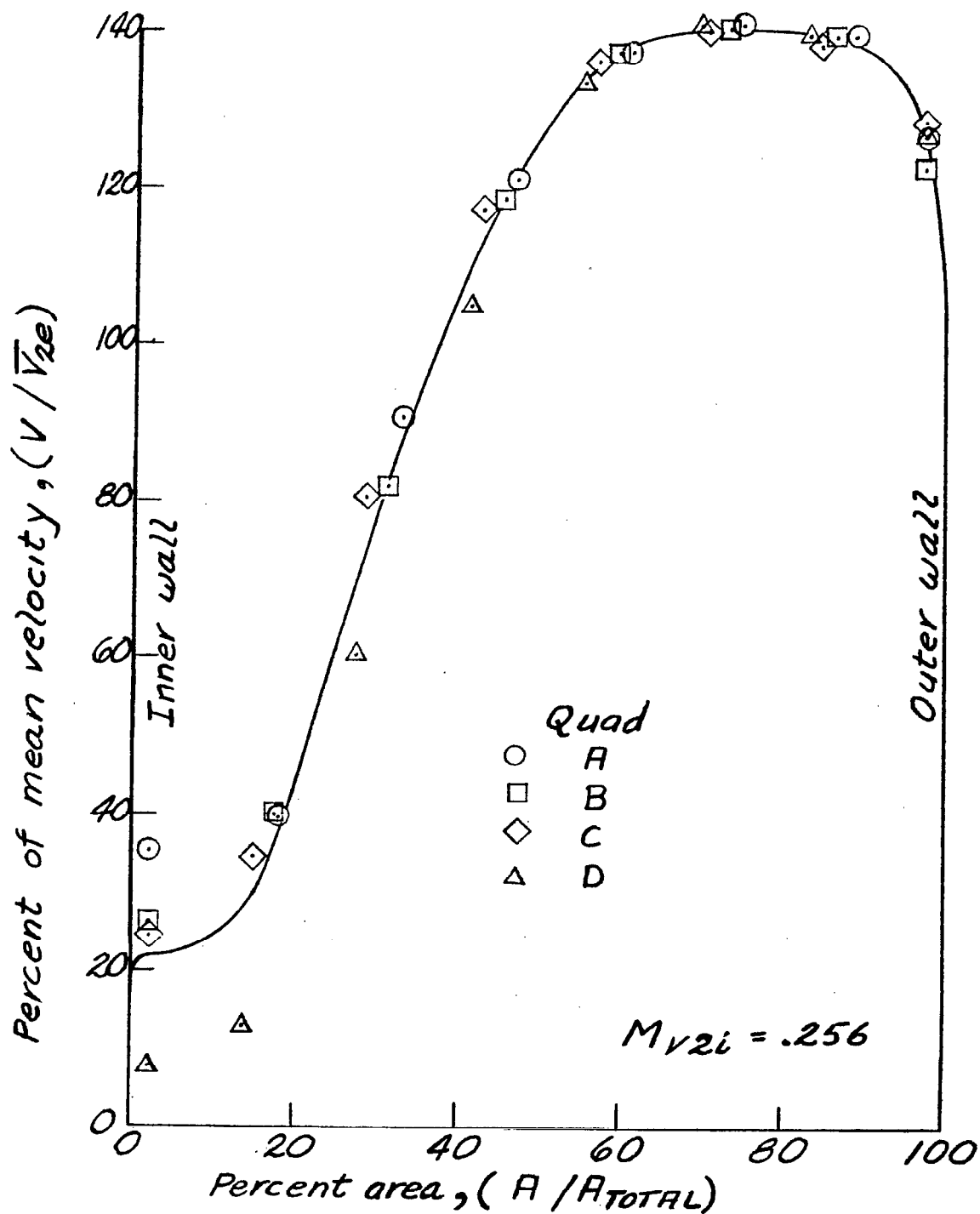
Figure 25.- Radial variation of velocity at station 2e. Test
configuration 2.
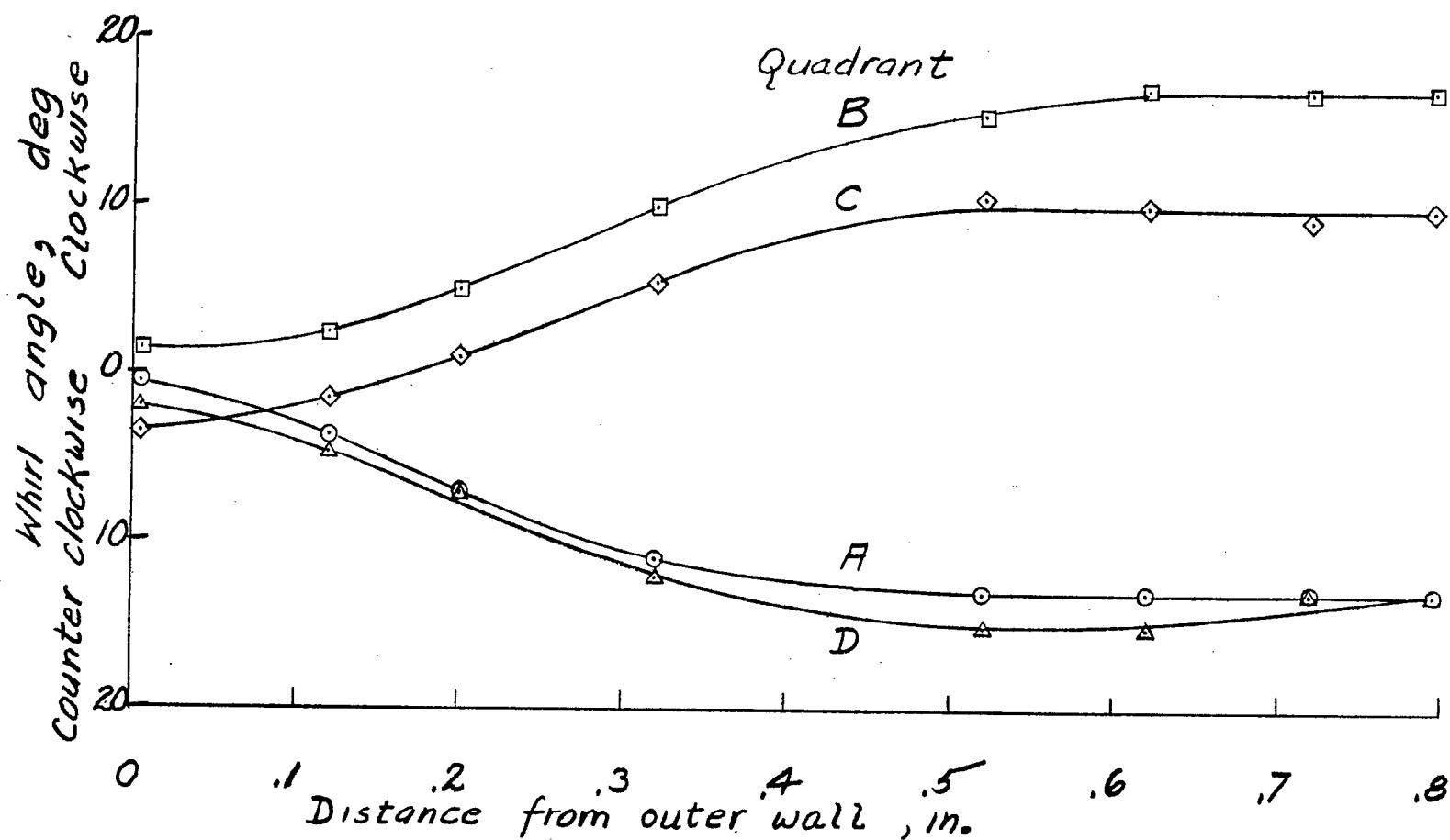
Figure 26.- Radial variation of whirl angle at station 2i as viewed from downstream.   Test configuration 3.
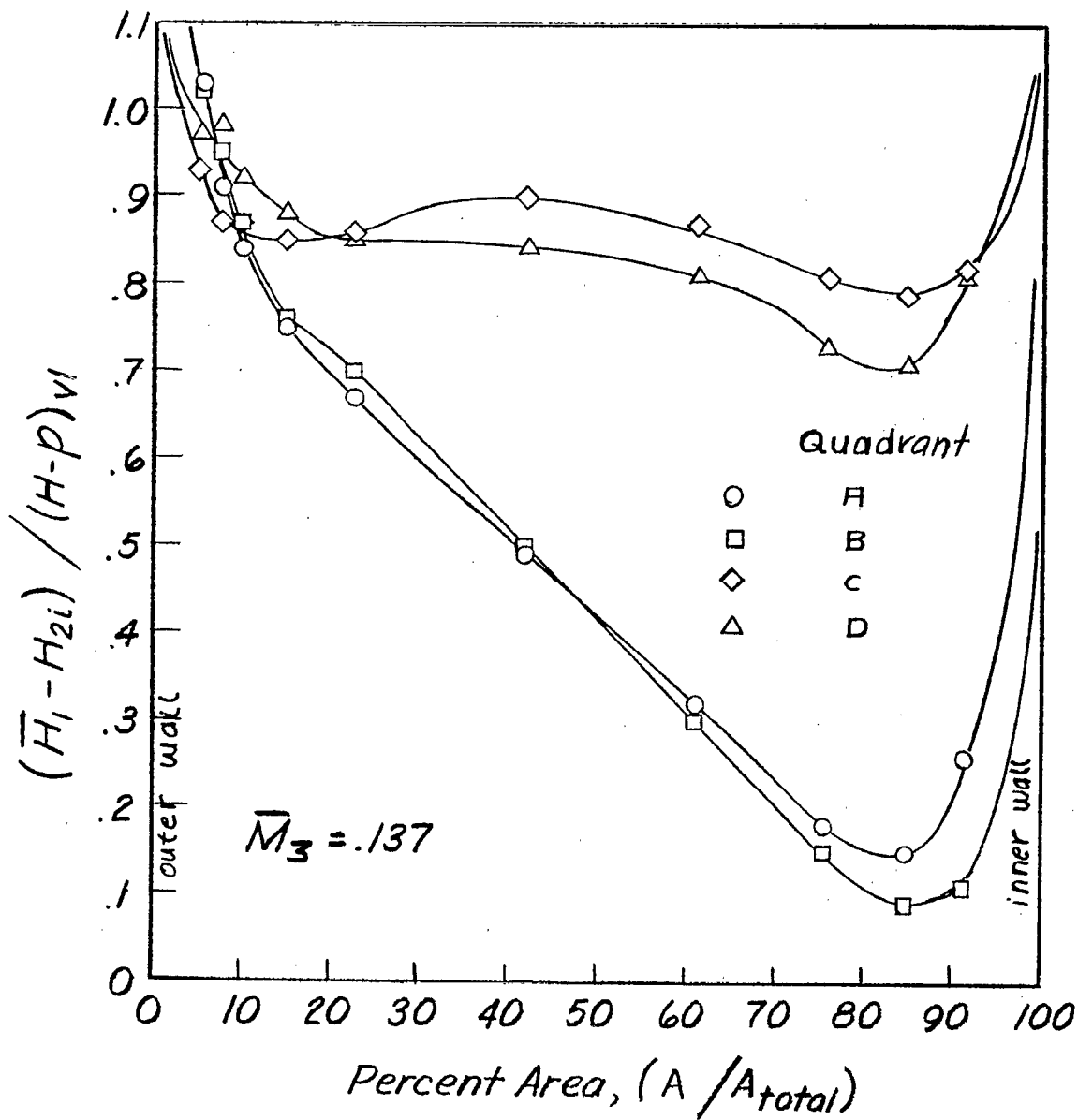
Figure 27.- Radial variation of total pressure at station 2i. Test configuration 3.
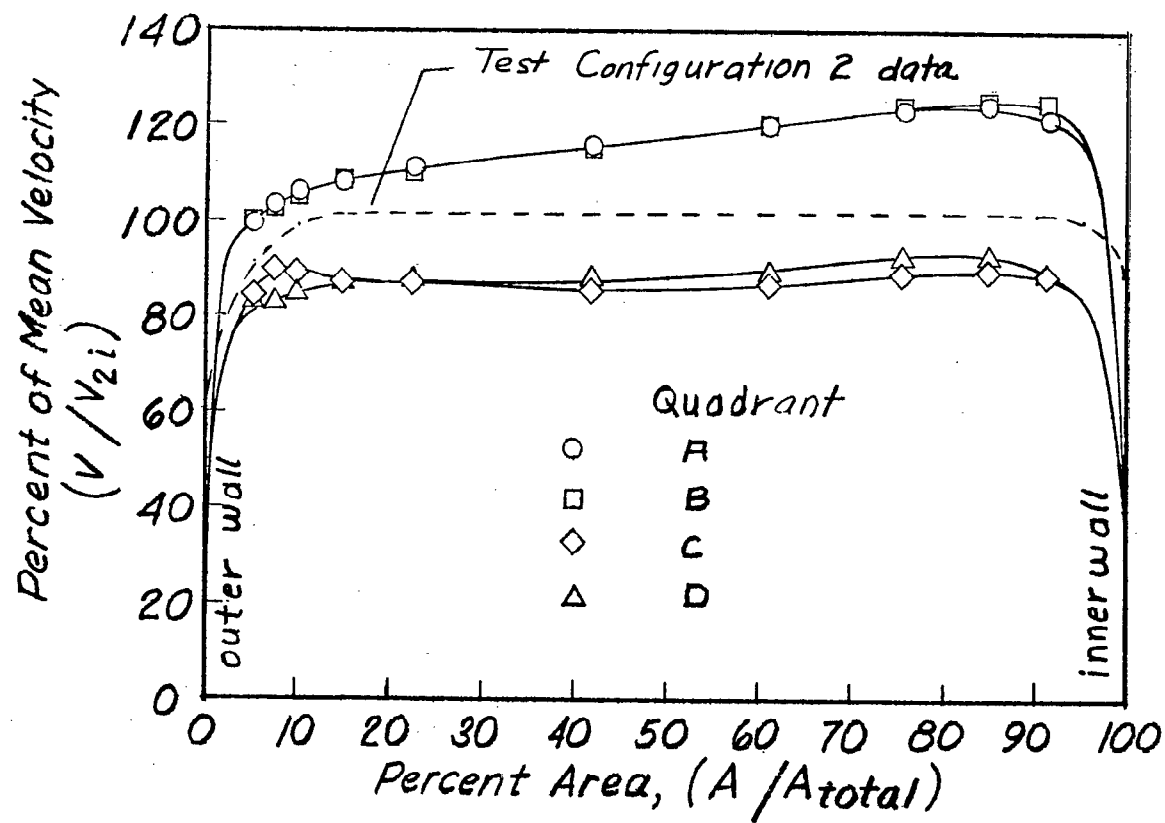
Figure 28.- Radial variation of velocity at station 2i.   Test configuration 3.
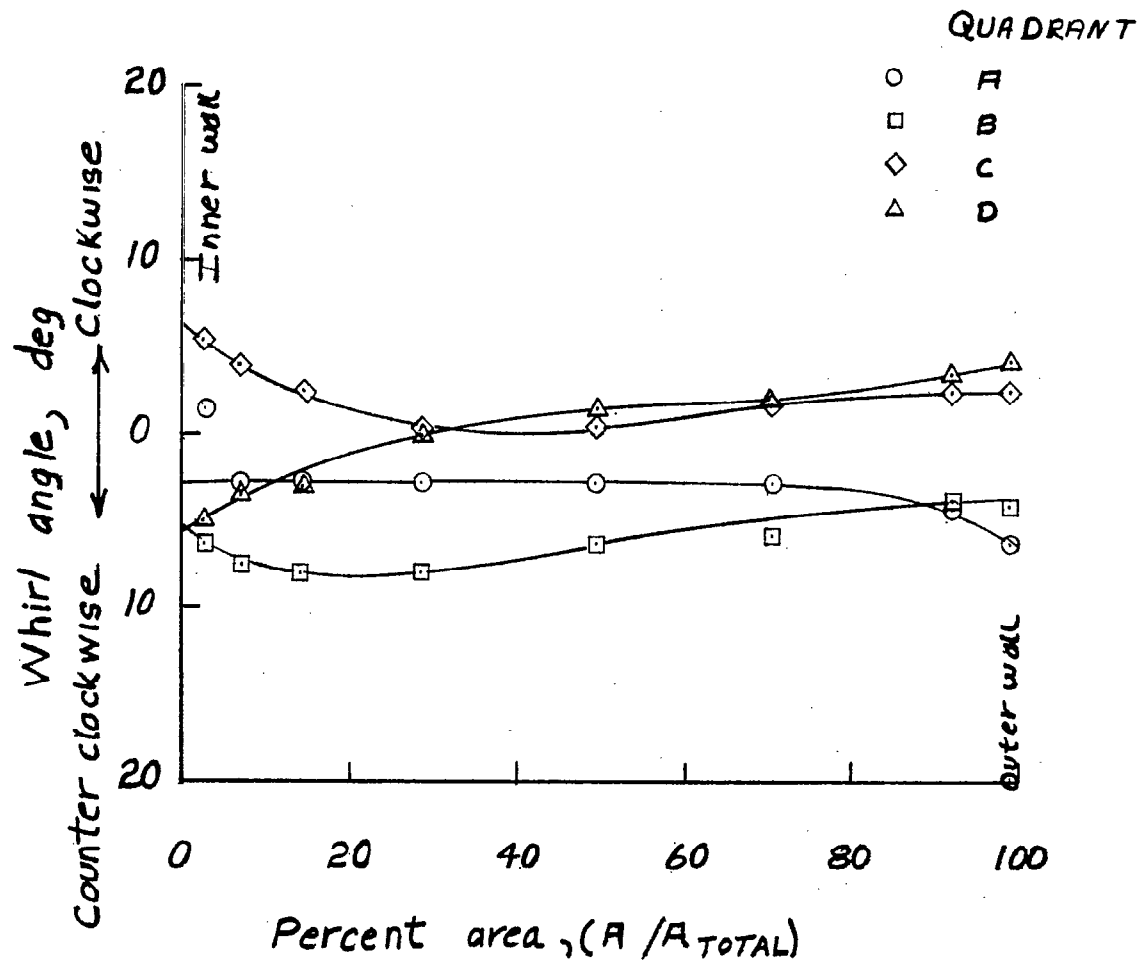
Figure 29.- Radial variation of whirl angle at station 2e as viewed from downstream.   Test configuration 3.
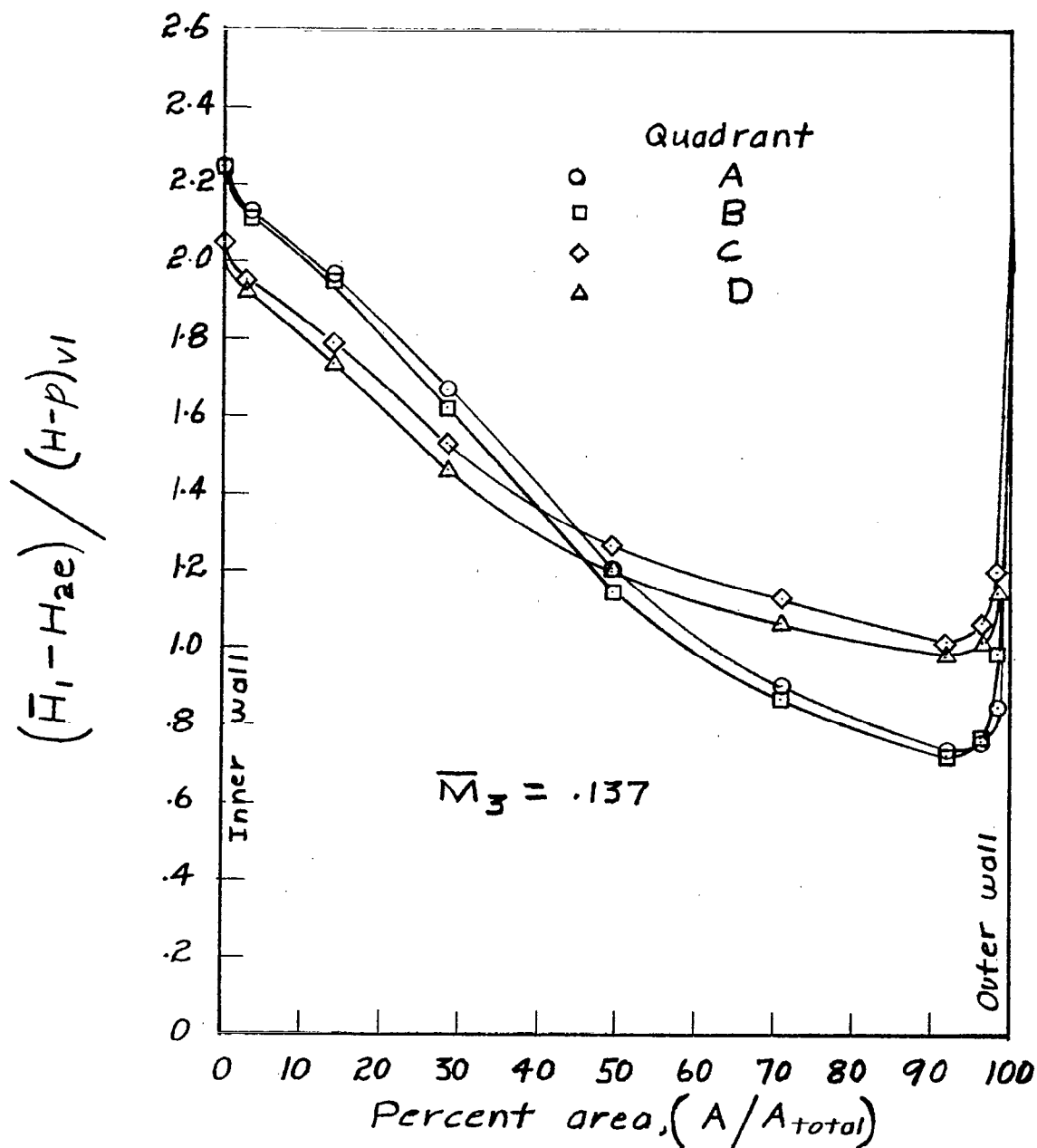
Figure 30.- Radial variation of total pressure at station 2e. Test
configuration 3.
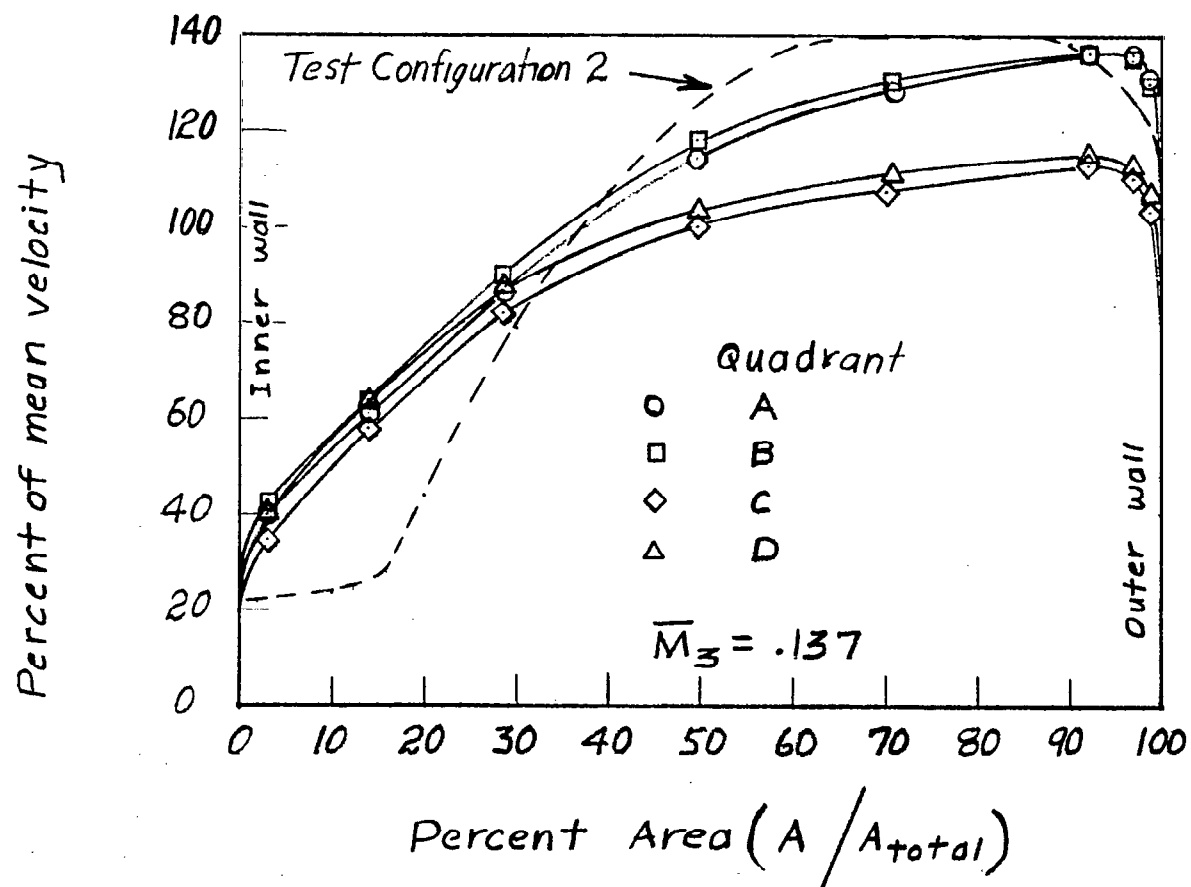
Figure 31.- Radial variation of velocity at station 2e. Test configuration 3.
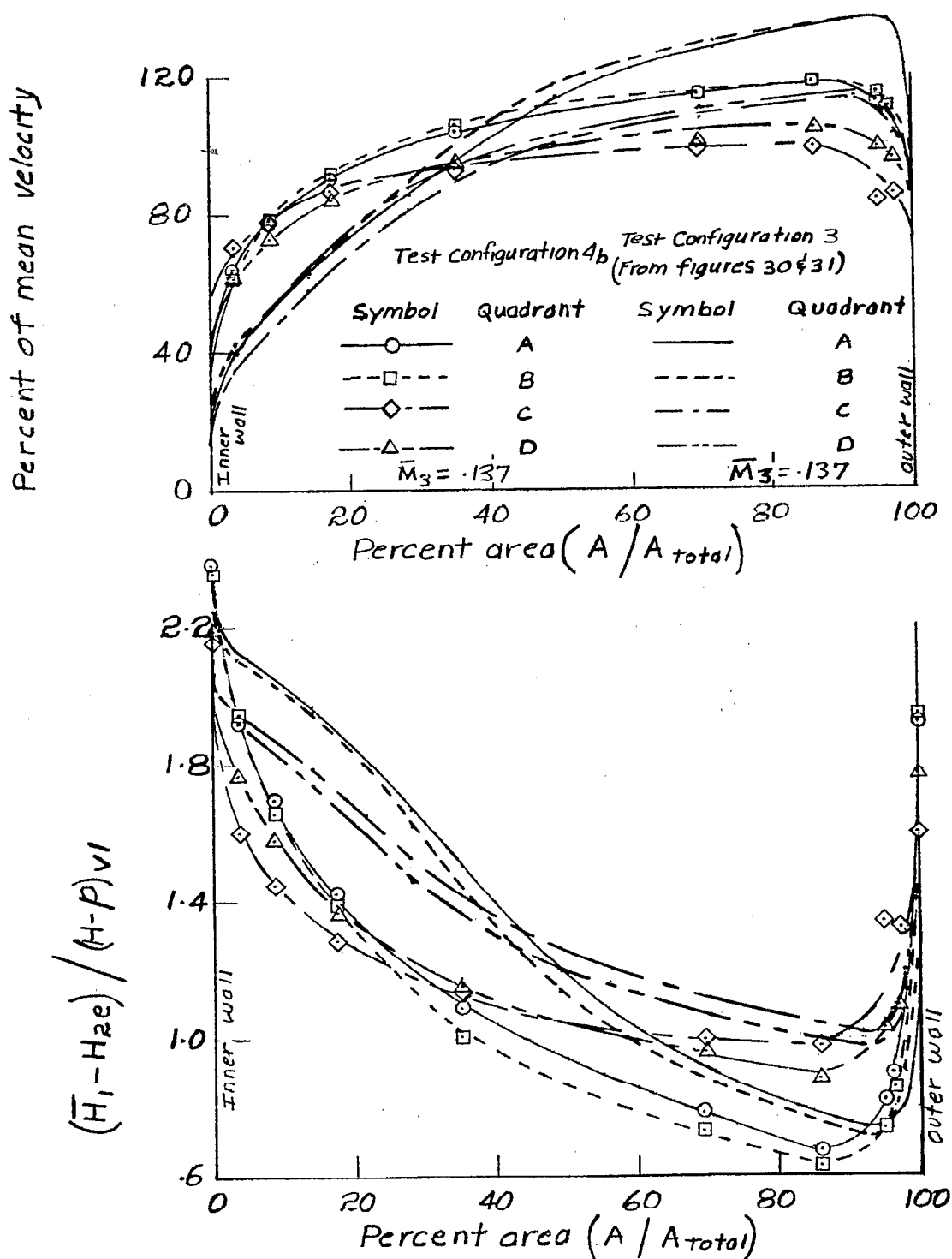
Figure 32.- Radial variation of total pressure and velocity at station 2e.
Test configuration 4b (header plate 2, guide vane configuration 1).
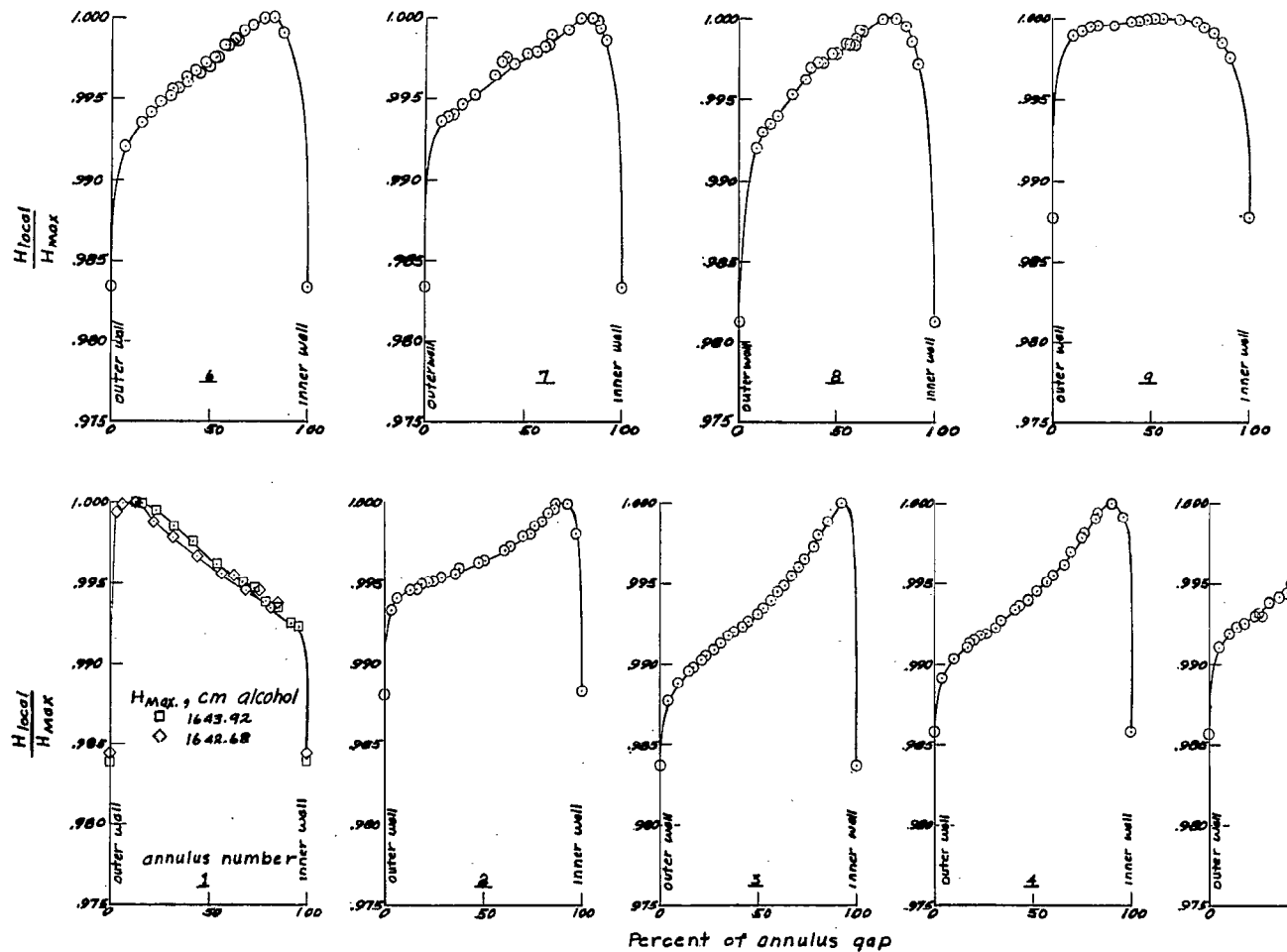
Figure 33.- Radial variation of total pressure in quadrant A, $2\frac{1}{2}$ inches downstream from the entrance to each annulus. Test configuration 4c $\overline{M}_3 \approx 0.135$.
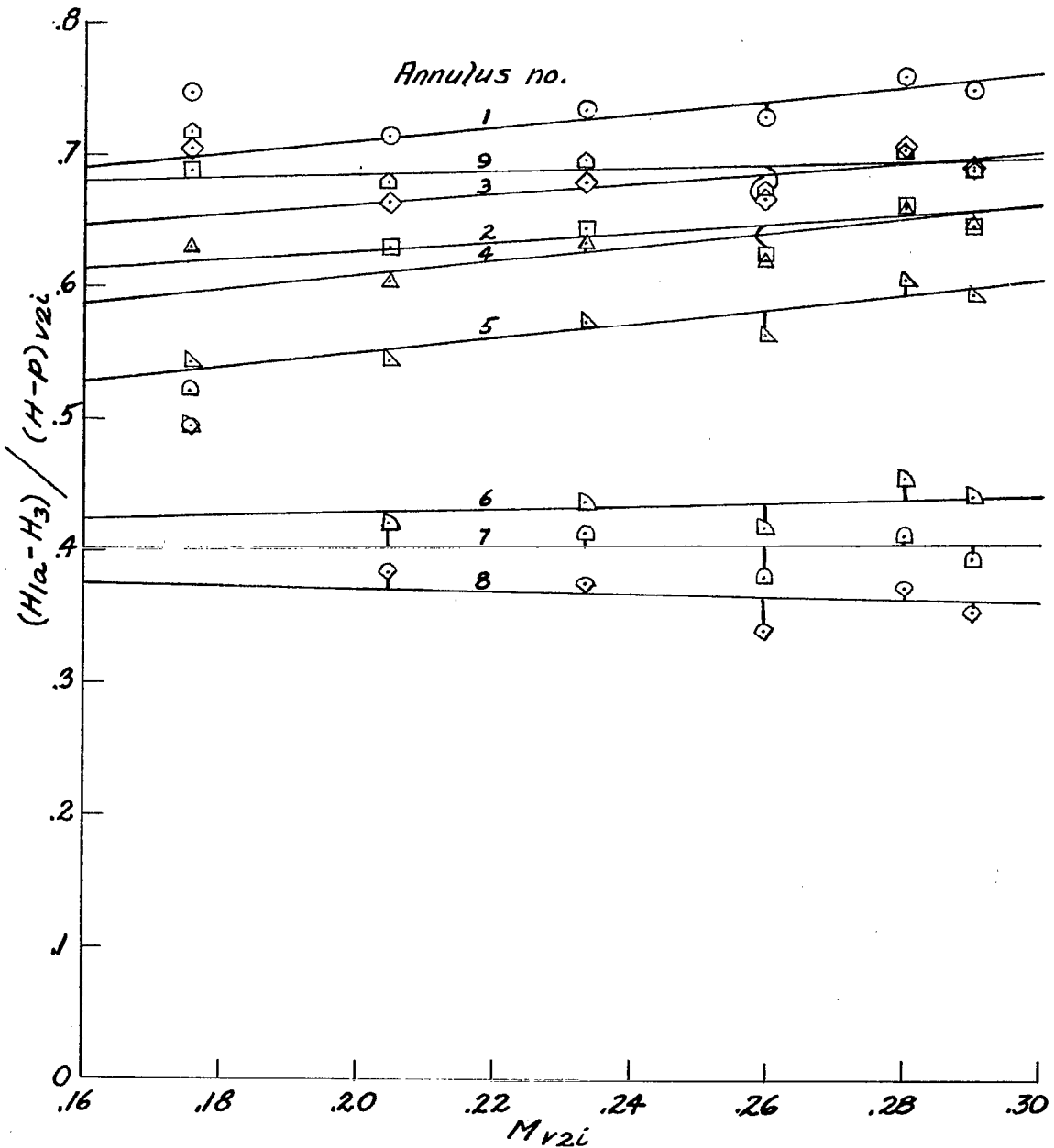
Figure 34.- Variation of the total-pressure-loss coefficient from the reference station to station 3 with Mach number. Test configuration 2.
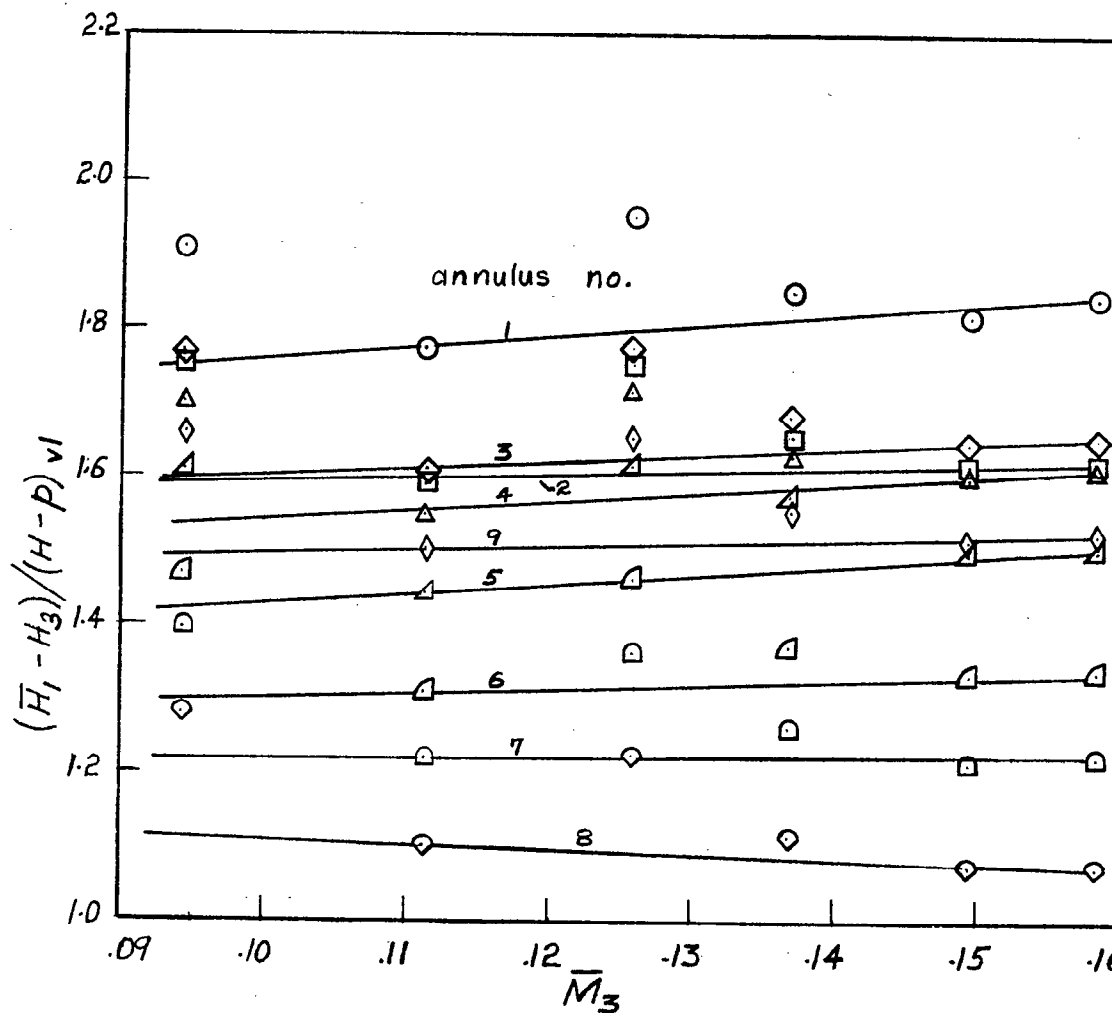
Figure 35.- Variation of the loss coefficient from station 1 to station
with Mach number. Test configuration 3. (Measurements made simulta-
neously with surveys at station 2i.)
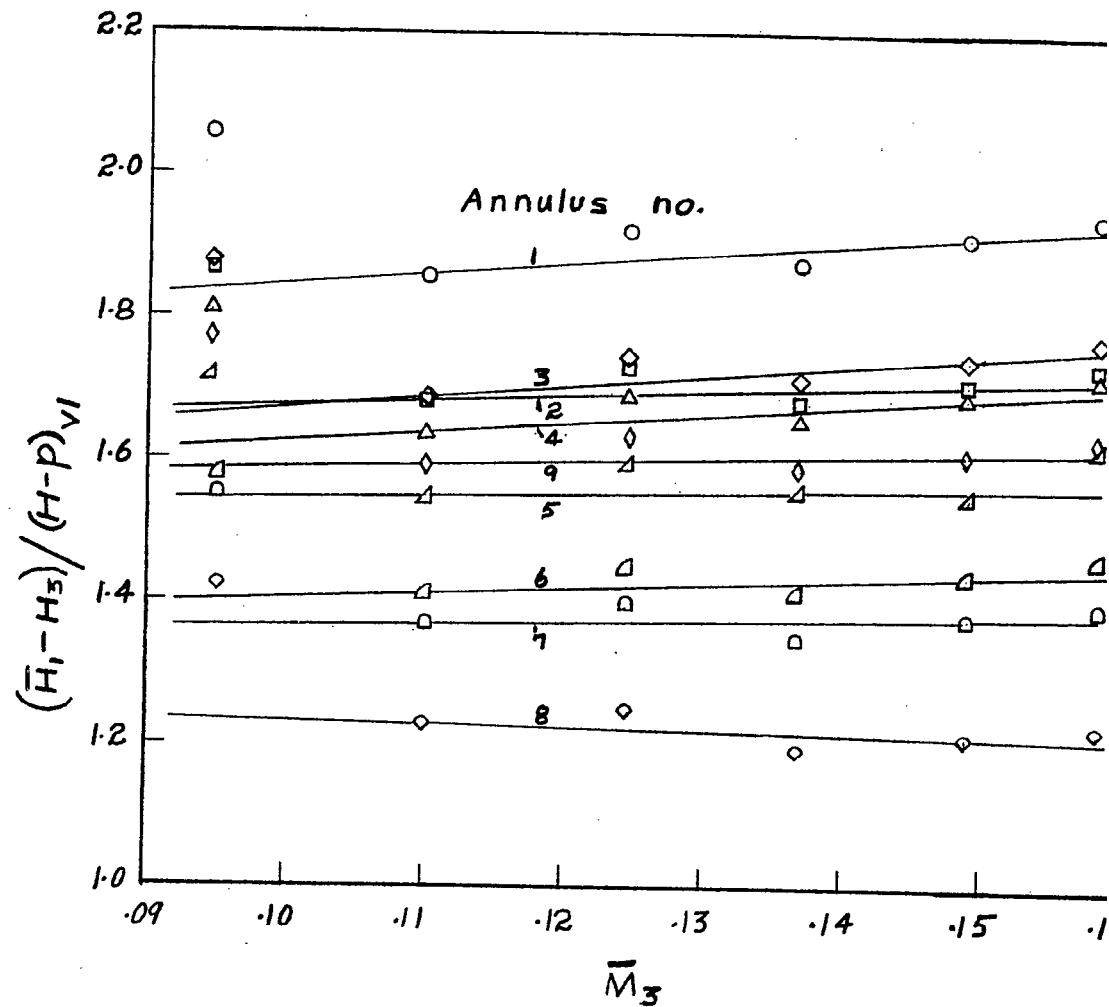
Figure 36.- Variation of the loss coefficient from station 1 to station with Mach number. Test configuration 3. (Measurements made simultaneously with surveys at station 2e.)
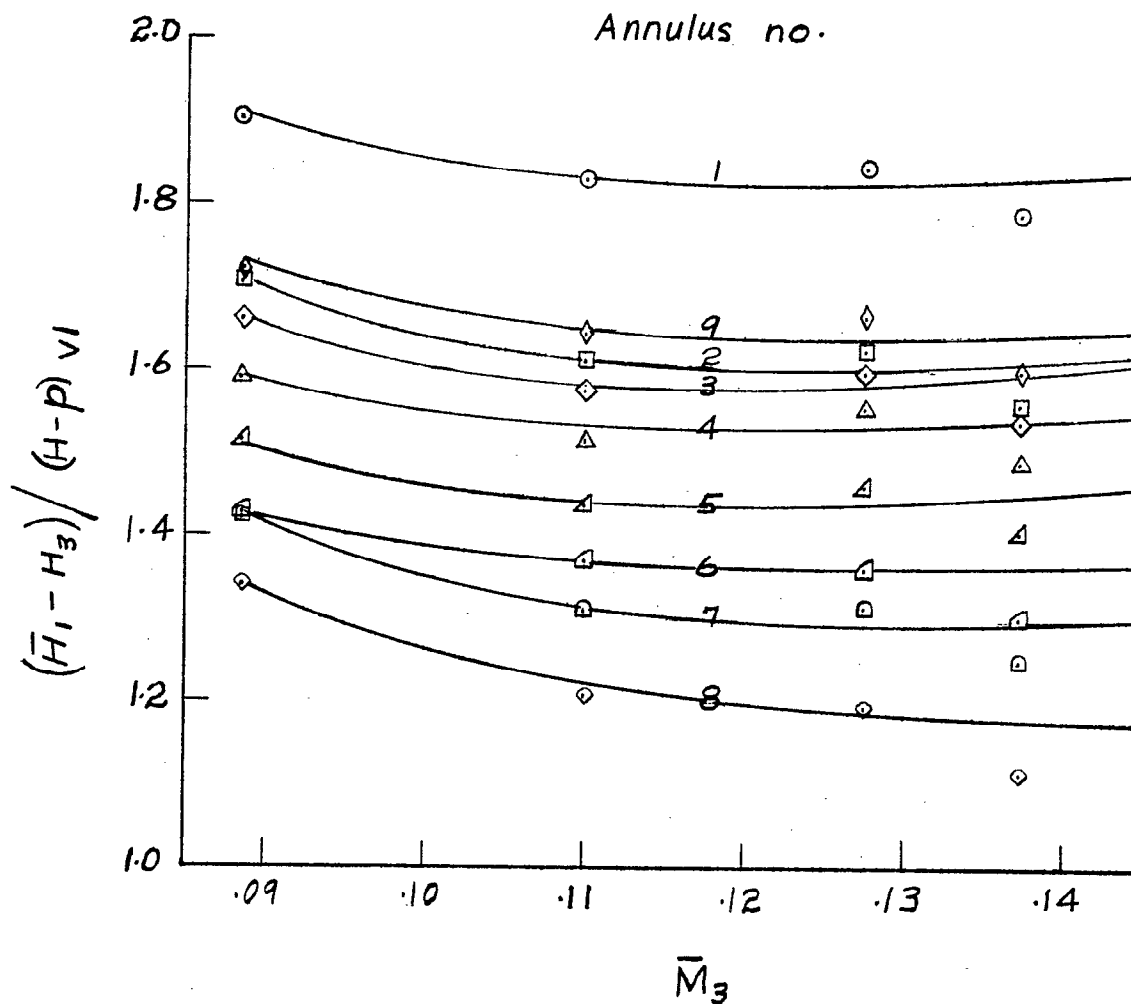
Figure 37.- Variation of the loss coefficient from station 1 to static
with Mach number. Test configuration 4b (header plate 2, guide var
configuration 1).
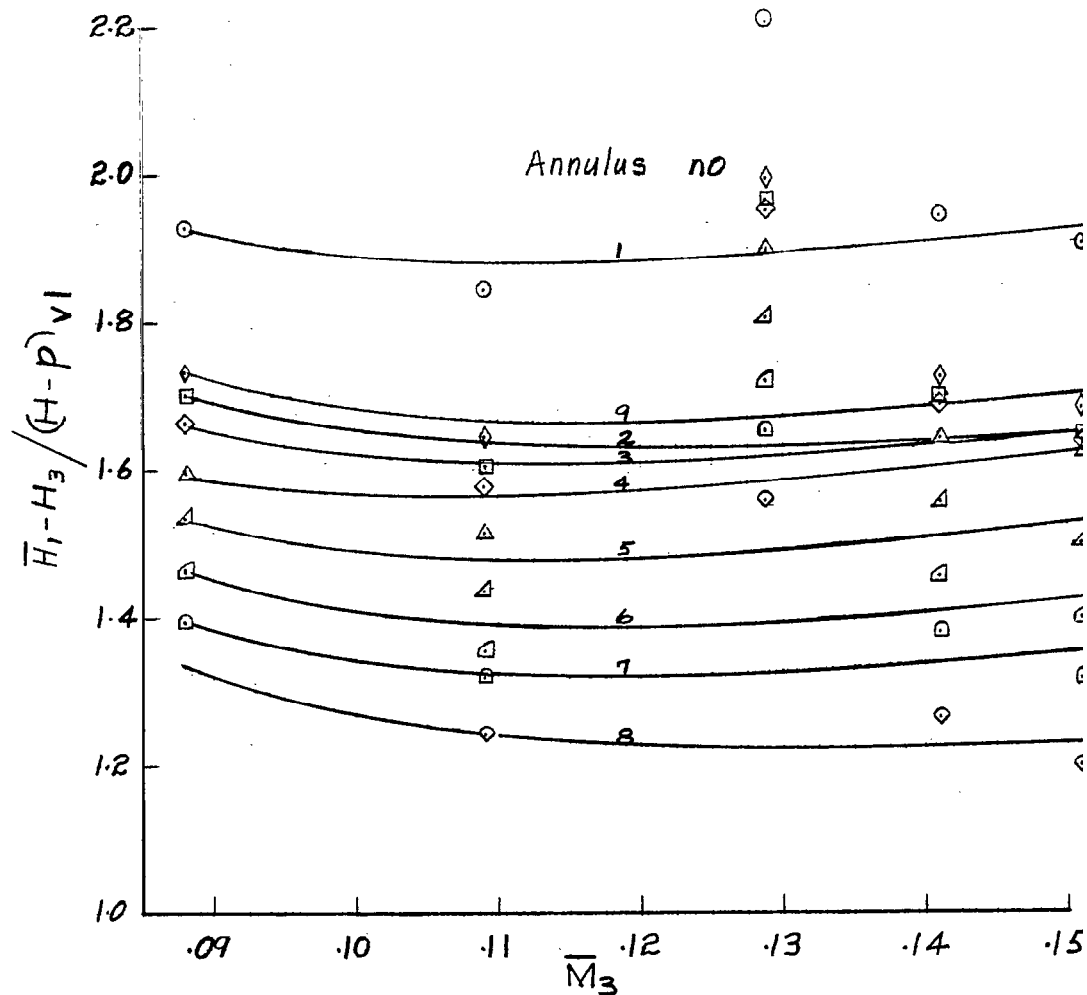
Figure 38.- Variation of the loss coefficient from station 1 to station
   with Mach number. Test configuration 4c (header plate 2, guide vane
   configuration 2, rear strut 2).
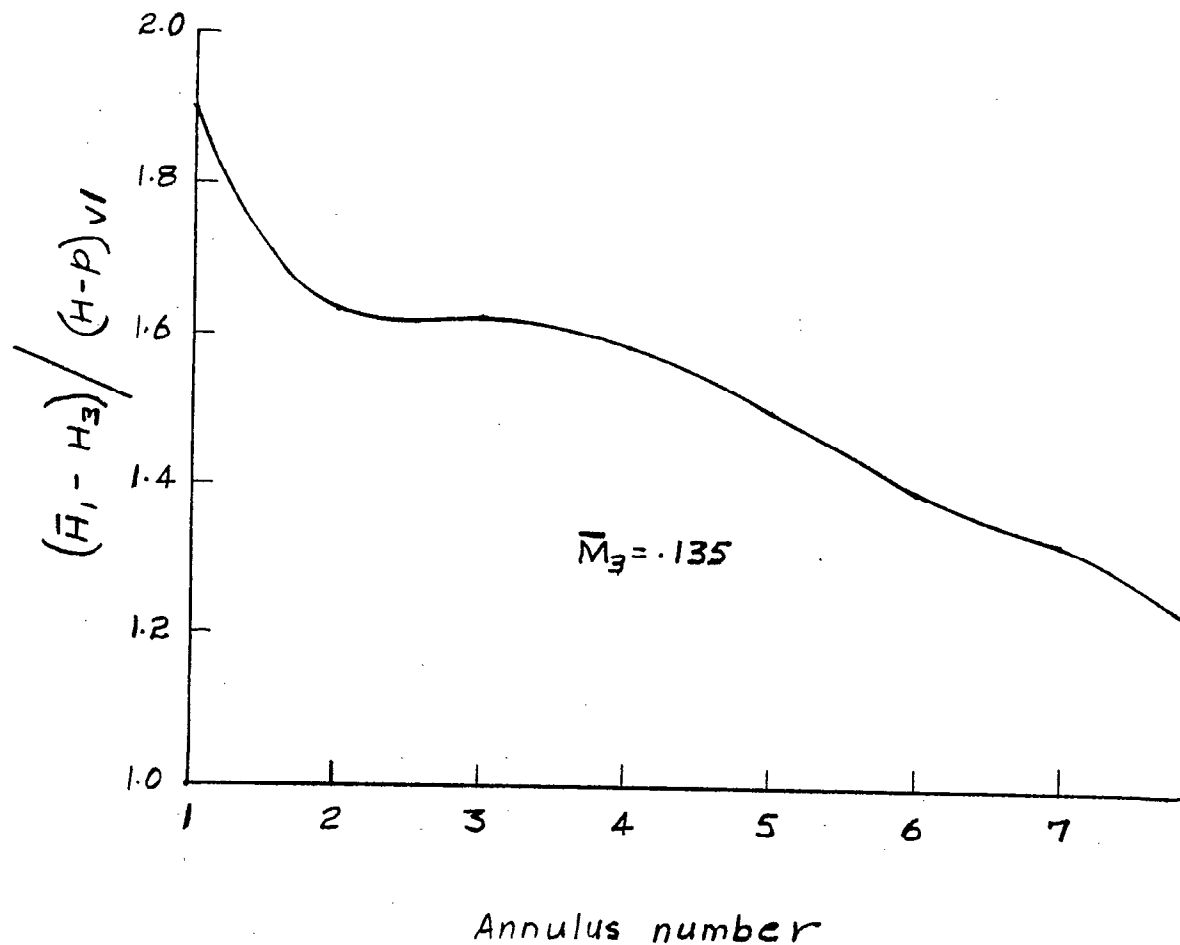
Figure 39.- Cross plot showing variation of the total pressure between annuli of the simulated reactor. Test configuration 4c (header plate guide vane configuration 2, rear strut 2); $\overline{M}_3 = 0.135$.
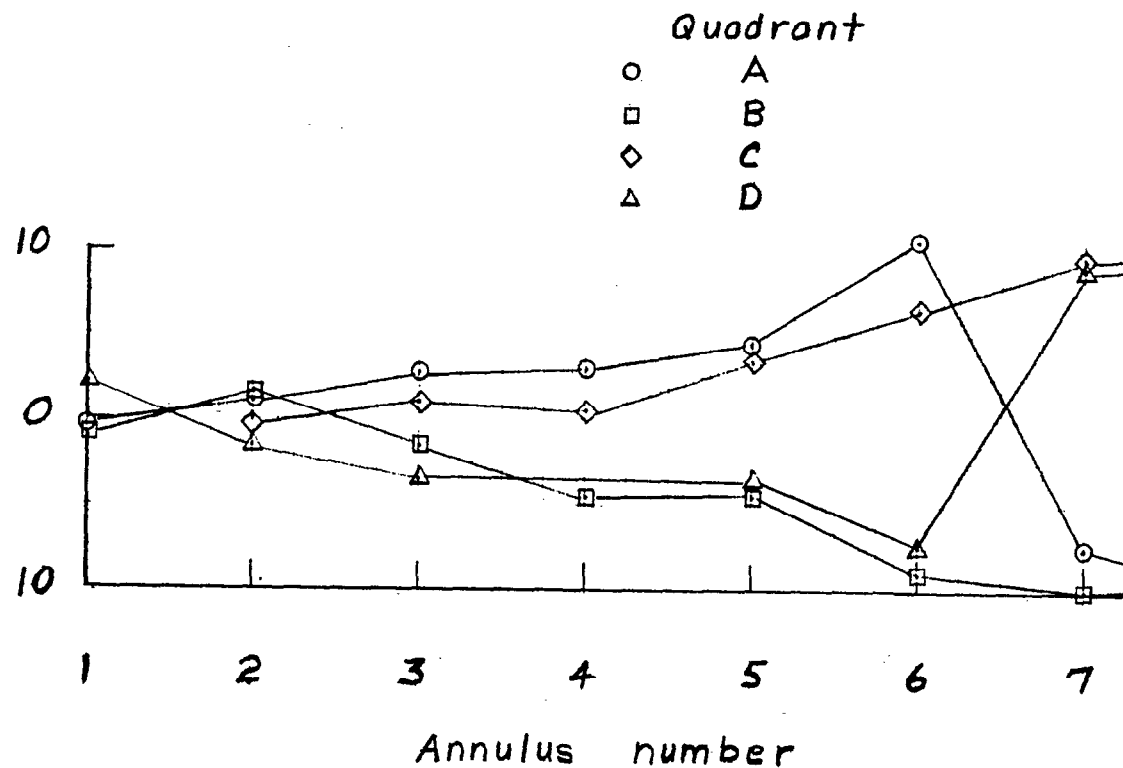
Figure 40.- Variation of the total pressure between quadrants in any annulus of the simulated reactor. Test configuration 4c (header guide vane configuration 3, rear strut 2); $\overline{M}_3 = 0.135$.
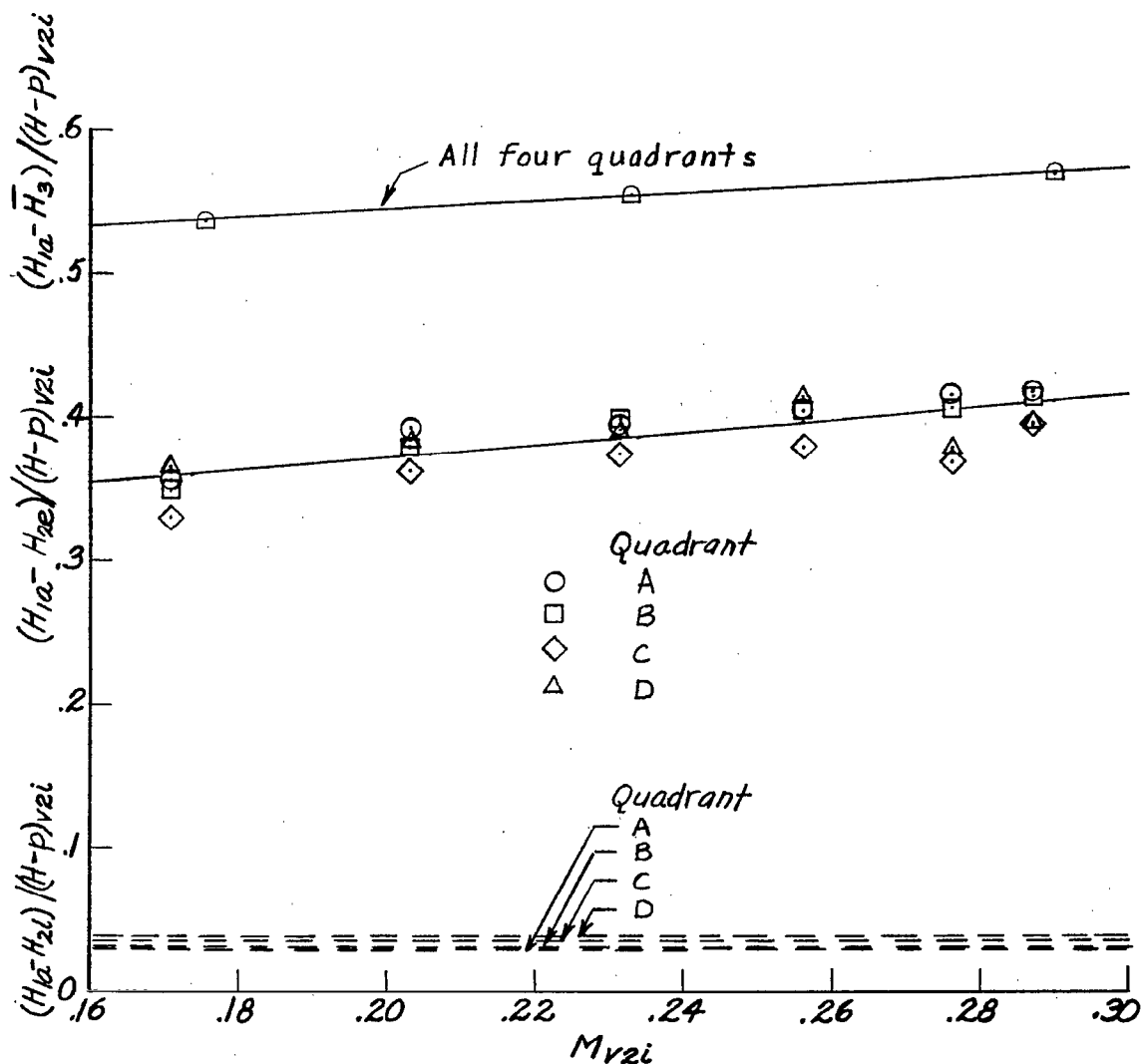
Figure 41.- Variation of the mean loss coefficients from the reference station to stations 2i, 2e, and 3 with Mach number. Test configuration 2.
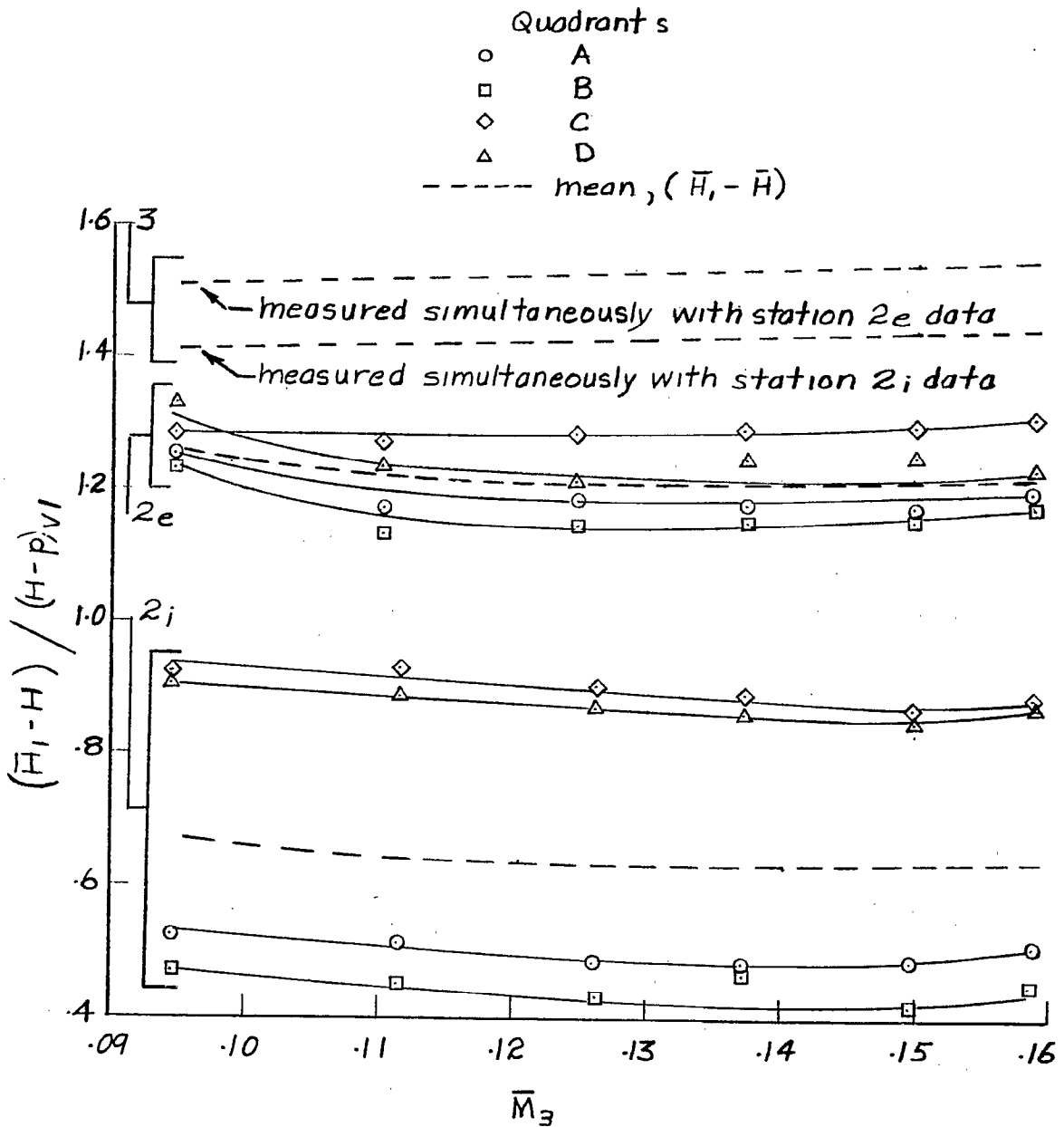
Figure 42.- Variation of the mean loss coefficients from station 1 to stations 2i, 2e, and 3 with Mach number. Test configuration 3.
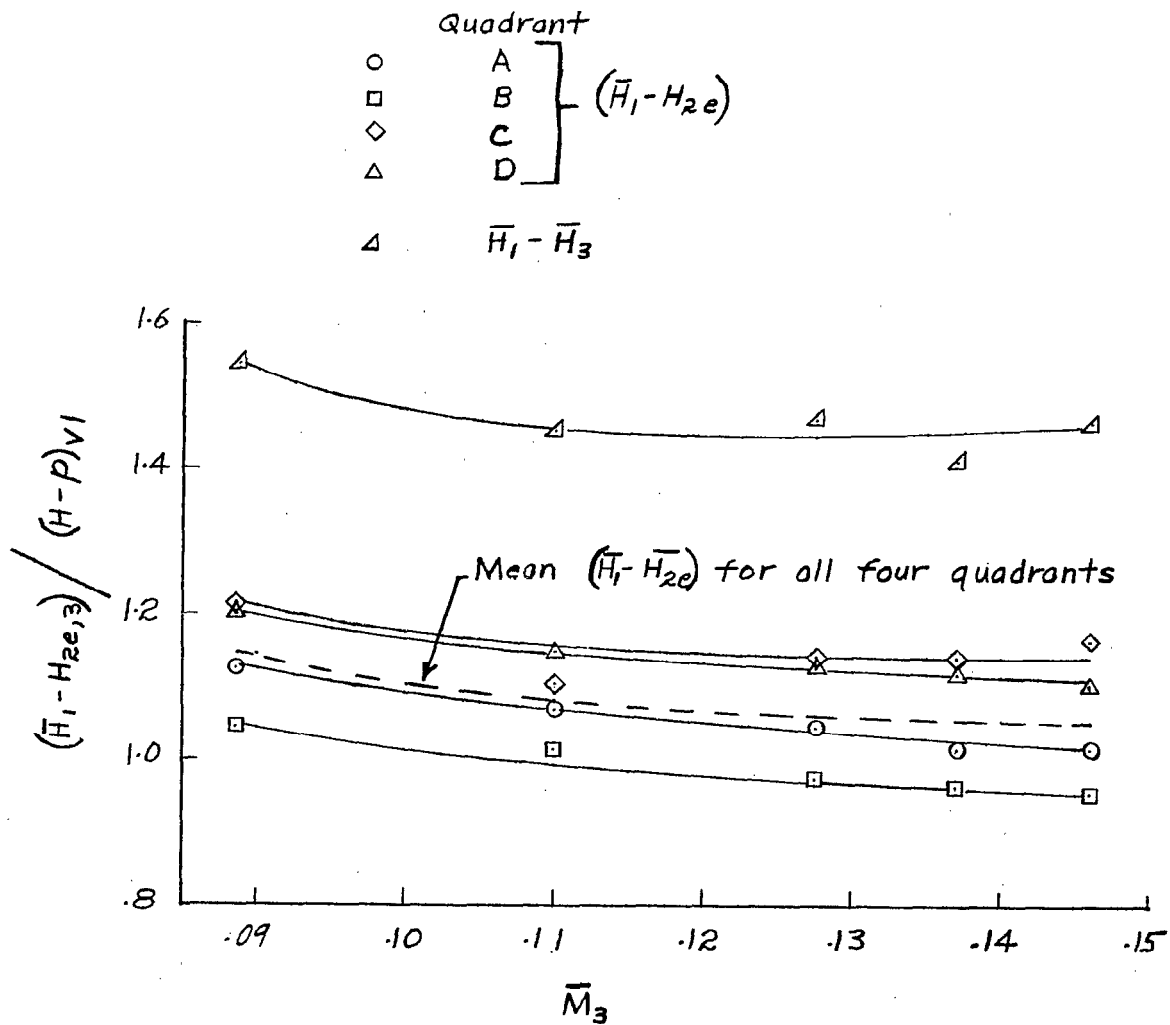
Figure 43.- Variation of the loss coefficients from station 1 to sta-
tions 2e and 3 with Mach number. Test configuration 4b (header
plate 2, guide vane configuration 1).
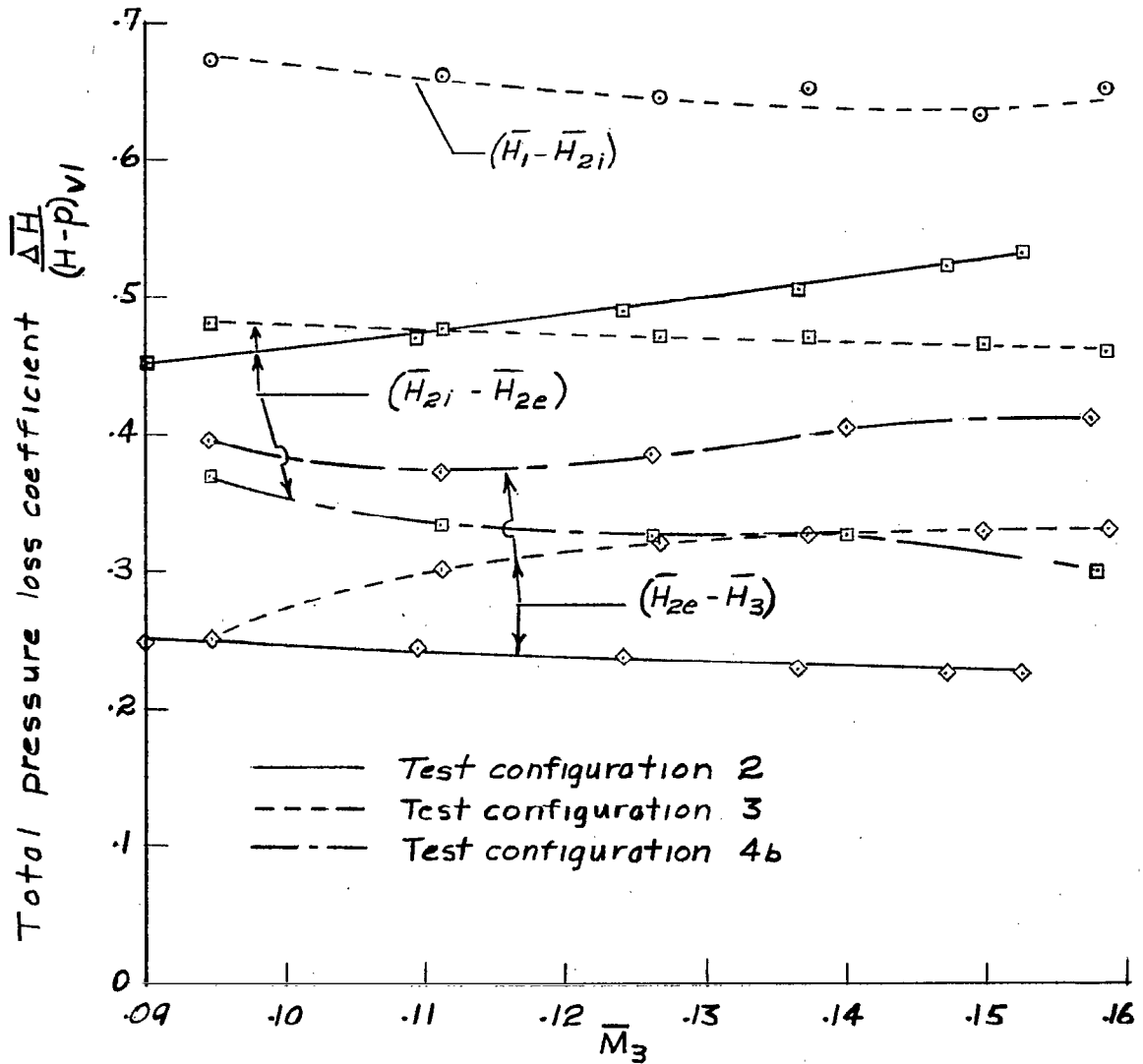
Figure 44.- Variation with Mach number of the loss coefficients of the individual duct elements located upstream of station 3.
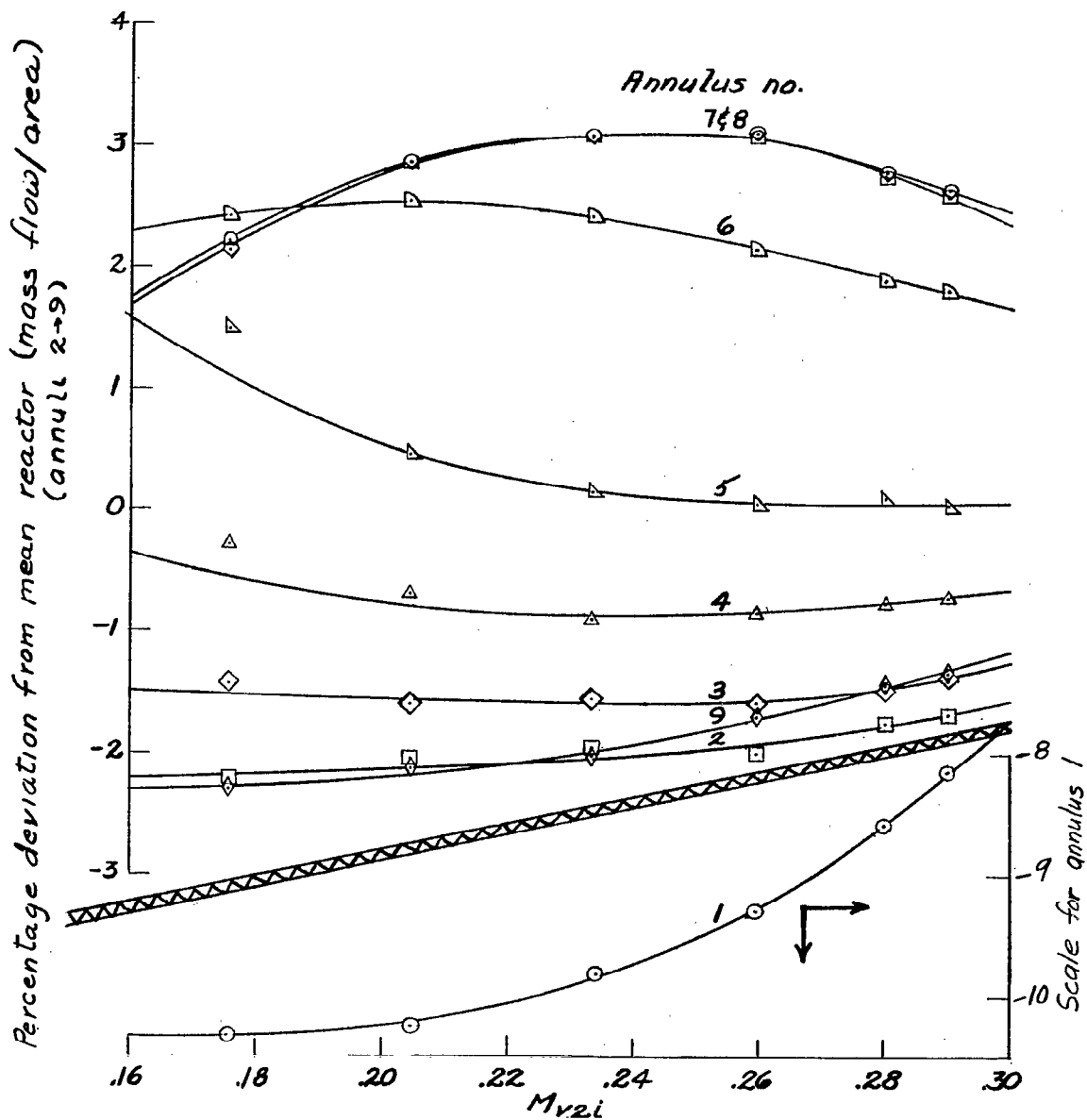
Figure 45.- Variation of the mass flow deviations in the simulated reactor with Mach number. Test configuration 2.

Figure 46.- Variation of the mass flow deviations in the simulated reactor with Mach number. Test configuration 3.
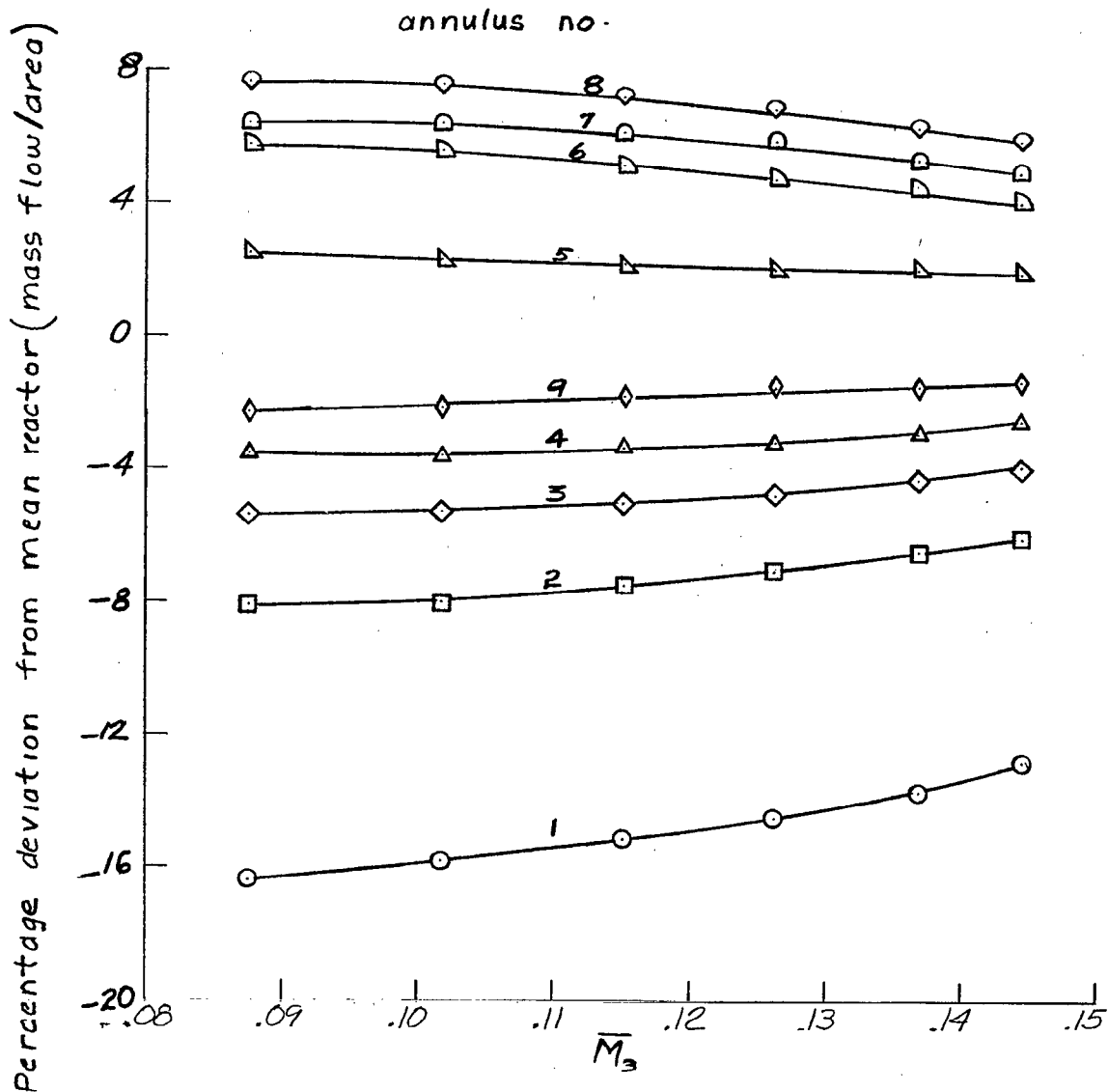
Figure 47.- Variation of the mass flow deviations in the simulated reactor with Mach number. Test configuration 4a (header plate 1, guide vane configuration 1).
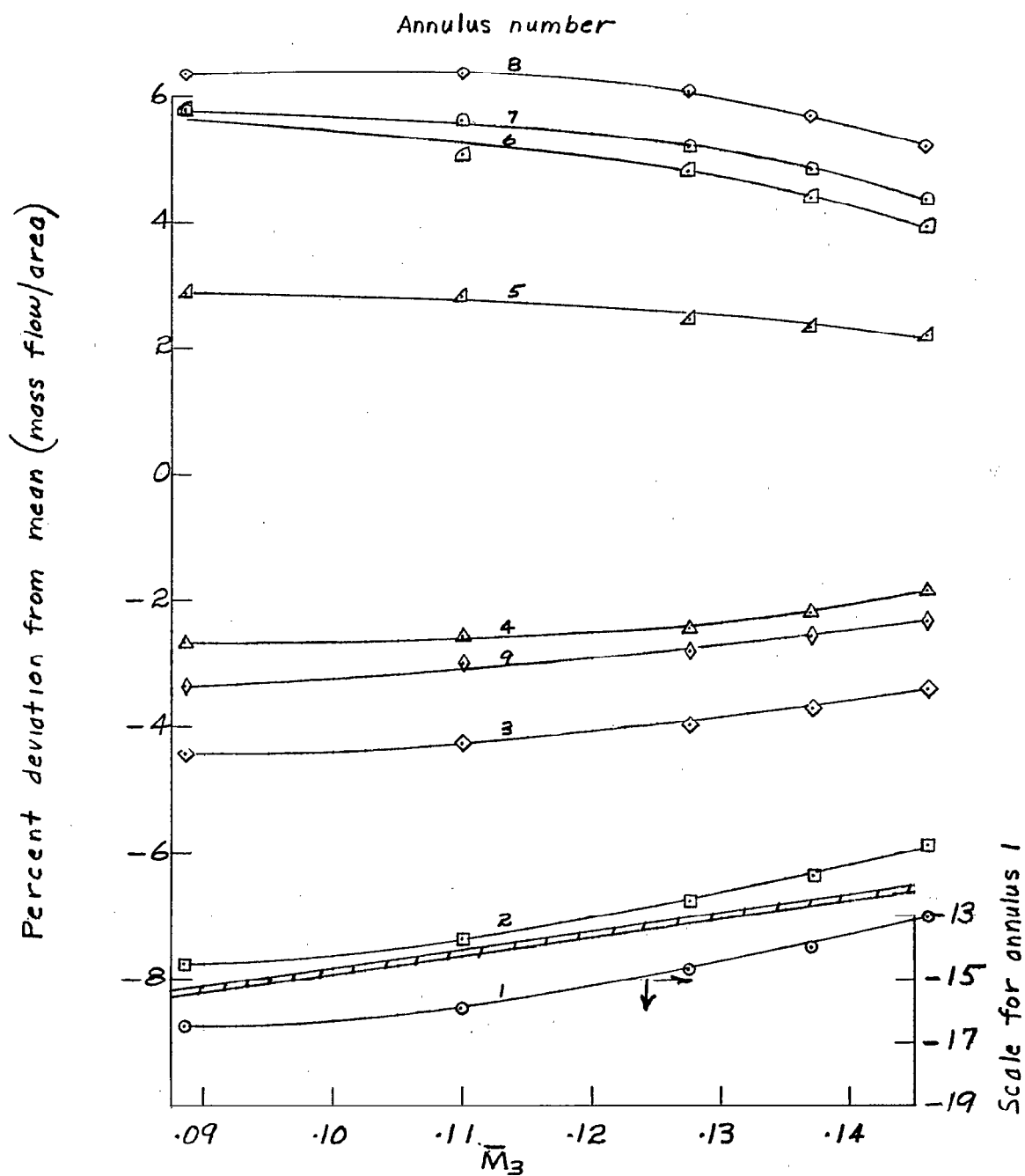
Figure 48.- Variation of the mass flow deviations in the simulated reactor with Mach number. Test configuration 4b (header plate 2, guide vane configuration 1).
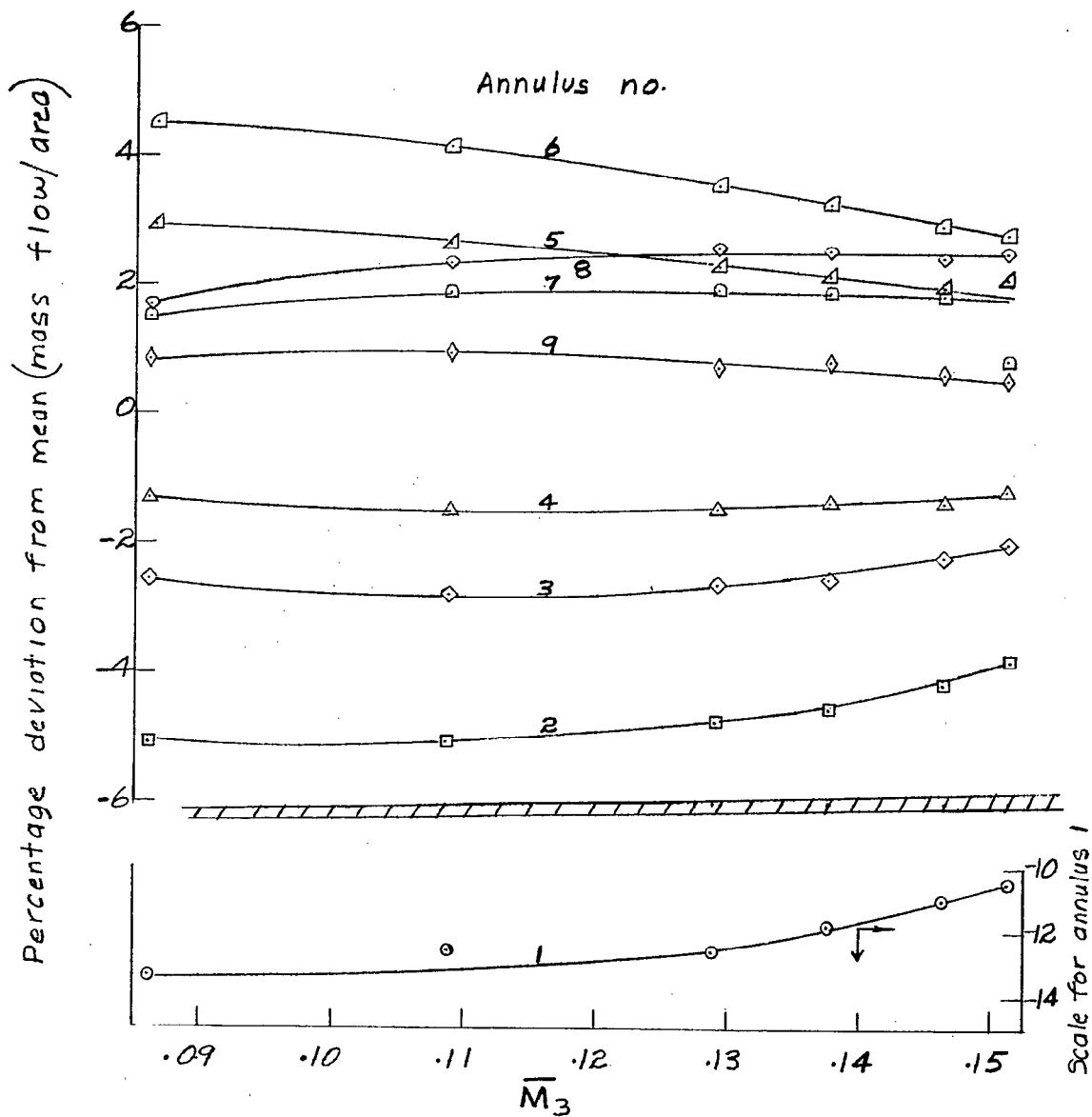
Figure 49.- Variation of the mass flow deviations in the simulated reactor with Mach number. Test configuration 4c (header plate 2, guide vane configuration 2, rear strut number 2).
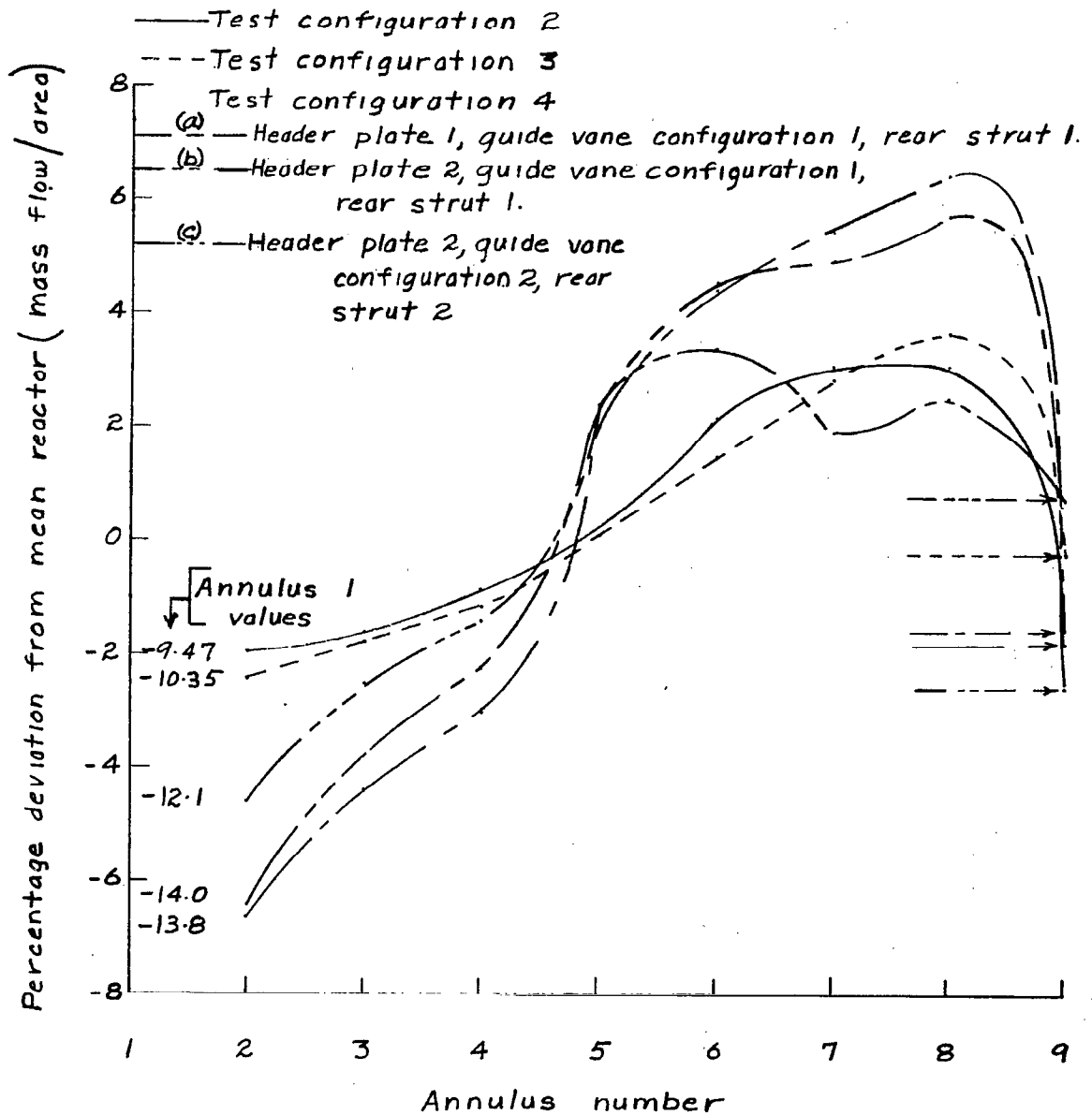
Figure 50.- Cross plots showing variation of the mass flow deviations in the simulated reactor with annulus number. $\bar{M}_3 = 0.135$.
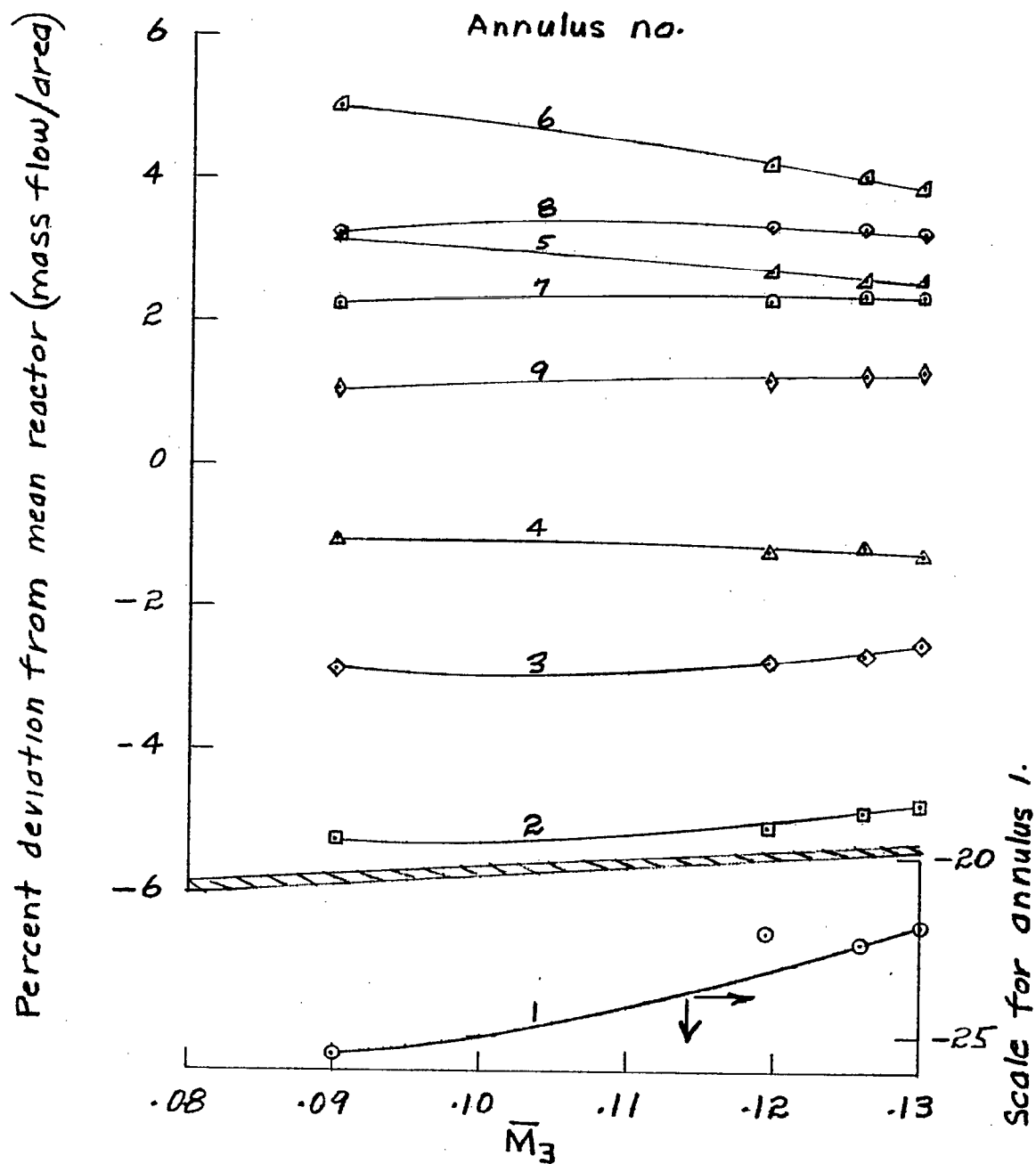
Figure 51.- Variation of the mass flow deviations in the simulated reactor with Mach number. Pipe 4 closed. Test configuration 4c (header plate 2, guide vane configuration 2, rear strut number 2).
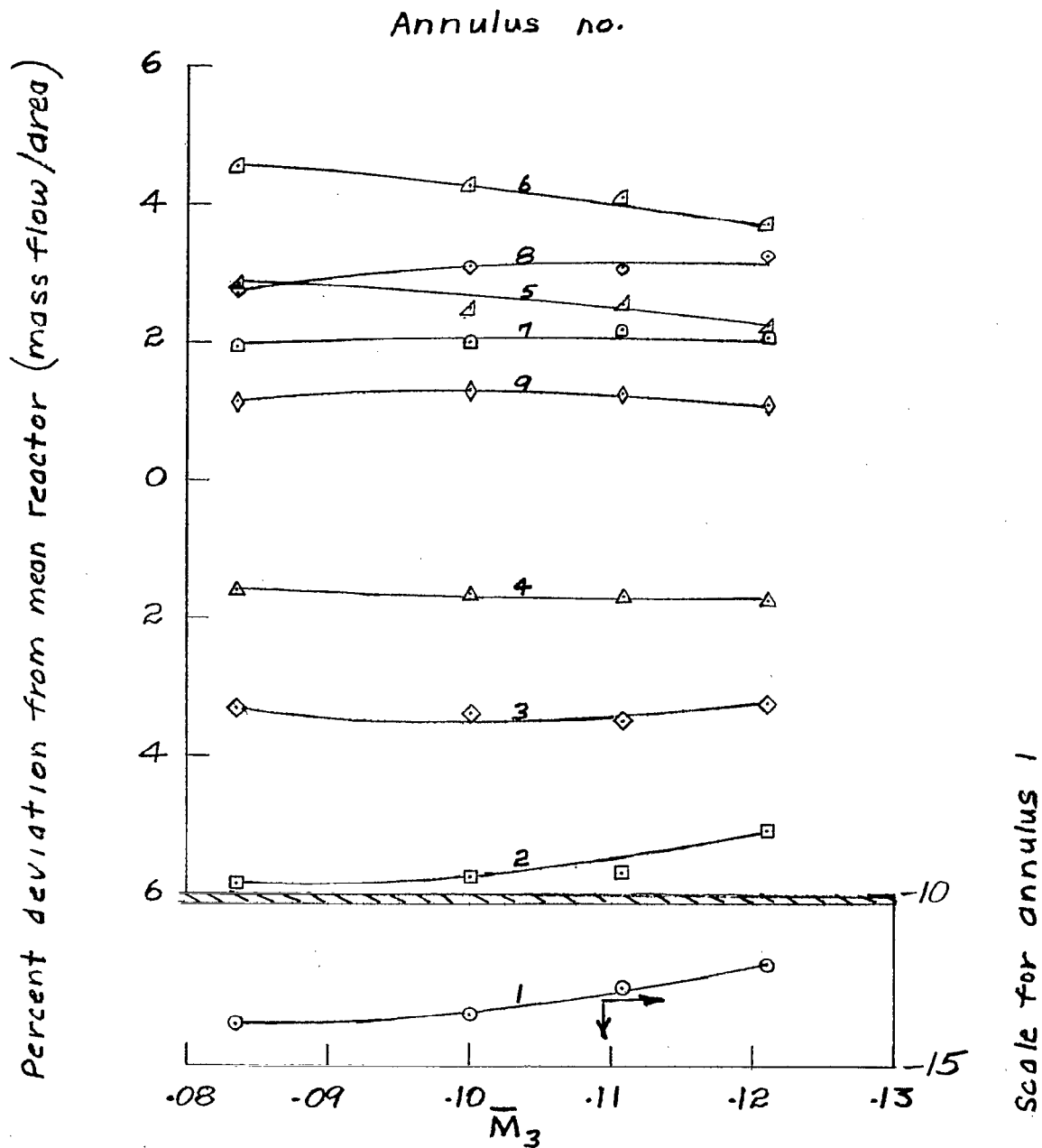
Figure 52.- Variation of the mass flow deviations in the simulated reactor with Mach number. Pipe 3 closed. Test configuration 4c (header plate 2, guide vane configuration 2, rear strut number 2).
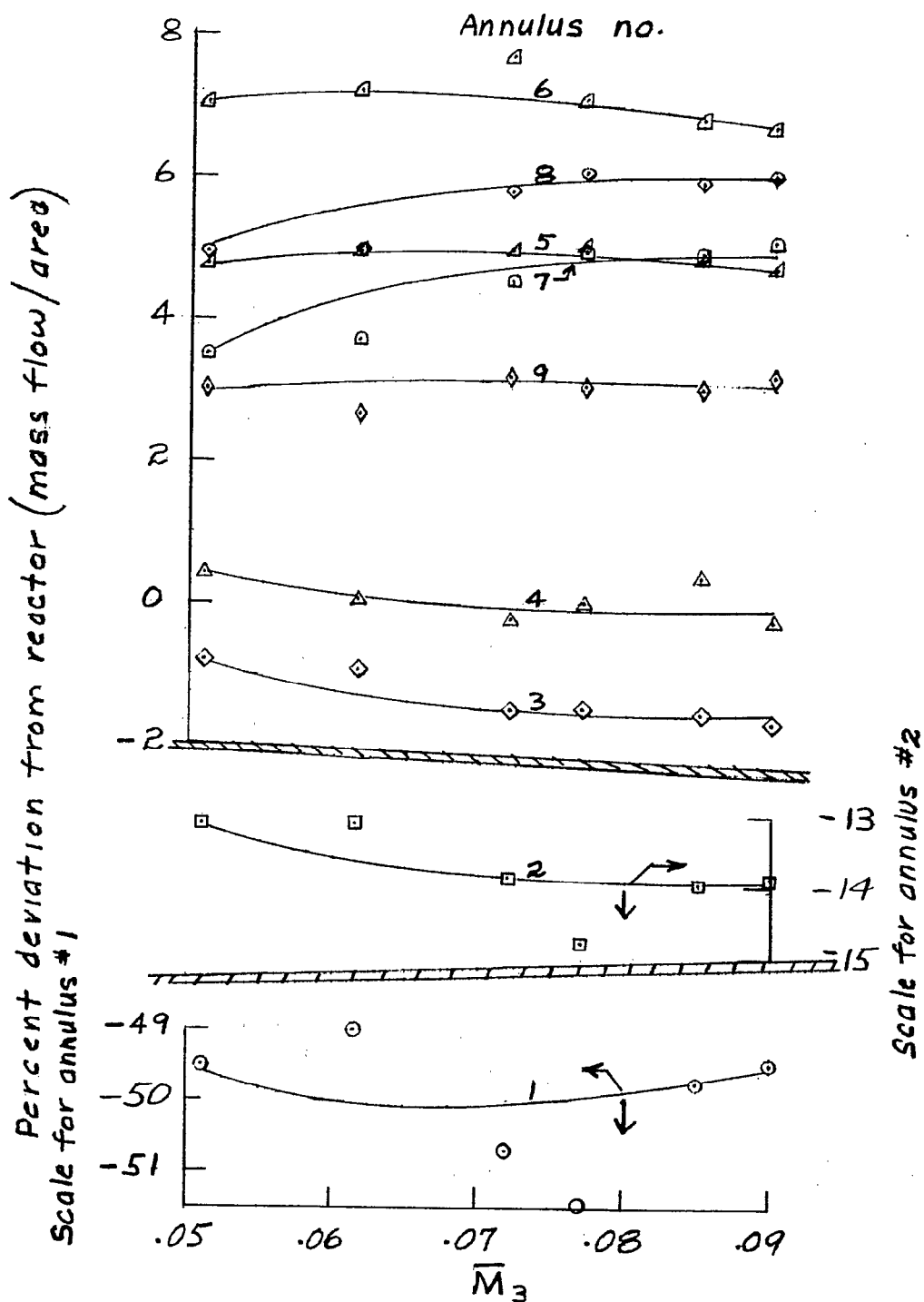
Figure 53.- Variation of the mass flow deviations in the simulated reactor with Mach number. Pipes 1 and 4 closed. Test configuration 4c (header plate 2, guide vane configuration 2, rear strut number 2).

Figure 54.- Variation of the mass flow deviations in the simulated reactor with Mach number. Pipes 2 and 3 closed. Test configuration 4c (header plate 2, guide vane configuration 2, rear strut number 2).
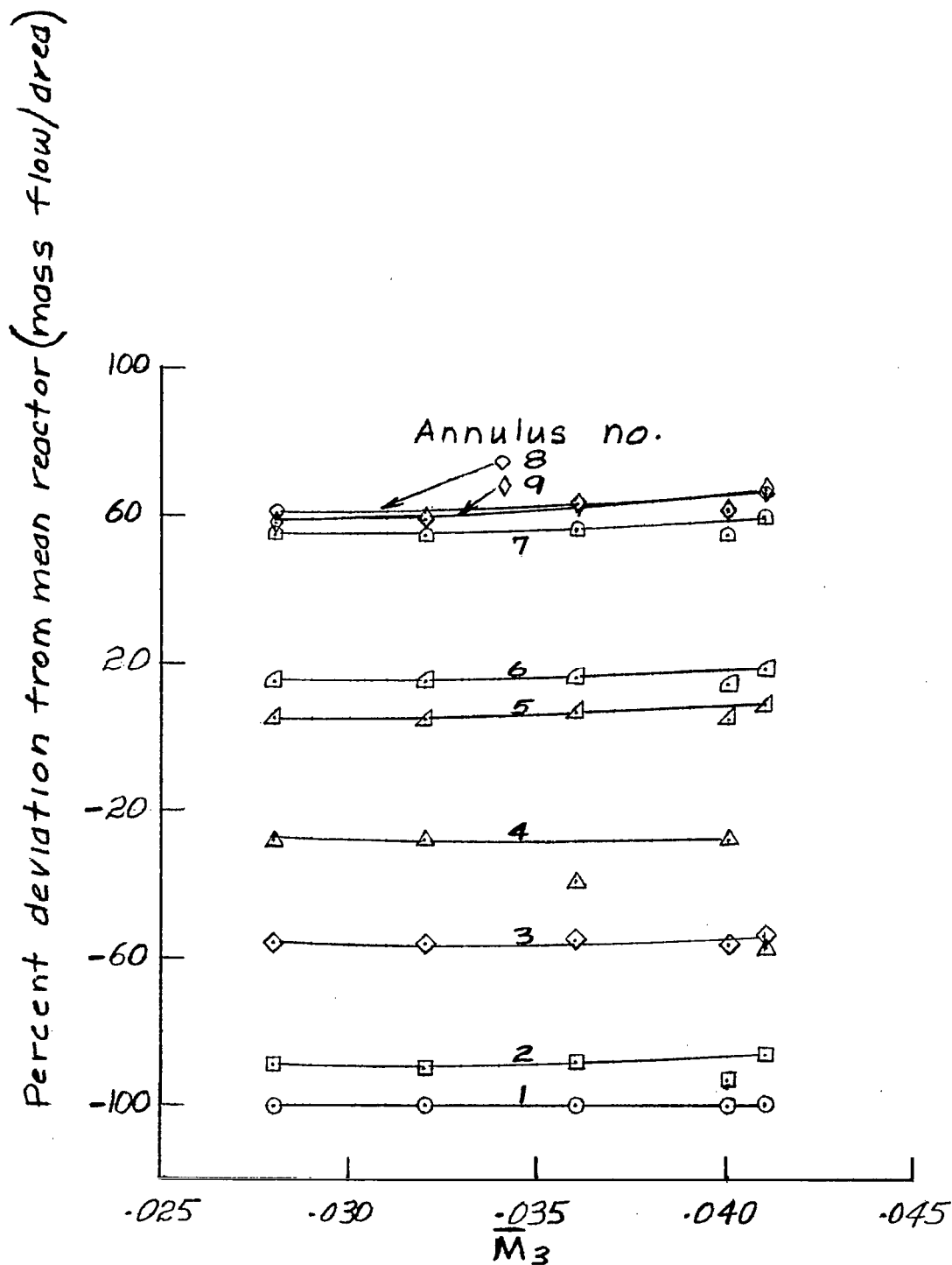
Figure 55.- Variation of the mass flow deviations in the simulated reactor with Mach number. Pipes 2, 3, and 4 closed. Test configuration 4c (header plate 2, guide vane configuration 2, rear strut number 2).
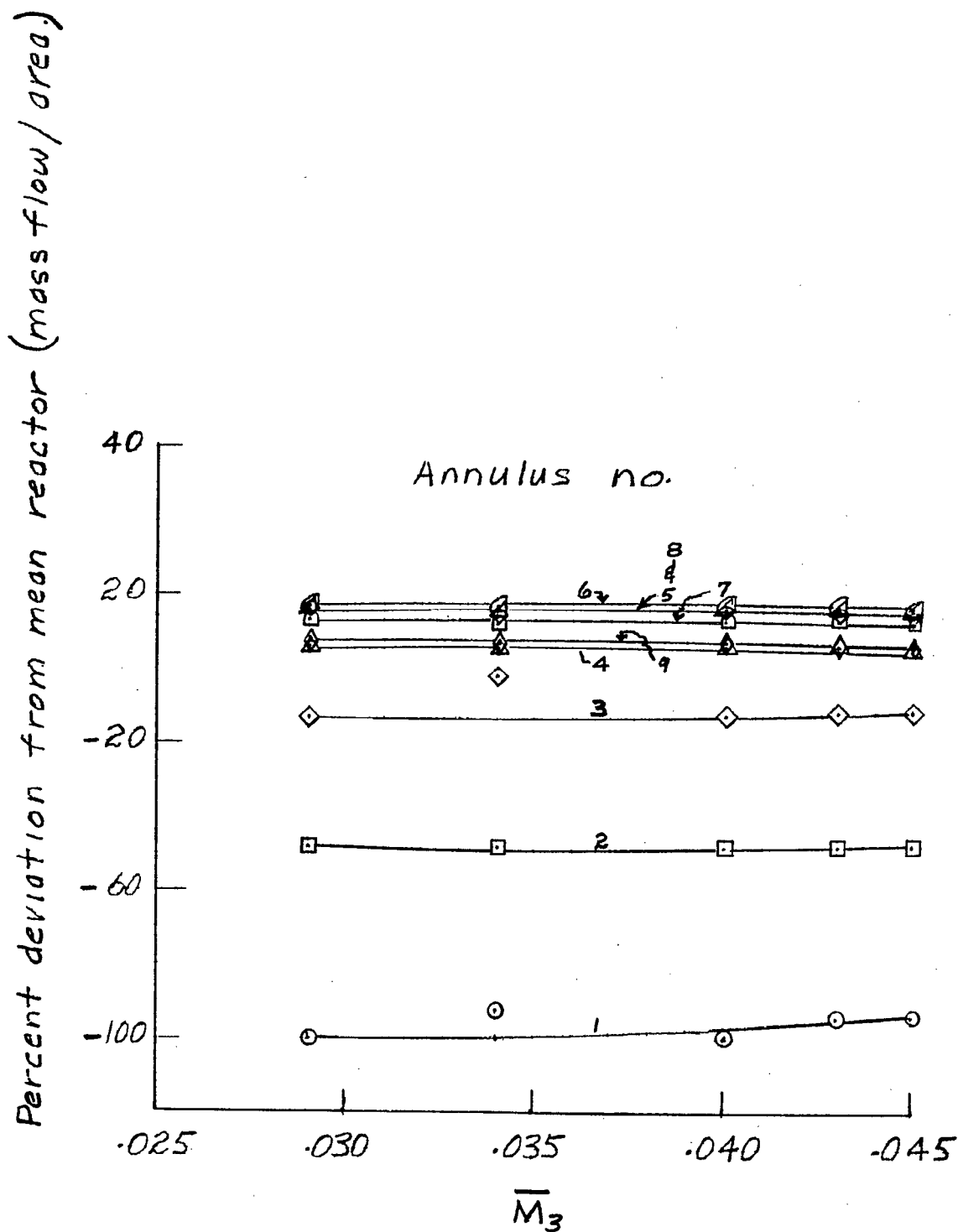
Figure 56.- Variation of the mass flow deviations in the simulated reactor with Mach number. Pipes 1, 2, and 4 closed. Test configuration 4c (header plate 2, guide vane configuration 2, rear strut number 2).
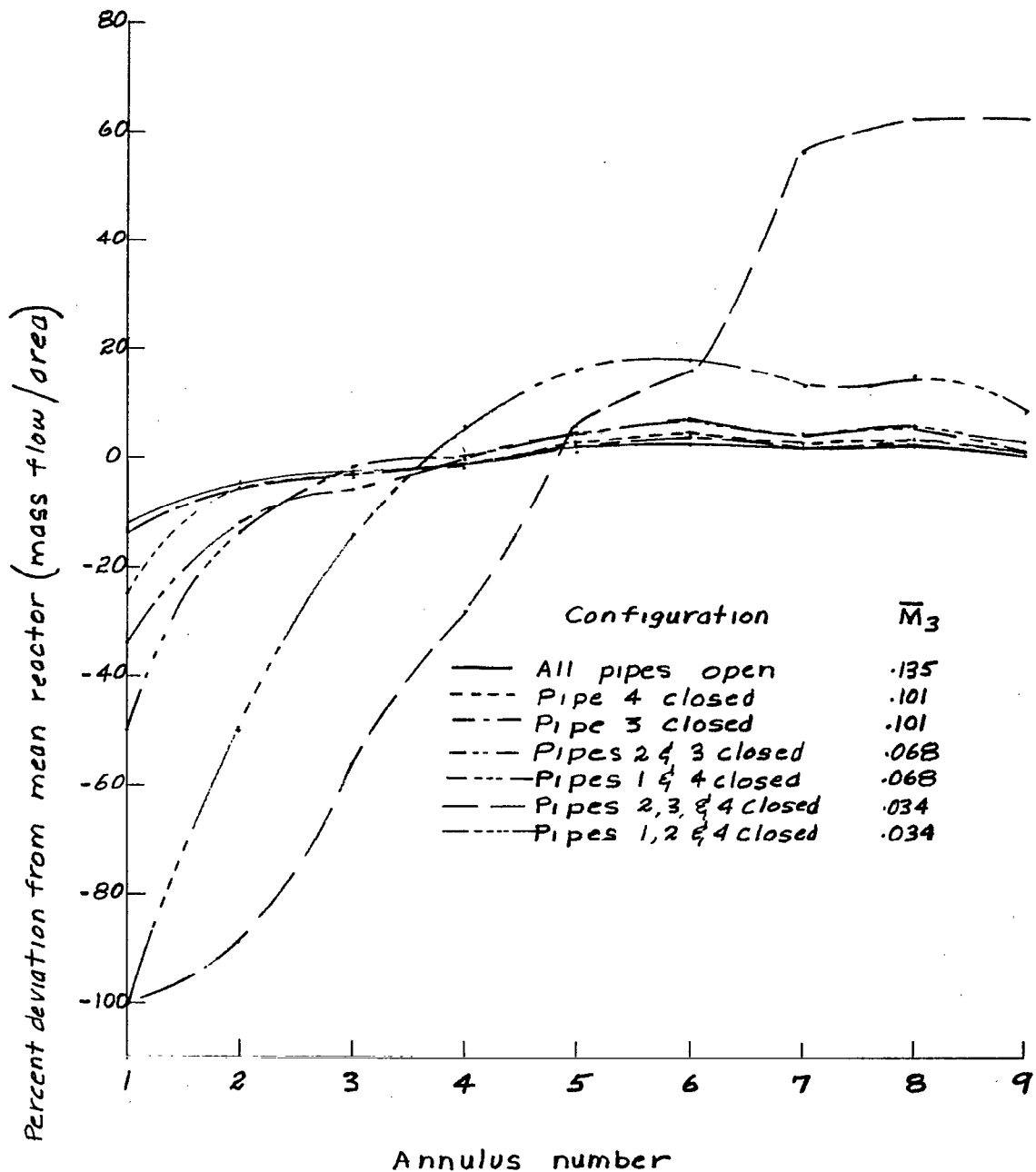
Figure 57.- Cross plots showing variation with annulus number of the mass flow deviations in the simulated reactor for the symmetrical and the six asymmetrical test conditions. Test configuration 4c (header plate 2, guide vane configuration 2, rear strut number 2).
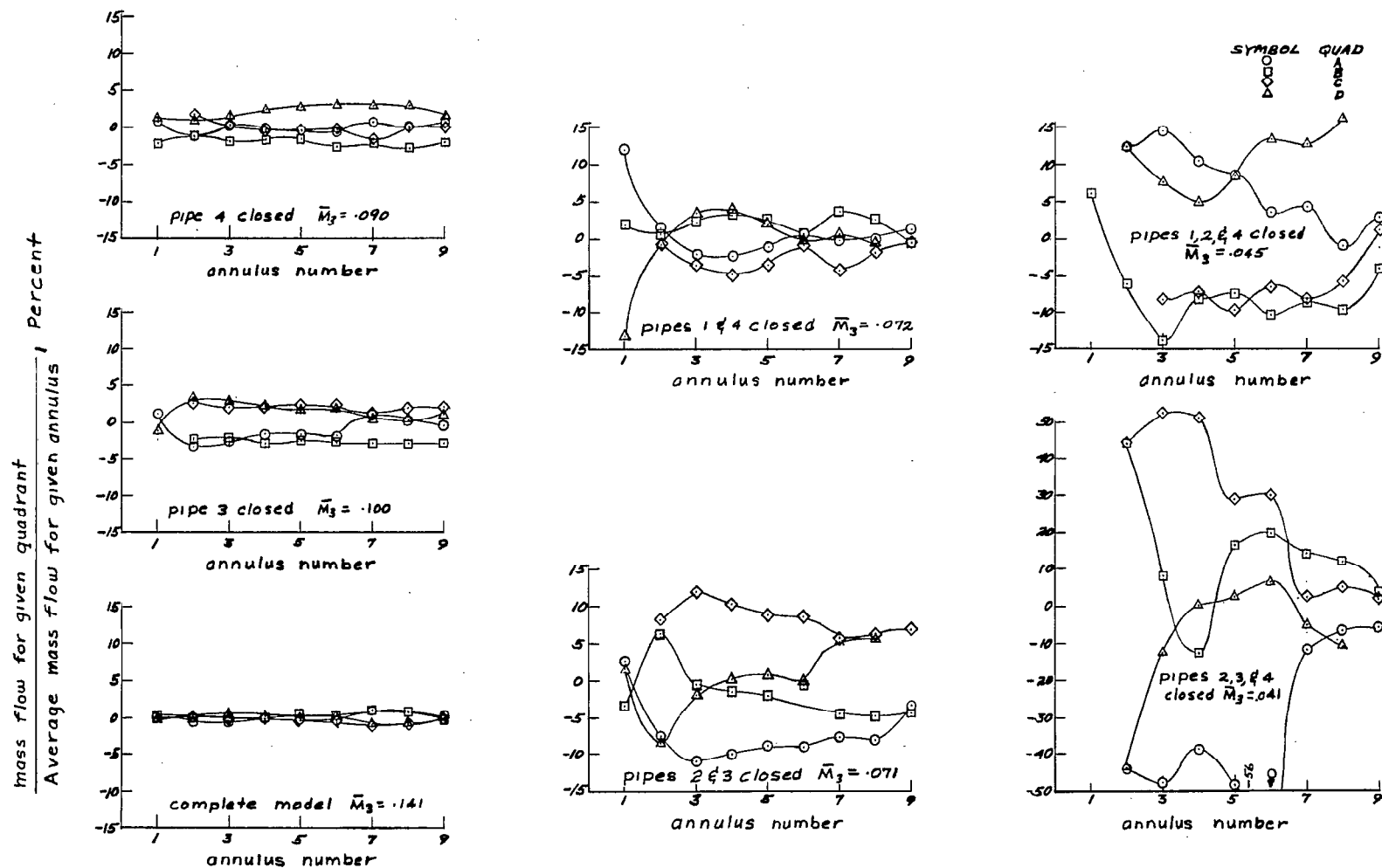
Figure 58.- Variation of mass flow between quadrants in any given annulus of the simulated reactor for the symmetrical and the six asymmetrical test conditions.
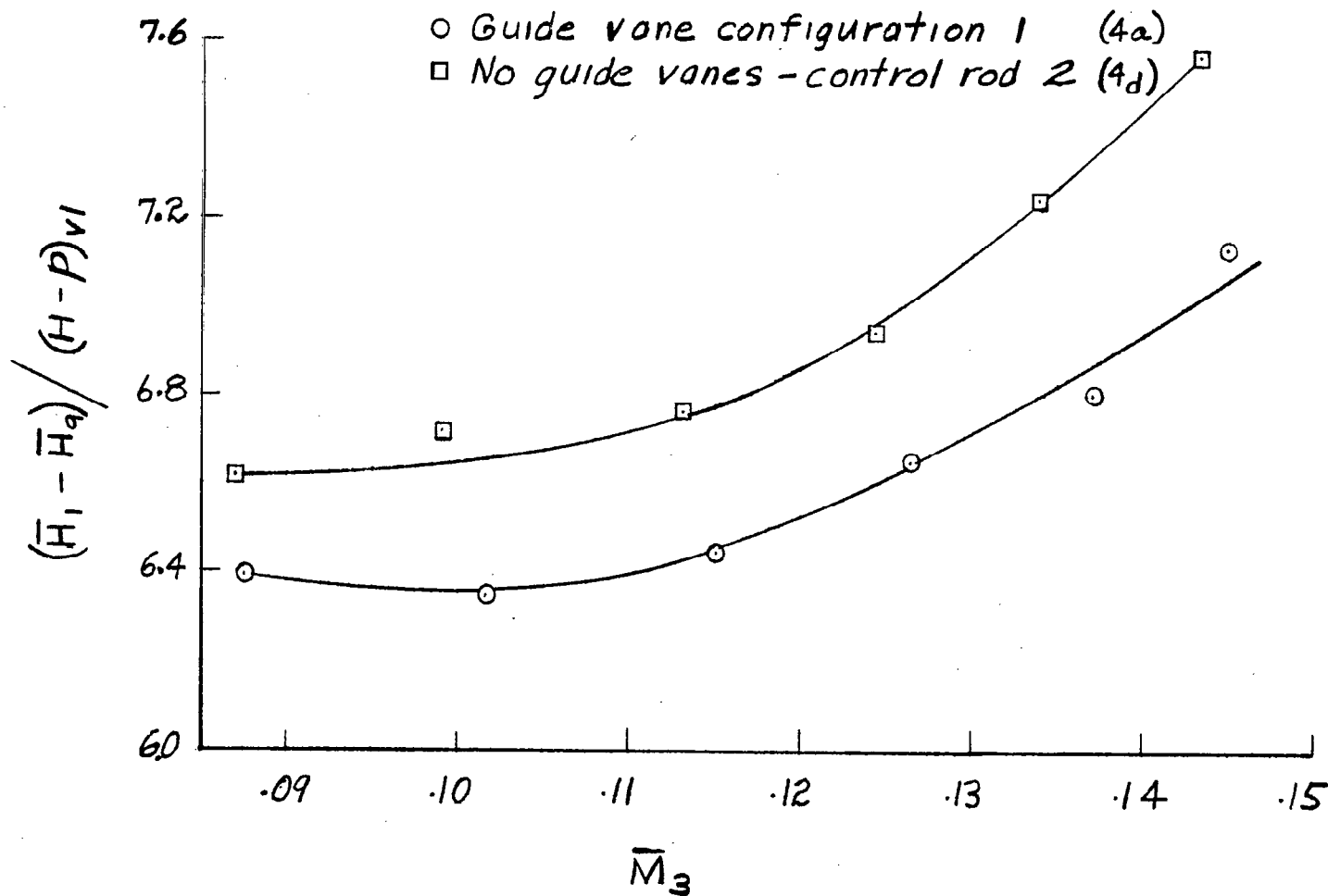
Figure 59.- Variation of the loss coefficient from station 1 to station 9 with Mach number. Test configurations 4a and 4d.
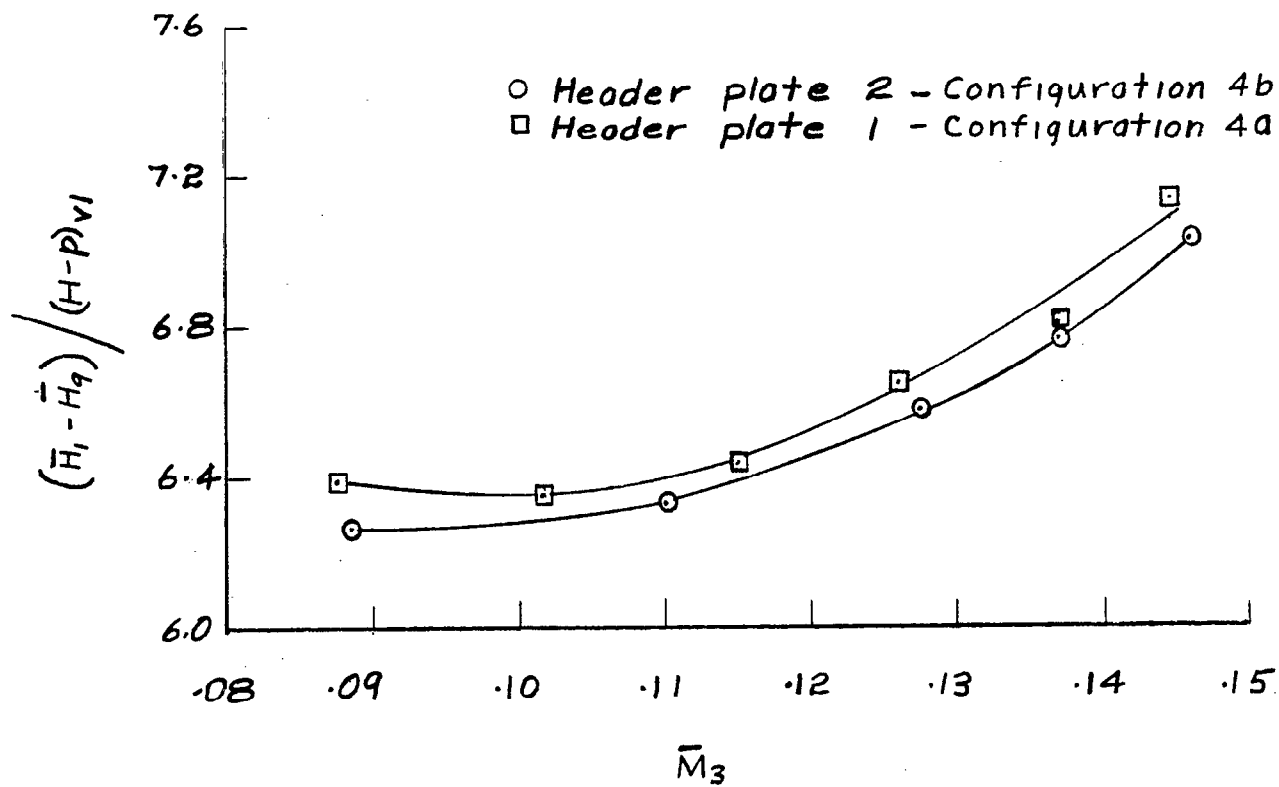
Figure 60.- Variation of the loss coefficient from station 1 to station 9 with Mach number. Test configurations 4a and 4b.

(a) Measured loss coefficient.

(b) Loss coefficient adjusted to a constant orifice-plate loss coefficient.
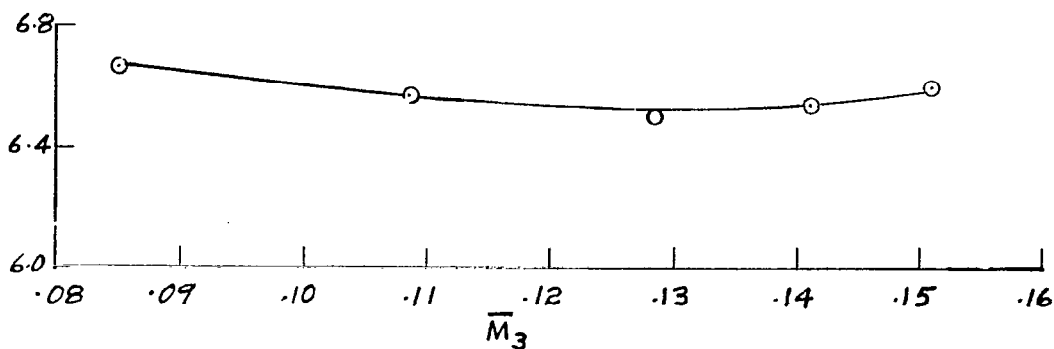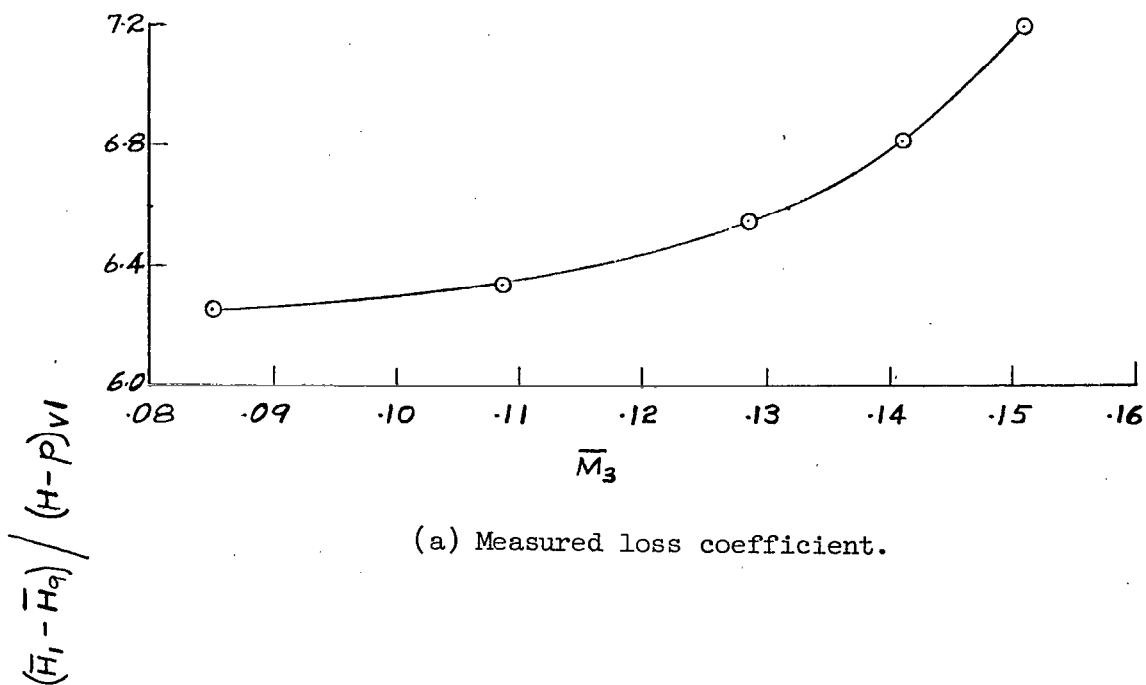
Figure 61.- Variation of the measured and the adjusted loss coefficients from station 1 to station 9 with Mach number. Test configuration 4c (header plate 2, guide vane configuration 2, rear strut 2).
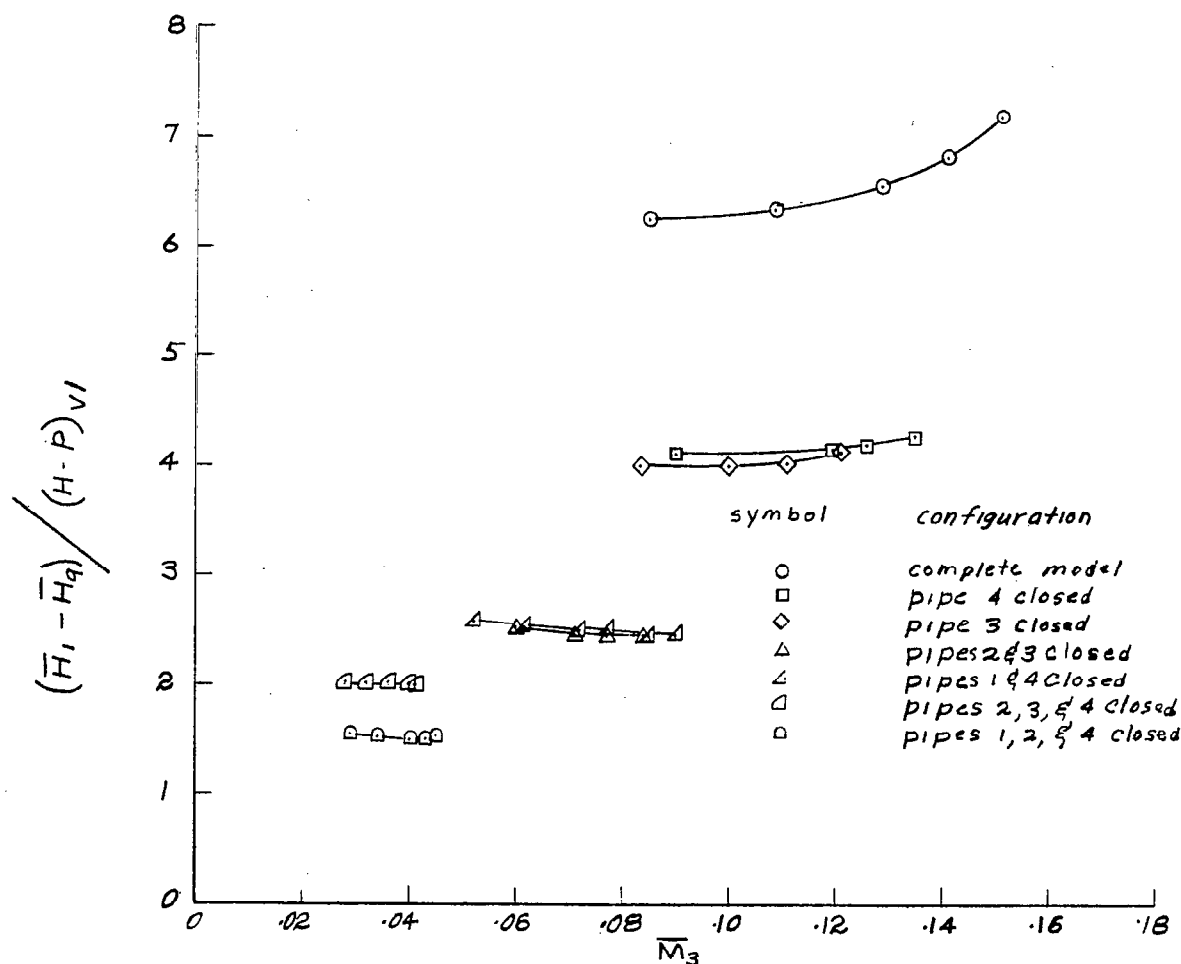
Figure 62.- Variation of the loss coefficient from station 1 to station 9 with Mach number for the symmetrical and the six asymmetrical test conditions. Test configuration 4c (header plate 2, guide vane configuration 2, rear strut 2).
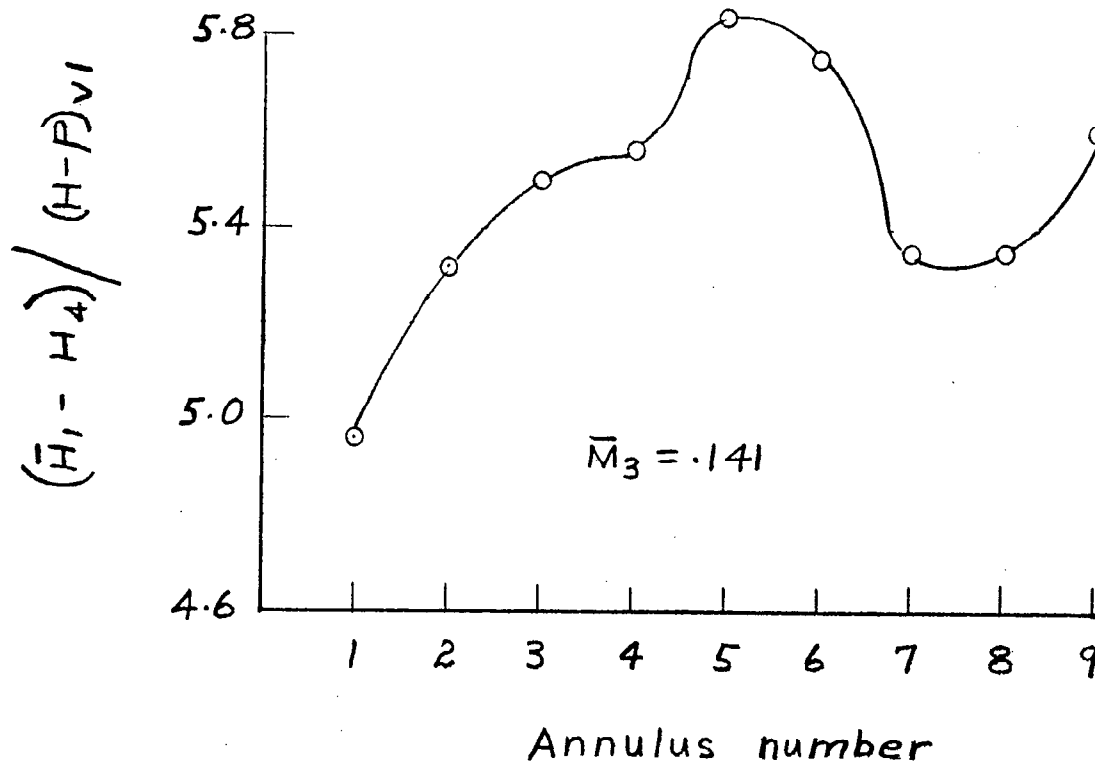
Figure 63.- Variation of the calculated total pressure loss from stations 1
to 4 with reactor annulus number. Test configuration 4c (header plate 2,
guide vane configuration 2, rear strut 2); $\overline{M}_3$ = 0.141.
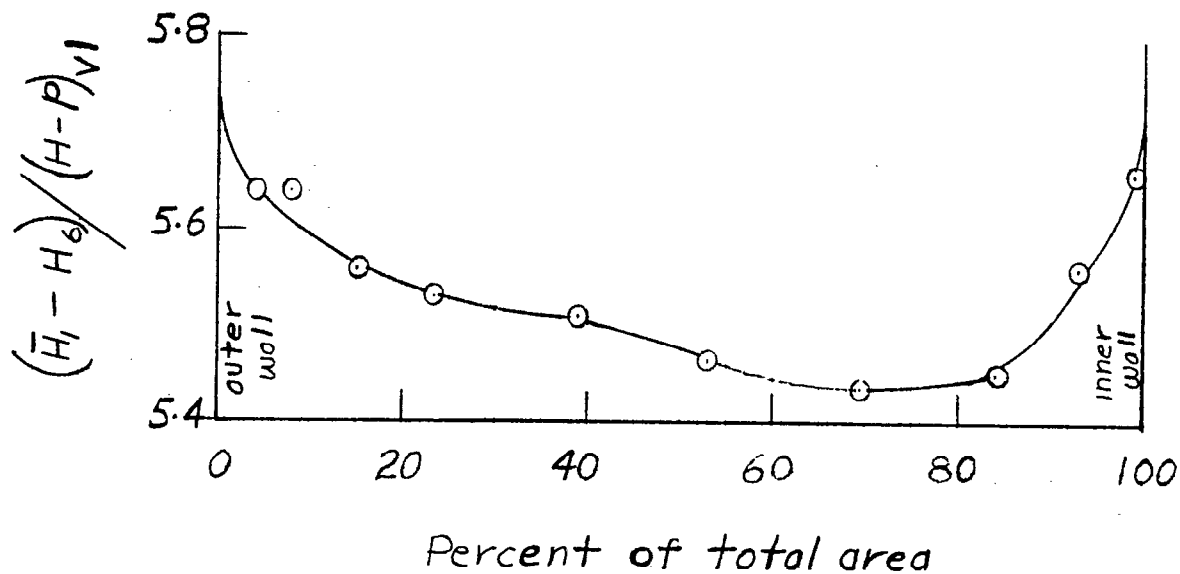
Figure 64.- Radial variation of the total pressure in the exit annulus at station 6. Data obtained at the 45° position of quadrant A for test configuration 4c.
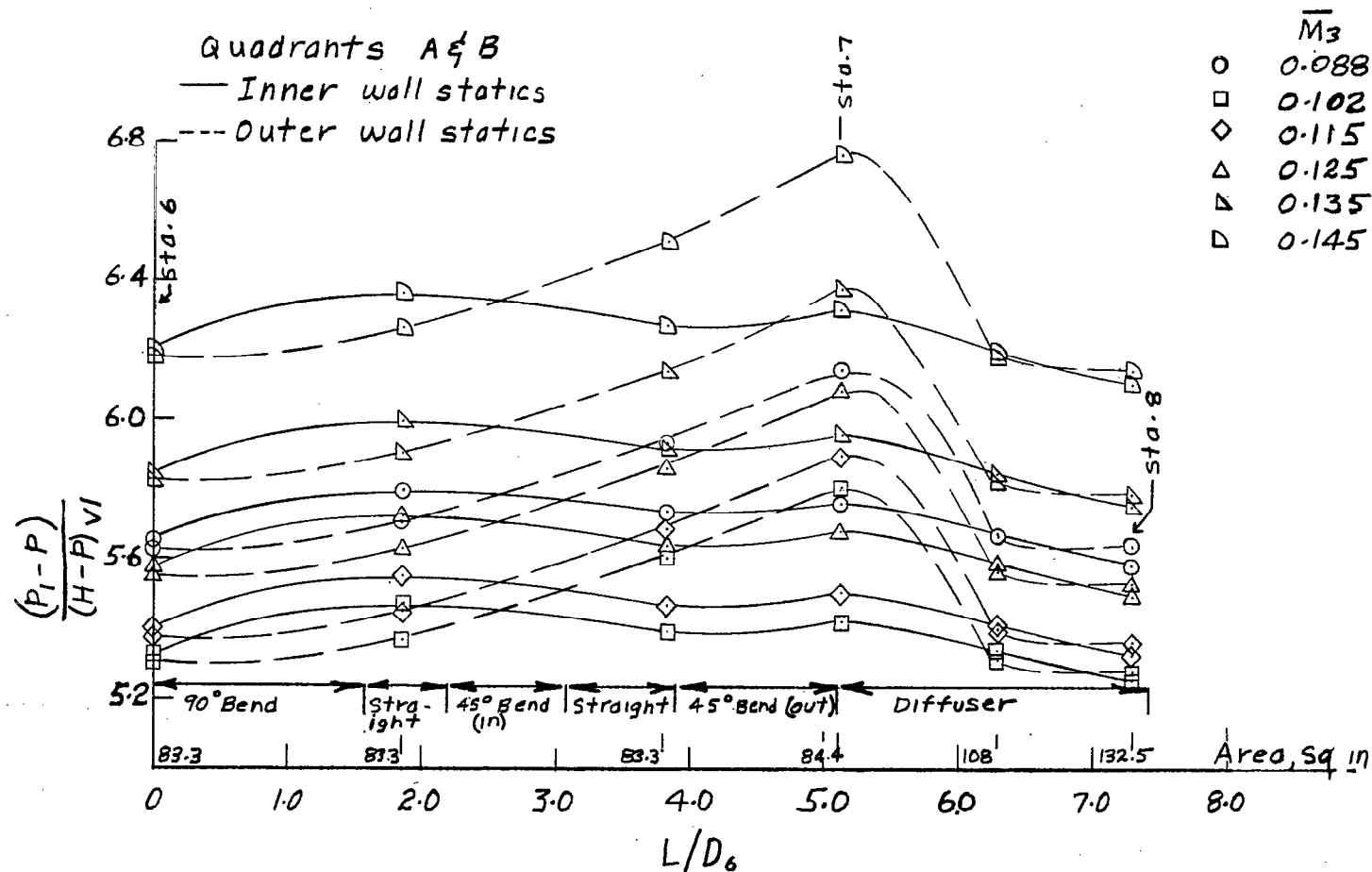
(a) Quadrants A and B.

Figure 65.- Exit annulus longitudinal static pressure distribution. Test
configuration 4a (header plate 1, guide vane configuration 1, rear
strut 1).
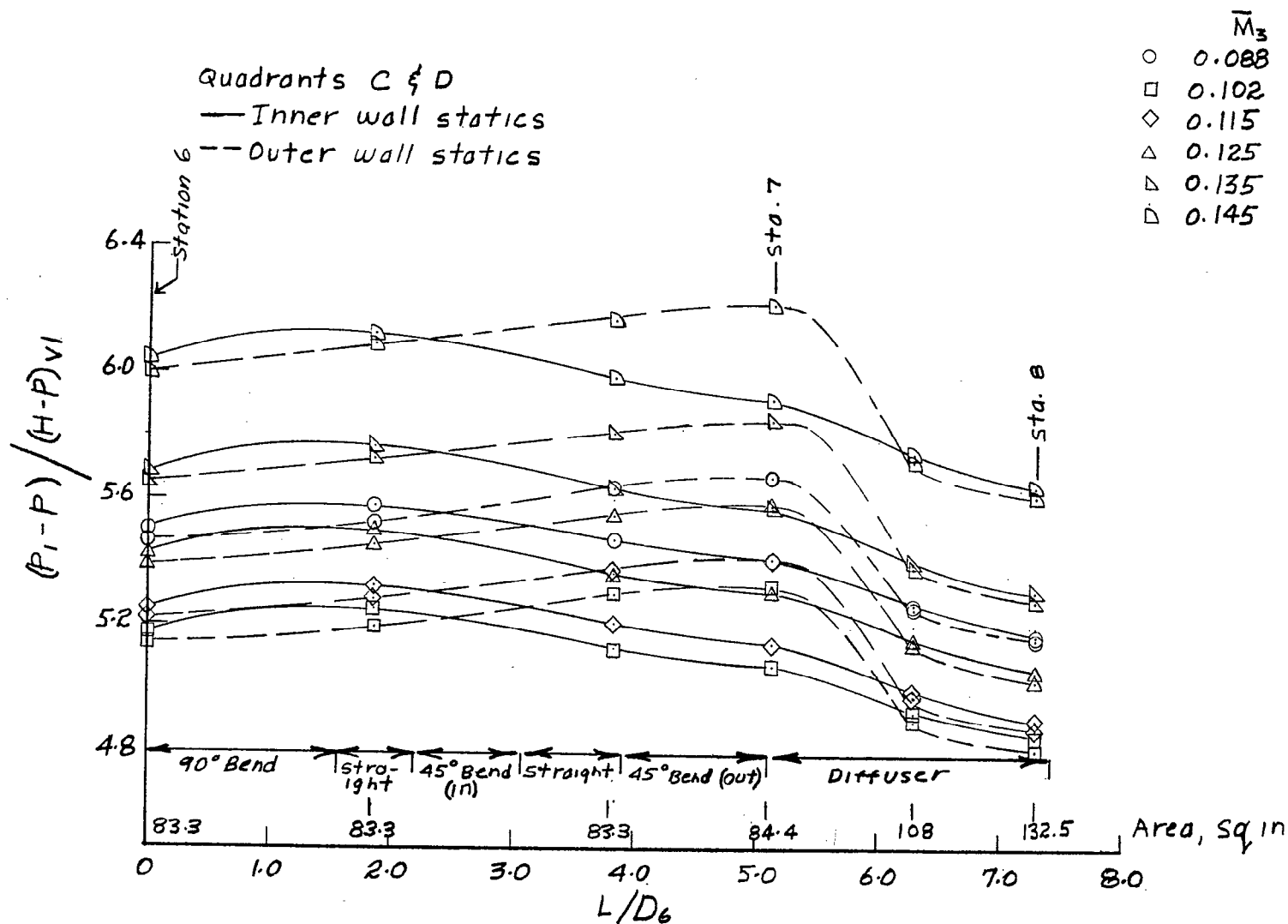
(b) Quadrants C and D.

Figure 65.- Concluded.
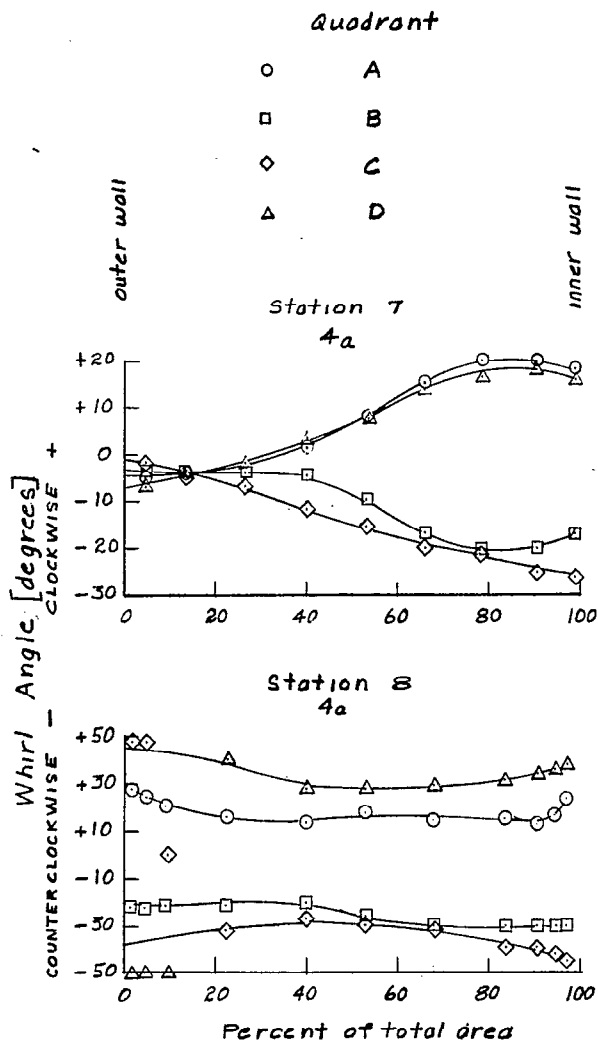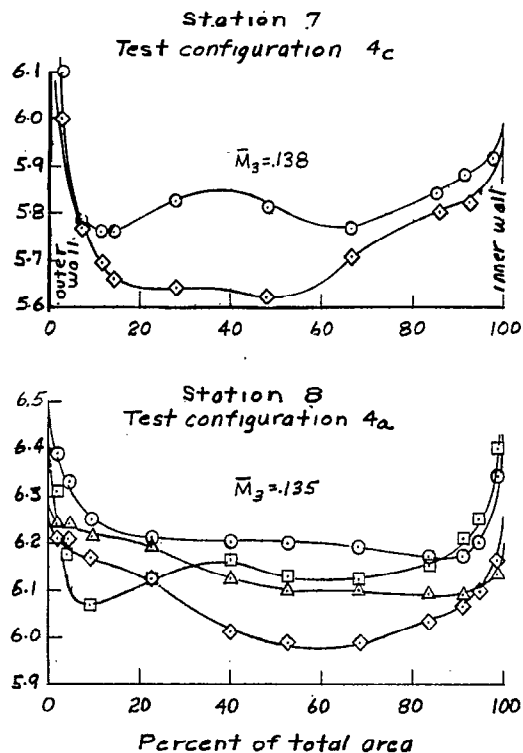
Figure 66.- Radial variation of total pressure and whirl angle in the exit annulus at stations 7 and 8. Test configurations 4a and 4c.

Station 7

Test configuration 4c
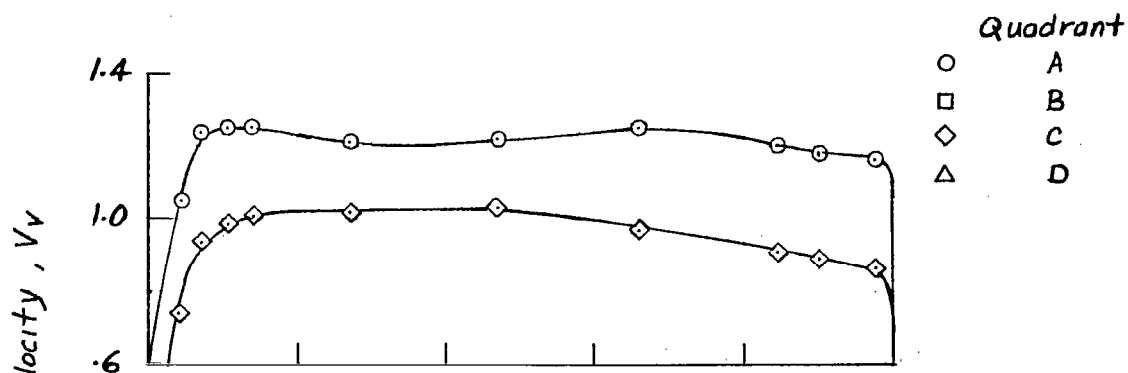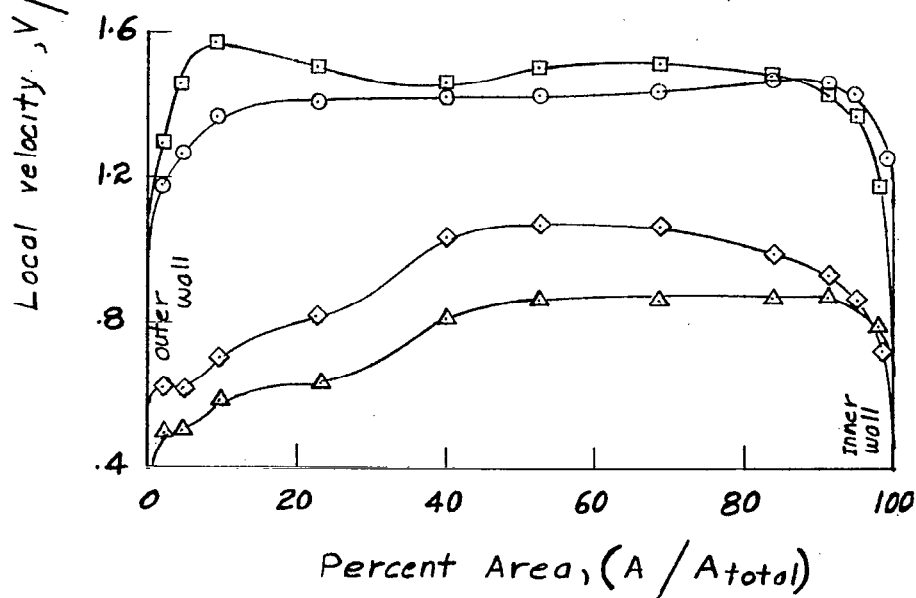
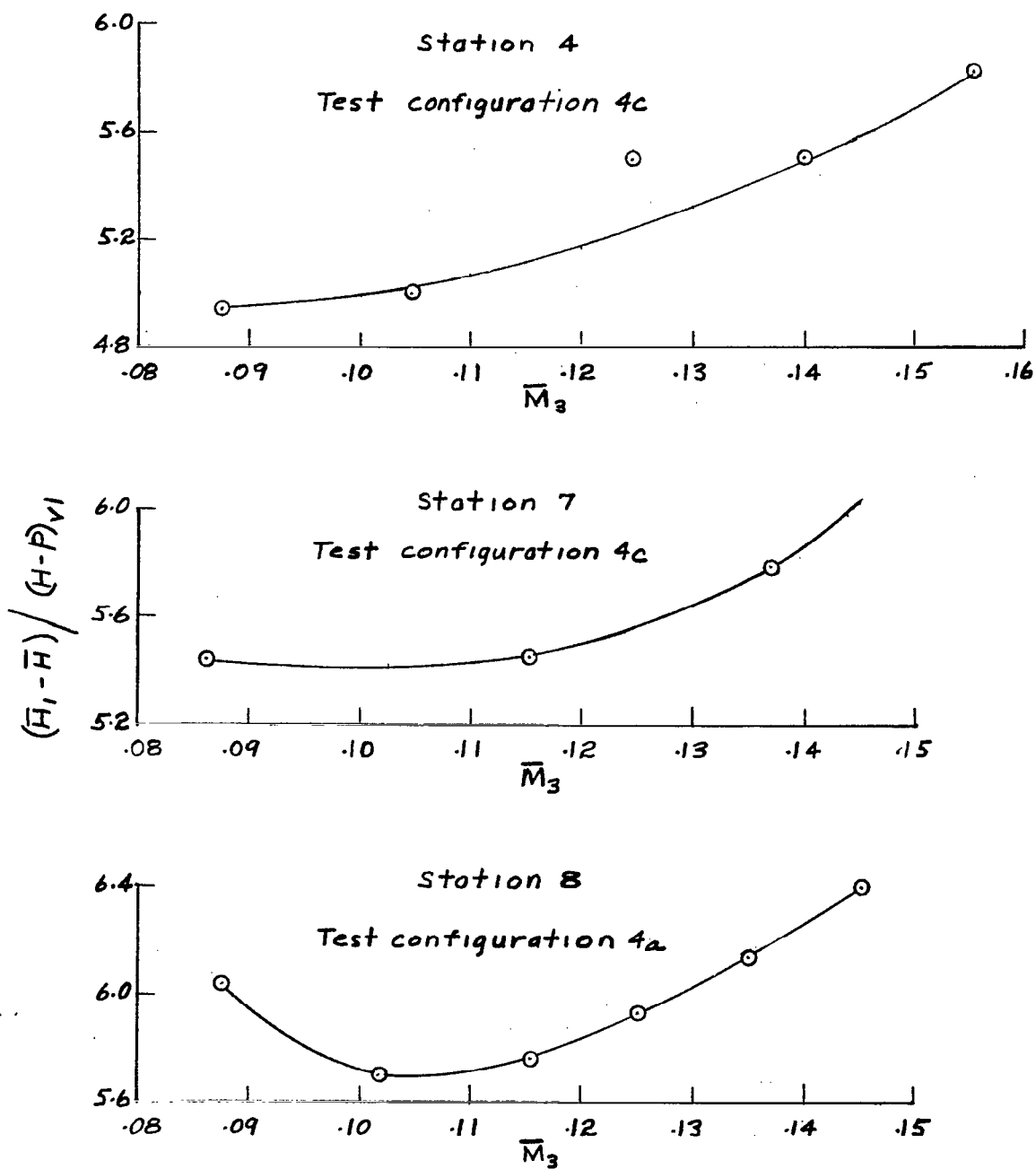Figure 67.- Radial variation of velocity at stations 7 and 8. Test configurations 4a and 4c.

Figure 68.- Variation of the mean loss coefficients from station 1 to stations 4, 7, and 8 with Mach number. Test configurations 4a and 4c.
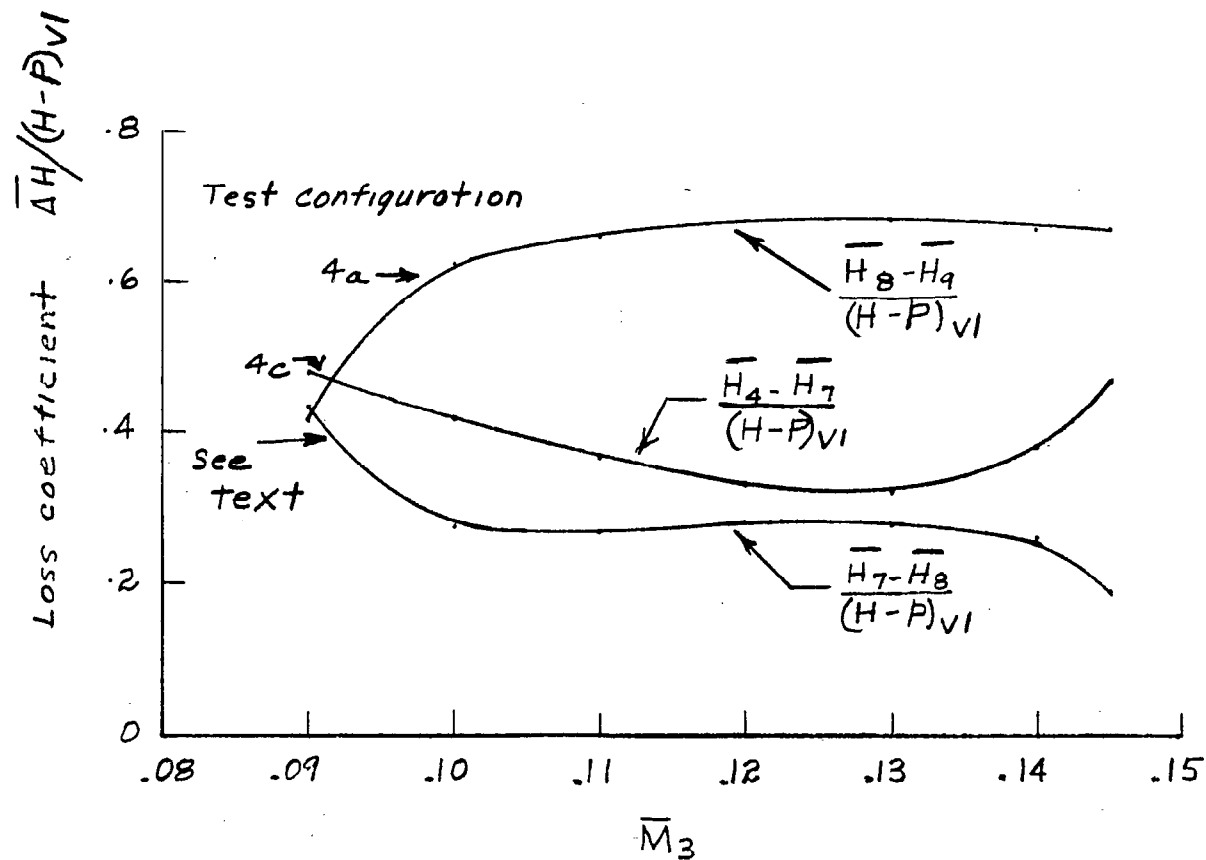
Figure 69.- Variation of the loss coefficients of the various duct elements downstream of the simulated reactor with Mach number. Test configurations 4a and 4c.
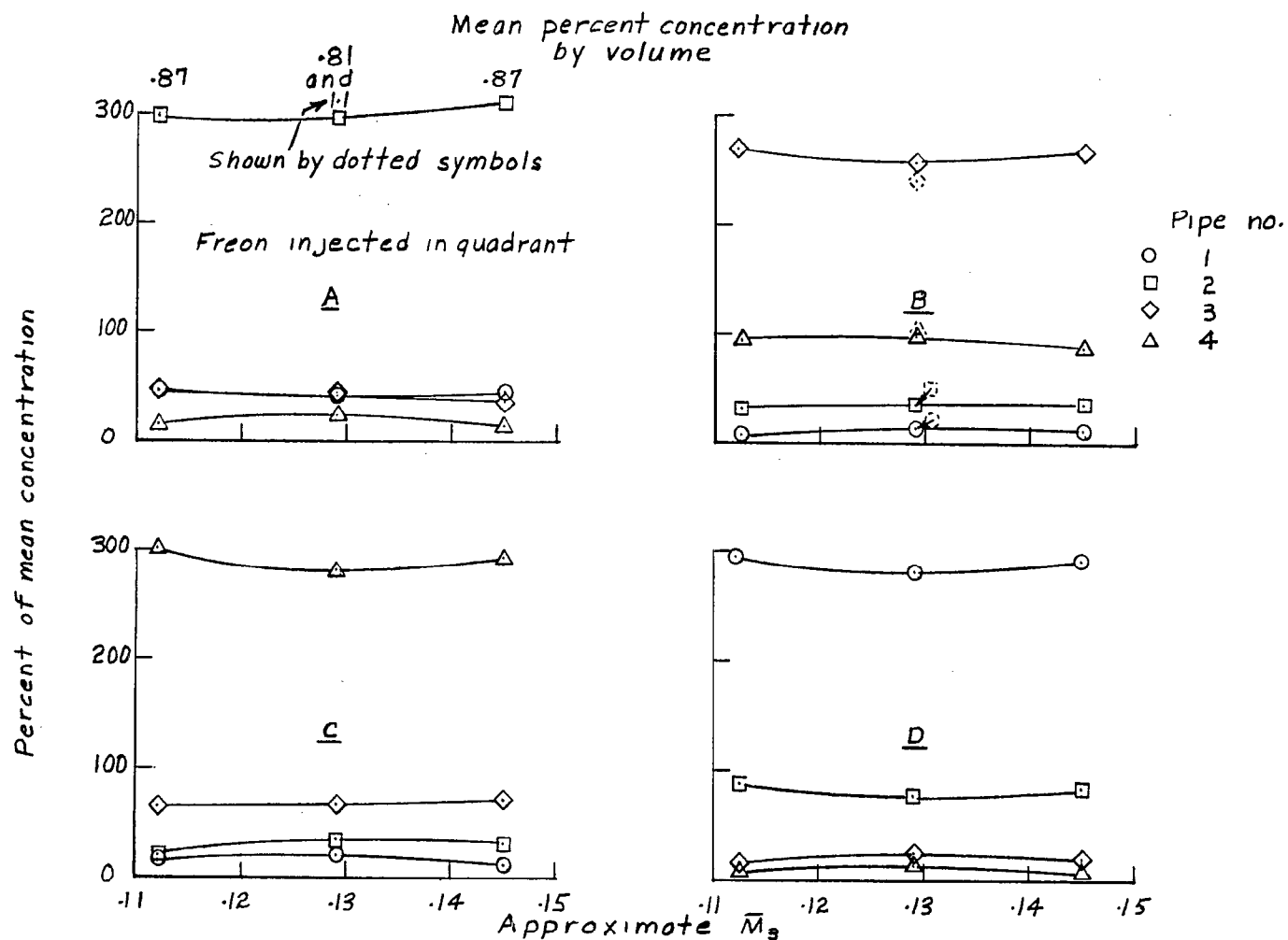
Figure 70.- Results of air-flow tracing test showing the percent of mean concentration in the various pipes for several airspeeds. Test configuration 4c.
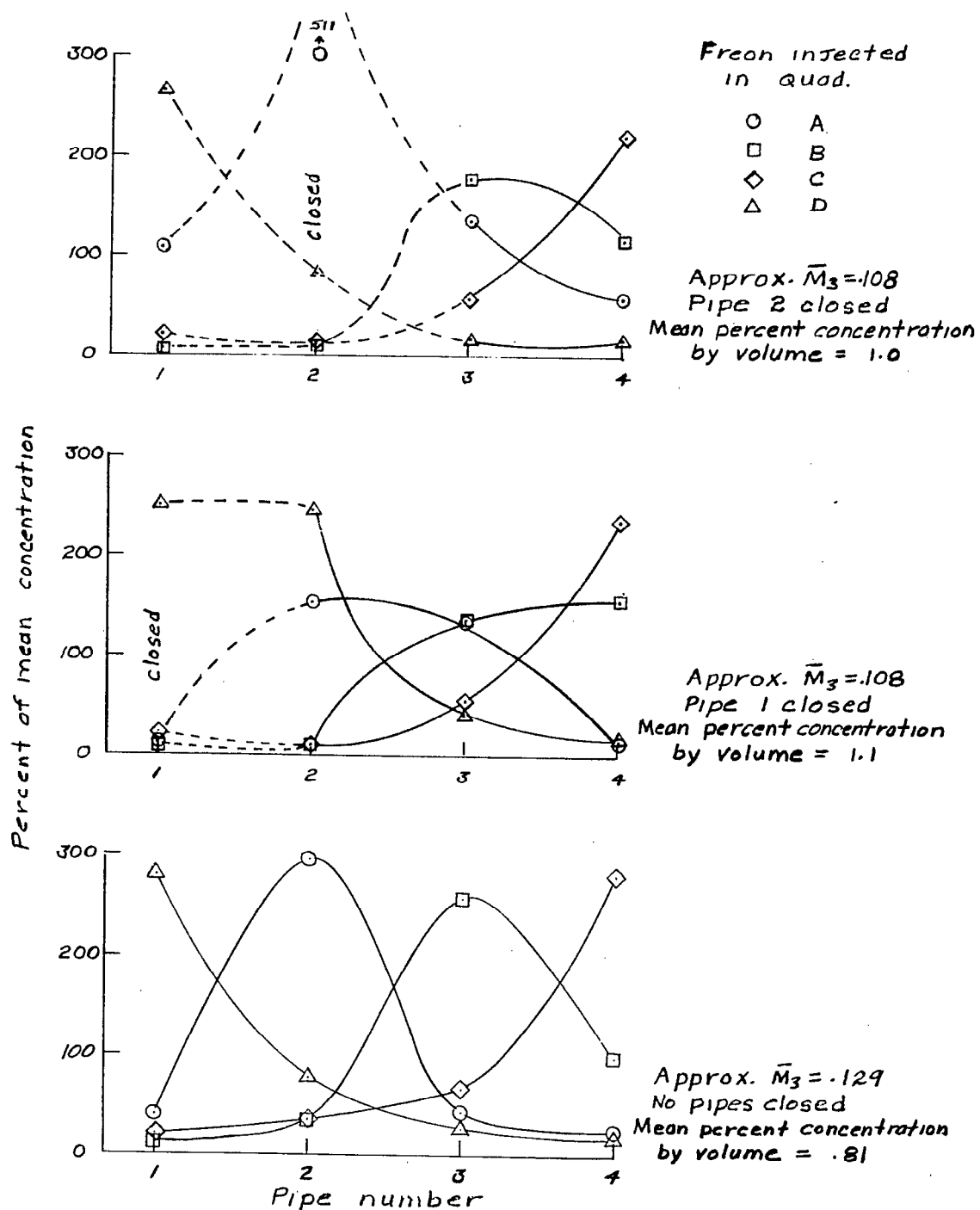
Figure 71.- Results of air-flow tracing test showing the percent of mean concentration in the various pipes for the symmetrical and two asymmetrical test conditions. Test configuration 4c.